LAPPEENRANTA UNIVERSITY OF TECHNOLOGY
FACULTY OF TECHNOLOGY
Master's Degree Programme in Technomathematics and Technical Physics

SYNTHESES OF NIOBIUM OXIDE IN THE PRESENCE OF MAGNETIC FILD AND DETERMINATION OF PHYSICAL PROPERTIES

Examiners: Professor, Erkki Lahderanta
MSc Elina Hujala

Supervisors: Professor, Erkki Lahderanta

Lappeenranta 22.05.2008

Anastasia Fadeeva
Punkkerikatu 5 C 41
53850 Lappeenranta
Phone: +358449325644

ABSTRACT

LAPPEENRANTA UNIVERSITY OF TECHNOLOGY
FACULTY OF TECHNOLOGY
Master's Degree Programme in Technomathematics and Technical Physics

Author: Anastasia Fadeeva

Title: **Syntheses of niobium oxide in the presence of magnetic field and determination of physical properties.**

Master's thesis

Year: 2008

106 pages, 57 figures and 17 tables.

Examiners: Professor, Erkki Lahderanta
MSc Elina Hujala.

Keywords: Magnetic field, oxide film, synthesis.

Now when the technology fast developing it is very important to control the formation of materials with better properties. In the scientific literature there is a number of works describing the influence of magnetic field on the properties and process of formation of materials. The goal of this master's thesis is to analyze the process of electrochemical synthesis of niobium oxide in the present of magnetic field, to compare properties of formed oxide films and to estimate the influence of magnetic field on the process and on the result of synthesis.

ACKNOWLEDGEMENTS

This master's thesis was carried out in the laboratory of Physics, Lappeenranta University of Technology in cooperation with laboratory of Thin Films, Petrozavodsk State University "PetrSU".

I wish to express my gratitude to Professor E. Lahderanta and Professor V. Malinenko for their guidance and support.
I also wish to express my gratitude to my friends, relatives and especially to my mum.

Lappeenranta, May 2008
Anastasia Fadeeva

SYMBOLS

Roman letters

B_T current efficiency
C capacity
d_{ox} oxide thickness
E electric field strength
E_a activation energy
E_{diff} differential electric field strength
F Faraday constant
f frequency
G free energy
g gyromagnetic ratio
I current
j density of current
M molar mass
m^* effective mass
T temperature
U voltage
U_f forming voltage

Greek letters

α forming coefficient
β Bohr magneton
δ critical factor
ε permittivity
ρ oxide density
τ relaxation time

TABLE OF CONTENTS

INDRODUCTION

Now in the scientific literature a number of works describing the influence of magnetic field on the properties and process of formation of materials exist. It is shown that the magnetic field applied during the formation of materials can influence on the structure of the material. The magnetic field leads to more perfect structure. Also properties of the materials are changed. Particularly the influence of magnetic field on the mobility of dislocations in a monocrystal of p-type silicon is revealed, the crystal hardening is observed, there is a change of ferroelectric properties, and the initial distribution of electrons is changed. It is established, that a short-term exposure to a weak magnetic field initiate long-term changes of the structure and physical properties of a wide class of nonmagnetic materials. Properties of materials are determined by spin states of microparticles which enter into the chemical reactions and form substance. The magnetic field can change the spin states of particles and thereby both the chemical reaction process and its result can be changed.

The influence of a magnetic field on electrochemical synthesis of materials is actively studied. Electrochemical synthesis is a process of two fluxes of the charged particles moving towards each other, their interaction and the reaction of oxide formation. The accelerating electric field is strong and the speeds of fluxes are high. Presence of magnetic field can influence on the movement of particles, their interaction and reactions of oxide formation. Consequently, applied magnetic field leads to a change of properties and structures of the formed material. The electrochemical synthesis is a process of a self-organizing of substance. It is a complex process. The magnetic field can change conditions of the course of the process, changing energy and spin states of reactive particles.

The purpose of the present study is to compare the kinetic characteristics of the synthesis of the niobium oxide in the presence of different magnetic field, investigation and analysis of optical, electrical and polarizing properties of the formed materials, and determination of permittivity.

1 THEORETICAL PART

1.1. Properties and growing processes of oxide

1.1.1. Basic characteristics of Niobium

Niobium is a chemical element that has symbol Nb, atomic number 41, and atomic weight 92.9064. Natural niobium consists of one stable isotope ^{93}Nb. The configuration of two external electron layers is $4s^2p^6d^45s^1$. The oxidation numbers are +5, +4, +3, +2 and +1 (the valencies are V, IV, III, II and I). Niobium is situated in the group VB, in the fifth period of the periodic table.

Atomic radius is 0.145 nm, Nb^{5+} ion radius has from 0.062 nm (correspond to the coordination number 4) to 0.088 nm (8), of Nb^{4+} has from 0.082 to 0.092 nm, Nb^{3+} ion radius has 0.086 nm, and Nb^{2+} has 0.085 nm. Energies of successive ionization are 6.88, 14.32, 25.05, 38.3 and 50.6 eV. The electron work function is 4.01 eV. [1]

Physical and chemical properties

Niobium is a glitter silver-grey metal with a body-centered cubic structure of the type α-Fe with a = 0.3294 nm. The melting temperature is 2477°C, the boiling temperature is 4760°C, and the density is 8.57 kg /dm^3.

Niobium is a chemical-steady element. Niobium oxide has about 10 crystalline modifications. B-form of Nb_2O_5 is stable by the normal pressure.

Table 1.1. Physical and chemical properties

Name	Formula	Density, g/cm^3	Melting point, ^{0}C	Boiling point, ^{0}C
Niobium	Nb	8.57	2468	4860
(V) oxide	Nb_2O_5	4.55	1512	

Table 1.2. Effective ion radiuses

ion	electron configuration	coordination number	crystallographic radius, Å	Effective ion radius, Å
Nb^{+5}	4p6	4	0.620	0.620
		6	0.780	0.640
		7	0.830	0.690
		8	0.880	0.740
O^{-2}	2p6	2	1.210	1.350
		3	1.220	1.360
		4	1.240	1.380
		6	1.260	1.400
		8	1.280	1.420

1.1.2. Natural oxide layer

Anodic oxide films are oxide layers, which are formed on the metal surface by the anodic polarization in the electrolyte solution, in the salt melts, in the oxygen plasma and in contact with some solid electrolyte [2].

All metals, except gold, are thermodynamically unstable and form an oxide film on the surface [3]. This film can exist because oxidation is exothermic reaction. Free energy decreases during this reaction.

$$xMe + \frac{y}{2}O_2 \rightarrow Me_xO_y$$

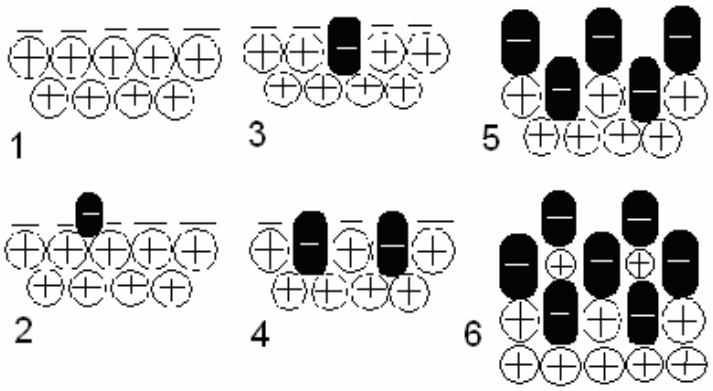

Figure 1.1. Scheme of forming of primary oxide with absorbed oxygen, where particles with plus are metal molecules and particles with minus are oxygen molecules [4].

Oxygen interacts with clean metal surface. The first stage of the reaction is oxygen absorption. Physically absorbed molecules dissociate on the metal surface and a chemisorbed monolayer of oxygen molecules is formed. After that oxygen molecules penetrate into the metal lattice, the metal lattice doesn't change, and this process can be regarded as the oxygen dissolution in the metal [4]. This process is shown in Figure 1.1. It occurs until the solubility limit is not reached, after this the process of oxide phase forming is started.

This process is finished after one or two oxide monolayers are formed and the penetration of the oxygen atoms inside the metal stopps. All this process occurs instantly [5].

Further oxide growth can continue by means of diffusion of the metal and oxygen ions due to electric field [3]. This process is slowly. Increasing of the film thickness decreases the reaction rate because of decreasing of electric field inside the film.

1.1.3. Bonds in oxides and structure of oxide films

Chemical bonds in the oxides are mixed ion-covalent bonds. An ionic bond is an electrostatic interaction between two oppositely charged ions, which are components of the chemical compound. The ion charge determines the main valence of the atom.

A covalent bond is an exchange electronic interaction between neighbouring atoms [6]. Paired electrons must have antiparallel spins. The interaction with third electron induces repulsion, meaning that the covalent bond is a saturated bond.

Amorphous oxide films are usually formed by anodic oxidization of metal [3]. There is no long-range ordering, no translation symmetry nor periodic space lattice in amorphous material. Theoretically, only ideal gas is completely disordered system. Amorphous solid has short-range order. There is a concrete coordination of the nearest neighbors. Those crystal regions are not homogeneous. They form a continuous net of structure units, which are six- or five-membered space ring. Relative position of particles is determined by the chemical nature and the type of interaction between particles. The bond length of the particle, situated in the centre of the other particles, is strongly fixed. But the angles are not strongly fixed, and distortion of the lattice increases with moving away from the center [7].

The structure scheme of the compound Me_2O_3 is shown in Figure 1.2 with amorphous form (a) and crystal form (b) [5].

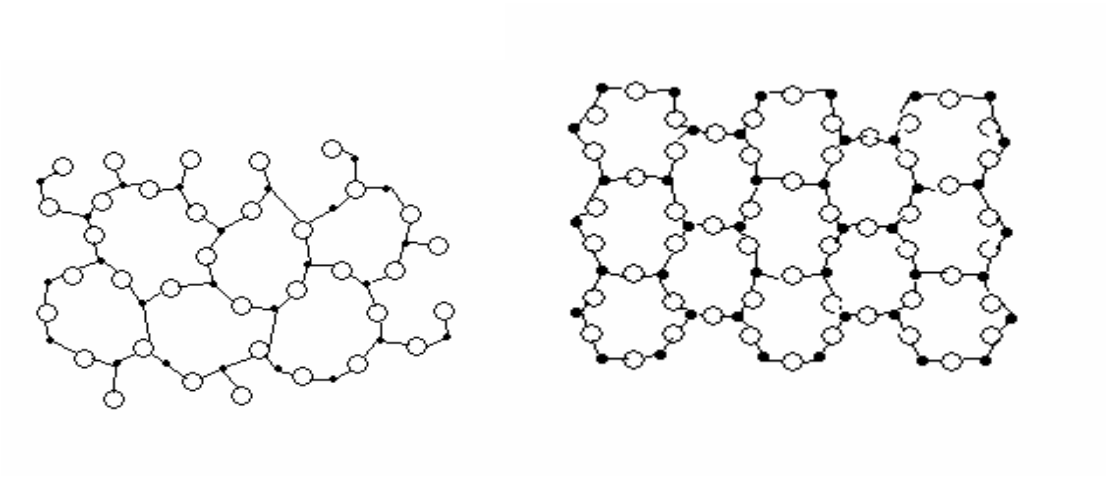

(a) (b)

Figure. 1.2. Structure scheme of compound Me_2O_3: a) amorphous form; b) crystal form.

1.1.4. Kinetics of mass and charge transport in electrostatic field.

Anodic oxide films on the metal or semiconductor surface are formed by applied electric field in electrolyte. Electric field shifts the equilibrium potential to the positive side. First, thin solid oxide layer is formed on the surface of the metal, as described in the previous chapter. This layer is insoluble in electrolyte, and electrostatic field is established in the oxide. Metal and oxygen ions start to move from one side of the oxide layer to another by means of applied electric field, and the oxide film grows. For forming every new layer of oxide it is needed additional voltage dU. This voltage is added to previously applied voltage [8].

Forming of oxide layer occurs only if there is transport of mass and (or) charge through the oxide film. The transport process is possible if there are a concentration gradient of movable particles (defects) and an electric field gradient. Electric field can be created by internal reasons such as redistribution of diffusion particles or by external reasons, for example, by applied potential [9].

A part of current forming oxide can be 100% or less it is determined by nature of the metal and conditions of oxide formation. A part of current (electron current) is used for oxidization reactions. Current is used also to dissolution of metal by transport of ions through the oxide to electrolyte. In addition the anodic film can be dissolution in electrolyte. This process is compensated by forming equivalent amount of oxide, it means that part of common current is used to this process. Niobium is a metal for which almost of all current is used to oxide formation. The thickness of niobium anodic films can be several hundreds nanometers. [9]

The main data, which give information about kinetic characteristics, are voltage and current characteristics. [10]

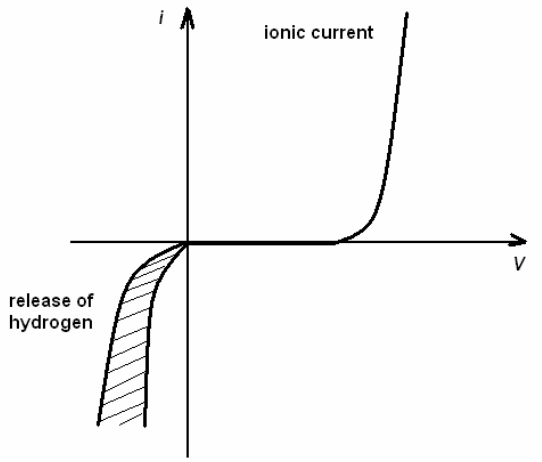

Figure 1.3. I-V characteristic of tantalum oxide electrode. [8]

Dependence *i(u)* of valve metal is shown in fig. 1.3. Current quickly increases with negative voltage, and hydrogen is produced on the electrode. Current of anodic polarization is vanishingly small, until voltage is enough for ionic current to be more than leakage current. At this voltage current starts to increase quickly with increasing of voltage. Anodic current is caused by release of oxygen and is connected with electric conductivity of the film.

When electric field strength is enough for existence of ionic current, process of oxide growth is started. There are two possible regimes of oxide growth; potentiostatic and galvanostatic regimes.

If film is weakly soluble during galvanostatic oxidization, the thickness of oxide film x is proportional to transmitted charge q and constant γ. According to Faraday law constant γ is:

$$\gamma = \frac{dx}{dq} = \frac{MB_T}{\rho nF}, \tag{1.1}$$

where M is molar mass of the oxide; ρ is the oxide density; B_T is the current efficiency; n is number of electrons needed to form of one oxide molecule; F is the Faraday constant; and x is the thickness of the film.

In these conditions also potential φ increases linearly with increasing of charge q, meaning that $d\varphi/dq$ = const, and

$$d\varphi / dx = E_{diff} = const, \tag{1.2}$$

where E_{diff} is differential electric field strength in the film. The E_{diff} is the field strength in new formed layers of the oxide. E_{diff} being constant means that strength of electric field does not change during growth of the film. If E_{diff} is constant, then voltage change is fater,

$$\frac{dU}{dt} = E_{diff}\frac{dx}{dt} = jE_{diff}\frac{M}{n\rho F}. \tag{1.3}$$

Ion conductivity of the solid is connected with defect transport in the solid. The defects are anion and cation lattice vacancies and interstitial ions. It is assumed that in the case of film growth there are interstitial ions with equivalent possibilities to move.

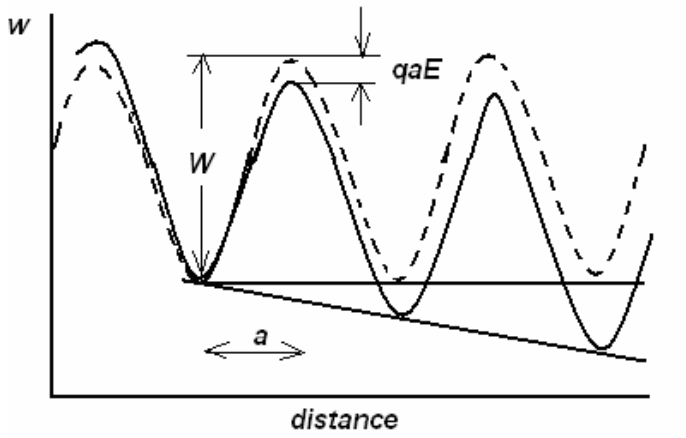

Figure. 1.4. Changing of potential energy of ion with distance: without field (dashed line) and when electric field is applied (solid line).

It is only first approximation, because niobium films are amorphous. Under thermal excitation and electric field the ions obtain enough energy to move over potential barrier to the next interstice. Potential energy is shown in figure 1.4. It is assumed that the ions make simple harmonic vibration with frequency v. If there is no electric field, the amount of ions which have enough energy W to transport over potential barrier is proportional to exp(—W/kT). If electric field is applied, the barrier height decreases from W to W-qaE for ions, moving along electric field, and increases from W to W+qaE for ions, moving against the field. Here q is charge of ion and a is the

distance between neighbouring maximum and minimum of potential energy. If the barrier is symmetric, a is a half of distance between two neighbouring maxima. If energy of the ion is enough and the ion has oscillation frequency v, the ion has v chances in a second to jump over the barrier. n is the number of mobile ions in the unit volume. Every moving ion carries charge q to the distance $2a$. Observable current is the difference between current of the ions, moving along electric field, and current of the ions, moving against the field.

Forward current is

$$\vec{j}_{\text{ion}} = 2anv\exp\left[-\frac{W-aqE}{kT}\right] \tag{1.4}$$

Backward current is:

$$\overleftarrow{j}_{ion} = 2a\left(n+2a\frac{\partial n}{\partial x}\right)v\exp\left[-\frac{W-aqE}{kT}\right]$$

where x is a distance through oxide. Term $\left(n+2a\frac{\partial n}{\partial x}\right)$ takes into account the concentration gradient.

Resistance of anode oxide films is so big that it is needed too high electric field to obtain measurable current. When electric field is high, backward current is negligible with respect to forward current. Therefore current is described by equation (1.4). Usually W is about 1 eV, for room temperature kT is about 1/40 eV and a is about 1Å. If strength of electric field is $6*10^6$ V/cm and $q = 5e$ (for Nb^{5+}) then qaE is about 0.3 eV. In this case forward-to-backward-current ratio is

$$\frac{\exp(-0.7\cdot 40)}{\exp(-1.3\cdot 40)} = \exp 24 \approx 10^{10}$$

This result is called the strong field approximation. It is typical for oxide films and equation (1.4) is the basic equation for theory of thin films.

In general case, the equation is

$$j_{\text{ion}} = \vec{j} - \overleftarrow{j} = 4anv\exp\left(-\frac{W}{kT}\right)sh\frac{qaE}{kT} - 4a^2\frac{\partial n}{\partial x}v\exp\left(-\frac{W+qaE}{kT}\right).$$

When electric field is weak (weak field approximation) and $qaE << kT$ then

$$sh\frac{qaE}{kT} \cong \frac{qaE}{kT}$$

and

$$\frac{W + qaE}{kT} \cong \frac{W}{kT}.$$

Therefore in the case of weak field approximation

$$j_{ion} = const \cdot E - const \cdot \frac{\partial n}{\partial x}$$

First term describes Ohm law, second term describes diffusion current and Fick law. Ohm law doesn't work for high electric field. In general case the ion current and the electric field are well described by equation

$$j_{ion} = 2AshBE. \quad (1.5)$$

In strong field approximation equation (1.5) is modified to Gentelshtulz and Betz equation

$$j_{ion} = A\exp BE, \quad (1.6)$$

where A and B are constants which are linearly depended on temperature.

In first approximation equation (1.3) satisfactorily describes dependence of current from electric field $j = f(E)$ [8].

Measurement of Jung [3] and other researchers showed that more successful than (1.5) are equations

$$j_{ion} = A^{/} \exp(\alpha E - \beta E^2) \quad (1.7)$$

$$j_{ion} = A^{//} \exp(B\sqrt{E}). \quad (1.8)$$

In these cases nonlinearities of dependence lg$j = f(E)$ are not big, but fundamental, for example, it explains temperature dependence of E [9].

In weak field approximation equation (1.5) is modified to

$$j_{ion} = 2ABE. \quad (1.9)$$

These equations do not fully describe process of film growth, because those do not take into account processes on metal-oxide and oxide-electrolyte boundaries.

Electron current is the part of anodic current in an anodic film with homopolar conductivity. Electron current decreases with increasing of electric field but not so quickly as common current. Thereby it is possible to separate these two current components and inverstigate each of these separately.

Electric conductivity of thin oxide films was observed by Charlsbe and Vermilja by means of Fraenkel theory [3]. According to this theory there is a potential barrier in the film. The barrier thickness is *2a* and the high is *u*. Electrons must go over the barrier. Electric field decreases the height of the barrier and increases probability of electron transport along-field direction.

If potential is less than the forming potential, then there is current though film. This current depends on strength of electric field

$$j_{el} = 2A\exp\left(-\frac{u}{kT}\right)sh\left(\frac{eaE}{kT}\right), \tag{1.10}$$

where A is constant, j_{el} is electron current density, E is electric field strength.

Electric field changes the lattice parameters and electrons are able to transport thought the symmetrical potential barrier.

Oxide films have semiconductor nature and conductivity is a result of electron emission to the conducting band by means of electric field. If electric field strength is $5\cdot10^6$ V/cm then the probability of tunneling conductance is 100 times more than by means of thermal excitation.

Conductivity of film increases by means of Schottky effect, and is given by

$$\sigma = A\exp\left(-\frac{E_g - |V_0|}{2kT}\right) = \sigma\exp\left\{\left[\frac{q^3E}{e}\right]^{1/2} \Big/ kT\right\}, \tag{1.11}$$

where E is electric field strength, E_g is energy gap, E_g - $|V_0|$ is energy gap when electric field is applied, q is charge of electron and ε is oxide permittivity.

According to this equation the dependence (ln i) vs. $E^{1/2}$ is linear.

For niobium oxide film Nb_2O_5, if the thickness is 2000 Å and voltage is 100 V then common current is 10^{-8} A/cm^2, and thereby resistance is 10^{15} oh • cm[8].

1.1.5. Motion of charged particles near interface and in bulk

Next questions are very important for understanding the oxide growth process: 1. Where do new layers form? Do those form on the internal or external interfaces or inside the bulk volume of the oxide? 2. Do oxygen and metal atoms move throught film from external and internal interfaces respectively to the opposite sides? 3. Do other atoms and ions penetrate to the oxide from electrolyte? If it happens, how do those move inside the film? 4. Do impurity atoms penetrate to the oxide from metal? If it happens, how do those move inside film?

Experiments with marked inert gas clearly showed that new niobium, tantalum, aluminum and wolfram oxide layers are formed on both the internal and external interfaces, but new zirconium and hafnium oxide layers are formed only on the internal interface. Ratio of the thickness of the oxide formed on the external boundary to the thickness of the oxide formed on the internal boundary is the transport number of metal, t_m. For niobium t_m = 0.29. Other independent methods also showed that both types of atom transport inside the oxide.

According to theory of disordered crystal there are four types of the ion defects in the oxide:

- The metal cation in interstice M_i^+,
- The vacancy in cation sublattice V_M^-,
- The anion in interstice A_i^-,
- The anion vacancy V_A^+.

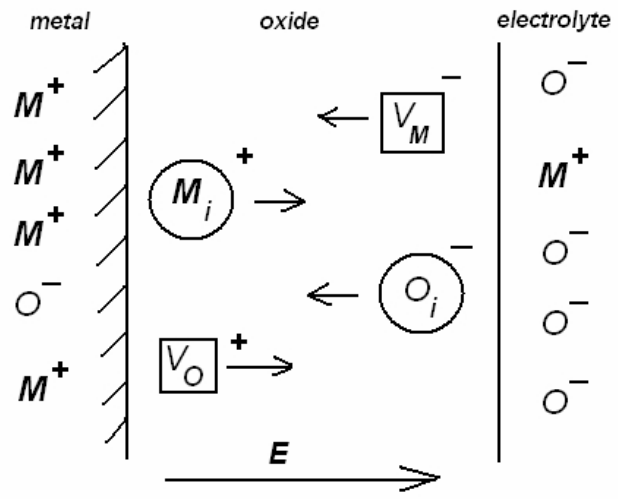

Figure. 1.5. Scheme of oxide growing, where M_i^+ and O_i^- are interstitial ions of metal and oxygen. V_M^- and Vo^+ are vacancies in the metal and oxygen sublittices [9].

If electric field is applied then the metal cations M_i^+ and the oxygen vacancies Vo^+ transport to the oxide-electrolyte boundary and the anions O_2^- and the metal vacancies V_M^- transport to the metal-oxide one. The cations M_i^+ interact with oxygen molecules or adsorb on the oxide-electrolyte surface ion O^{-2} or OH^- and new layers of oxide is formed. The same result is obtained by forming the vacancy in the metal sublattice on the oxide-electrolyte surface. The metal ion forms new layer of oxide, and the vacancy is formed in the previous layer. Thereby the vacancy move to the internal interface where it interacts with metal atom, and oxide is formed. By analogy, the interstitial oxygen ions and oxygen vacancies transport though film and form new layers on the internal boundary, fig. 1.5. Transport of ion defects is occurred by means of applied electric field and (or) diffusion. Diffusion is caused by concentration gradient of ion.

Processes on the external and internal interfaces make the film growth more complicated. The influence of the metal-oxide boundary was investigated by Mott and Cabrera [3]. The electric field strength is described by Poisson equation

$$\frac{\partial E}{\partial x} = \frac{4\pi}{\varepsilon}\rho ,$$

where E is the electric field strength, x is the distance, ρ is density of volume charge, and ε is permittivity. Full volume charge is the difference between positive charge of the mobile ions and negative charge of all immobile particles. Charge of electrons does

not give important contribution to full volume charge. This is shown by weak electron current.

If the density of volume charge is not big then electric field is not considerable changed in the thin film. In this case current is controlled by velocity of displacement ions from the metal to the oxide. Current through the barrier is described by similar equation as for current inside oxide. But the concentration of ions in the oxide volume *2an* is replaced by the concentration of ions on the boundary n'. The concentration of ions on the boundary is constant and doesn't depend on electric field. Therefore current through the barrier is:

$$j = n'\nu' \exp\left[-\frac{W' - qa'E}{kT}\right] \tag{1.11}$$

Where the character stroke means that parameters are concerned to the inter barrier. The ion concentration is not fixed, but it is self-regulating until current through oxide, described by formula (1.12), is not exactly equal to the barrier current.

$$j = 2an\nu \exp\left[-\frac{W - qaE}{kT}\right] \tag{1.12}$$

This implies $n = n_0$, where n_0 from (1.11) and (1.12) is

$$n_0 = \frac{(n'\nu')^{a/a'}}{2a\nu} \exp\left(\frac{W - W'\dfrac{a}{a'}}{kT}\right) j^{(1-a/a')}. \tag{1.13}$$

Equation (1.11), establishing linkage between *E*, *j* and *T*, has a form similar to the Vervei equation [9]. Equation (1.13) shows that n_0 strongly depends on electric field. Here are no restrictions on the concentration of the mobile ions, but in the case of real system restrictions can exist.

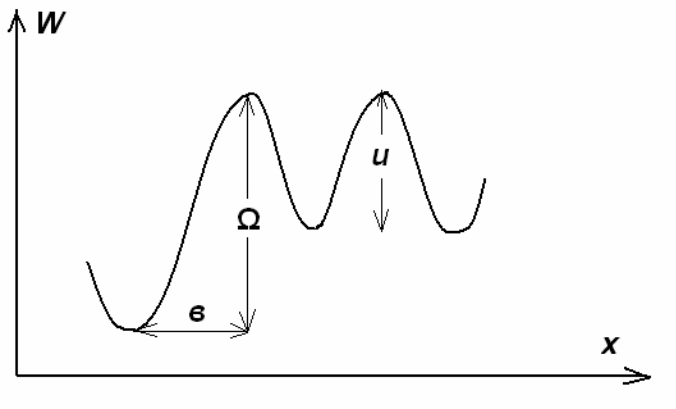

Figure. 1.6. Potential energy dependence on distance for ion outgoing from metal to oxide.

Figure 1.6 shows, when ion goes from the metal to the oxide, the first barrier Ω situated on distance *b* is bigger than the others situated inside the film [11].

Consider film as a lattice of the stoichiometric composition. The ions transport through film by means of electric field. Taking into account volume charge, behavior of this kind of system depends on critical factor δ. The critical factor is dimensionless quantity and depends on parameters of the oxide lattice and experimental conditions:

$$\delta = \beta\gamma n_0 D = \left[\frac{4\pi q^2 (m_s \nu_s)^{a/b}}{kr\nu}\right] \exp^{(u-\varphi a/b)/kT} \frac{D}{T} j^{(1-a/b)}.$$

Here *u* is the activation energy; *2a* is the distance between two equilibrium positions; *v* is oscillation frequency of the ion in the interstice; v_s is oscillation frequency of the metal atom on the surface; n_o is concentration of the ions when $x = 0$; φ is diffusion activation energy; m_s is surface density of the metal ions; and *D* is the film thickness.

In the case of small δ, when volume charge has not big value, growth kinetics is determined by processes on the oxide-metal surface.

If the value of the critical factor is about 10 (δ ~ 10) and the thickness of the film is about 1000 Å then the growth velocity of the oxide is almost determined by film mass. In the presence of the strong applied electric field, electrons are removed from the film, and movement of the ions is not electrically compensated. Therefore volume charge arises.

Equation of average electric field is

$$\overline{E} = E_0 + \frac{1}{\beta}\left\{\left(1+\frac{1}{\delta}\right)\ln(1-\delta)-1\right\}, \tag{1.14}$$

where E_0 is a value of the surface charge; $\beta = qa/kT$ and a is distance between maximum and minimum of potential energy.

Equation (1.14) shows that for any point of the film electric field is determined by the value of surface charge and parameter β connected with volume charge.

Equation (1.14) has a simply dependence form for $\delta >> 1$ and $\delta << 1$ but complicated form when $\delta \approx 1$.

1.1.6. Transport processes and reactions on phase boundaries

Oxide is formed by means of transport of charge and (or) mass through film. This transport is possible if concentration gradients of mobile particles and electric potential exist. Electric field can be created by redistribution of diffusing particles or by external reasons for example by applied potential.

Reactions on the metal-oxide interface are [12]

$$M \rightarrow M_i^{z+} + ze^- \tag{1.15}$$

$$t_a(M_i^{z+} + \frac{z}{2}O_o \rightarrow MO_{z/2} + \frac{z}{2}V_o^{\bullet\bullet}) \tag{1.16}$$

and

$$y(M_i^{z+} + V_M^{z'} \rightarrow M_M) \tag{1.17}$$

Reactions on the oxide-electrolyte interface are

$$(t_c - y)(M_i^{z+} + \frac{z}{2} H_2O \rightarrow MO_{z/2} + zH_{aq}^{+}) \tag{1.18}$$

$$y(M_M + \frac{z}{2} H_2O \rightarrow MO_{z/2} + zH_{aq}^{+} + V_M^{z'}) \tag{1.19}$$

$$t_a \frac{z}{2}(V_O^{\bullet\bullet} + H_2O \rightarrow O_O + 2H_{aq}^{+}) \tag{1.20}$$

and

$$\alpha(MO_{z/2} + zH_{aq}^{2} \rightarrow M_{aq}^{z+} + H_2O) \tag{1.21}$$

Total reaction is:

$$M + \beta \frac{z}{2} H_2O \rightarrow \beta MO_{z/2} + \alpha M_{aq}^{z+} + \beta zH_{aq}^{+} + ze^{-}$$

Where t_c and t_a are part of transport cation and anion respectively, α and β are part of dissolved metal and part of metal which is spent on forming oxide respectively, M_M is the metal cation, O_O is the oxygen anion, V is the ion vacancy, M_i^{z+} is the intermediate ion.

Forming of oxide includes transport of the negative and positive quasi-ions through the oxide. Oxide forming takes place on phase boundaries according to reactions (1.15) – (1.21).

1.2. Influence of magnetic field on the process of oxide growth

1.2.1. Influence of constant magnetic field

At the present time many investigations works which estimate influence of magnetic field on properties and formation of materials exist.

Zubric [13] investigated influence of magnetic and electric field on condensation of thin films of tellurium. The model was made and experiments confirmed model validity. Following conclusions were made.

Magnetic and electric fields influence on condensation process of thin films and it is possible to control structure ordering. The molecules of adsorb vapor is polarized by electric field. Magnetic moments are created by means of temperature oscillations. Magnetic moments interact with magnetic field, and the crystallization centers are created.

Investigation of the surface was made and the optimal conditions of structure forming was estimated. These conditions made it possible to obtain structurally perfect tellurium on the nonoriented substrate. These papers describe possibility to form more perfect structure by influence of electric and magnetic fields.

Paper [14] show influence of electric and magnetic field on the liquid-solid transition and the structure of obtained solid materials. Applied magnetic field increases convective stream during liquid-solid transition. Also magnetic field changed nature, structure and kinetic of the forming. Lorenz force plays important role in these processes.

Group of scientific which are Osipjan, Morgynov, Baskakov, Orlov, Skvorcov, Inkina, Tanimoto [15] investigated influence of crossed constant and variable microwave magnetic fields on the monocrystal of the p-type silicon. Resonance influence on the dislocation mobility was established. Frequency of variable and inductance of constant magnetic fields which proved maximum effect of influence satisfy the conditions of stimulation of the electron paramagnetic resonance (EPR) in defects of structure. It is shown that the influence of magnetic field on the plasticity is spin-dependent in silicon.

Another paper is “Spin micromechanics of plasticity physic” [16] by Morgynov. Influence of spin of defects on the mechanical properties and plasticity is described. This publication is conclusion of series of experiments with different materials and magnetic field. Effects of influence of magnetic field are characterized by next factors: 1) Effects become more significant if magnetic field is not only constant but crossed constant and variable. 2) Effects become more significant in high temperatures

or in the some temperature interval. 3) Effects appeared with a dalay after exposure to magnetic field. 4) Exposure to magnetic field must be long-term, 10 second or more. 5) Effects depend on type of impurities. 6) Effects depend on interconnection between surface and volume properties of material in magnetic field.

Levin, Postnikov and Palagin [17] discovered the effect of selective influence of magnetic field on temperature of the ferroelectric transition. The height of maximum of dielectric permittivity multiply increases in the Curie point for triglycinesulphate (TGS) and dihydrophosphate (KDP) of potassium. This effect is occurred due to process of transformation of defect in real crystal. This process is spin dependent.

In most studies the reason for influence of weak magnetic field is the change of the spin states of the reagents. Theoretical models of influence of weak magnetic fields on radical chemical reactions are based on the assumption of the canceling of the spin forbidding of transition by means of magnetic field [18].

It is established, that a short-term exposure to weak magnetic field initiate a long-term changes of the structure and physical properties in wide class of nonmagnetic materials.

In study [19] influence of pulsed magnetic field causes a radical change of initial electron distribution. Observed decrease of fusion temperature of a crystal is explained by weakening and breakage of the bond in the vacancy complex occurred by means of pulsed magnetic field.

Possibility to control the structural ordering of thin films by means of magnetic field is theoretically proved. Under influence of electric field the molecules of adsorbed pair are polarized. The magnetic moment appears due to temperature oscillations. This magnetic moment interacts with applied magnetic field, and crystallization centers are formed.

The main conclusions from those studies are:

- Influence of magnetic field can lead to formation of more perfect structure.
- Magnetic field can change microstructure of materials.
- Influence of magnetic field can be selective.
- To determine influence of magnetic field on the structure or formation of materials it is necessary to consider presence of spin states of defects.

1.2.2. Energy spectrum of electron in constant homogeneous magnetic field

First we consider influence of strong magnetic field on energy spectrum of electron gas with magnetic field induction B in the direction along the axis z. Electrons can move in three directions. For simplicity, we assume that electrons have isotropic effective mass m^* [20].

Magnetic field influences on the orbital motion of electrons and on the spin orientation by means of respective magnetic moments. Hamiltonian function of the electron in magnetic field is:

$$\hat{H} = \frac{1}{2m^*}\left(\hat{\bar{p}} + q\hat{\bar{A}}\right)^2 + \beta\mu_B\left(\hat{\sigma}\bar{B}\right)$$

Where $\hat{\bar{p}} = -i\hbar\nabla$ is momentum operator; A is vector-potential of magnetic field and q is electron charge.

Second term in Hamiltonian function describes interaction between spin magnetic moment and magnetic field. Here $\mu_B = qh/2m^*$ is Bohr magneton; g is gyromagnetic ratio of the electron and σ is operator of electron spin.

In the case of integer quantum Hall effect the role of spin is not important and the Hamiltonian function can be simplified

$$\hat{H} = \frac{1}{2m^*}\left(\hat{\bar{p}} + q\hat{\bar{A}}\right)^2 . \qquad (1.22)$$

If vector-potential is described as $A_x = 0$, $A_y = B^* x$, $A_z = 0$ with $B = rotA$ then only one magnetic field component is not equal to zero, $B_z \neq 0$.

Permutation relation of momentum operator is

$$A_j P_j - P_j A_j = i\hbar \frac{\partial A_j}{\partial P_j} \quad \text{with} \quad j = x, y, z \quad . \tag{1.23}$$

In addition let vector-potential satisfies condition of calibration.

$$div\overline{A} = 0 \tag{1.24}$$

Using equations (1.24) and (1.22) the Hamiltonian function (1.22) can be modified

.

$$\hat{H} = -\frac{\hbar^2}{2m^*}\nabla^2 + \frac{1}{m^*}\left[B_x\left(-i\hbar\frac{\partial}{\partial y}\right)\right] + \frac{q^2B^2x^2}{2m^*} \quad . \tag{1.25}$$

Equation (1.25) has equivalent form:

$$\hat{H} = -\frac{\hbar^2}{2m^*}\left[\frac{\partial^2}{\partial x^2} + \left(\frac{\partial}{\partial y} + \frac{iqBx}{\hbar}\right)^2 + \frac{\partial^2}{\partial z^2}\right] \quad . \tag{1.26}$$

Schrödinger equation for Hamiltonian (1.26) is

$$\left[\frac{\partial^2}{\partial x^2} + \left(\frac{\partial}{\partial y} + \frac{iqBx}{\hbar}\right)^2 + \frac{\partial^2}{\partial z^2} + \frac{2m^*E}{\hbar^2}\right]\psi(xyz) = 0 \tag{1.27}$$

Vector-potential components do not depend on *y* and *z* direction, therefore equation (1.27) has solution:

$$\psi(xyz) = e^{i(k_z z + k_y y)}\varphi(x) \,. \tag{1.28}$$

Solution (1.28) is substituted into equation (1.27) and equation of wave function φ(x) is:

$$-\frac{\hbar^2}{2m^*}\frac{d^2\varphi}{dx^2} + \frac{1}{2m^*}\left(\hbar k_y + qBx\right)^2\varphi = \left(E - \frac{\hbar^2 k_z^2}{2m^*}\right)\varphi \tag{1.29}$$

Next signs are used:

$$E' = E - \frac{\hbar^2 k_z^2}{2m^*} \quad , \quad x = x' + x_0 \quad , \text{ where } \quad x_0 = -\frac{\hbar k_y}{Bq} \quad ,$$

We obtain equation (1.29) in the form

$$-\frac{\hbar^2}{2m^*}\frac{d^2\varphi}{dx'^2}+\frac{q^2B^2}{2m^*}x'^2\varphi=E'\varphi \quad . \tag{1.30}$$

Equation (1.29) coincides with quantum equation of harmonic oscillation which frequency is:

$$\omega_c=\frac{Bq}{m^*} \quad .$$

Its solutions are well known. The energy E' is quantized by the law:

$$E'=\hbar\omega_c\left(n-\frac{1}{2}\right) \quad \text{where n=1,2,3..} \tag{1.31}$$

Eigenfunctions are:

$$\varphi(x)=\sqrt{\gamma}\exp\left\{-\frac{(x-x_0)^2}{2\gamma^2}\right\}H_n\left(\frac{x-x_0}{\gamma}\right) \tag{1.32}$$

Where $\gamma=\hbar/Bq$ is magnetic length; $H_n\left(\frac{x-x_0}{\gamma}\right)$ is Hermitian polynomial.

Energy of electron consists of two parts in magnetic field:

$$E=\frac{\hbar^2k_z^2}{2m^*}+\hbar\omega_c\left(n-\frac{1}{2}\right) \quad . \tag{1.33}$$

First term describes energy for electron moving along the z axis, along the magnetic field. Magnetic field does not influence on this component of electron energy. Movement of electron is quantized in the plane which is perpendicular to magnetic field. This movement is described by second term of equation (1.33). If amount of k_z is fixed then energy spectrum of electron is series of equally spaced levels with distance $\hbar\omega_C$ between the levels. These levels are called Landau levels.

Energy spectrum is divided into the row of sublevels. Taking into account quantization increases the lowest energy level by amount $0.5\hbar\omega_C$. Thereby the energy spectrum is strongly modified in the present of magnetic field.

1.2.3. Charge particle in crossed magnetic and electric fields

According to Ohm law the current density in isotropic medium in weak electric field without magnetic field is [21]:

$$\bar{j} = \sigma \overline{E}\,, \tag{1.34}$$

where σ is conductivity

$$\sigma = en\mu\,. \tag{1.35}$$

Where n is concentration of uncombined carriers of charge, μ is drift mobility:

$$\mu = \frac{e}{m_n^*}\langle \tau \rangle \quad . \tag{1.36}$$

In (1.36) τ is relaxation time or average transit time of charged particles. Angle brackets mean energy averaging:

$$\langle \tau \rangle = \frac{\int_0^\infty \tau W^{3/2} \exp\left(-\frac{W}{k_0 T}\right) dW}{\int_0^\infty W^{3/2} \exp\left(-\frac{W}{k_0 T}\right) dW}$$

Projections of orthogonal coordinates are:

$$j_x = \sigma E_x\,,\ j_y = \sigma E_y\,,\ j_z = \sigma E_z\,.$$

In the case of anisotropic medium the current is homogeneous and linear function of all electric field components equation (1.34) can be written in the next form:

$$j_x = \sigma_{xx} E_x + \sigma_{xy} E_y + \sigma_{xz} E_z$$

$$j_y = \sigma_{yx} E_x + \sigma_{yy} E_y + \sigma_{yz} E_z$$

$$j_z = \sigma_{zx} E_x + \sigma_{zy} E_y + \sigma_{zz} E_z\,.$$

The short form is:

$$j_i = \sum_k \sigma_{ik} E_k\,,$$

Where indexes i and k take on values x, y, z.

Electrical conductivity tensor is:

$$\sigma_{ik} = \begin{pmatrix} \sigma_{xx} & \sigma_{xy} & \sigma_{xz} \\ \sigma_{yx} & \sigma_{yy} & \sigma_{yz} \\ \sigma_{zx} & \sigma_{zy} & \sigma_{zz} \end{pmatrix} .$$

Electrical conductivity tensor is symmetric tensor and components with symmetric indexes are equal, $\sigma_{ik} = \sigma_{ki}$.

If the charge particles move in the present of magnetic field B and electric field is zero $E = 0$, then the Lorentz force exists:

$$\overline{F} = e\left[\overline{v} \times \overline{B}\right]. \tag{1.38}$$

The Lorentz force is the force on moving charged particles in the presence of magnetic field B. This force is perpendicular to the velocity of the particle that why it does not influence on the amount of velocity, it changes only direction of velocity.

Therefore charge particles move in a circular orbit in the present of magnetic field B. The cyclotron frequency of motion is

$$\omega_c = \frac{Bq}{m^*} \tag{1.39}$$

and the cyclotron radius is

$$r_c = \frac{v}{\omega_c} \quad . \tag{1.40}$$

In the case of crossed electric E and magnetic B fields $\left(\overline{E} \perp \overline{B}\right)$ the next force exists:

$$\overline{F} = e\overline{E} + e\left[\overline{v} \times \overline{B}\right] \tag{1.41}$$

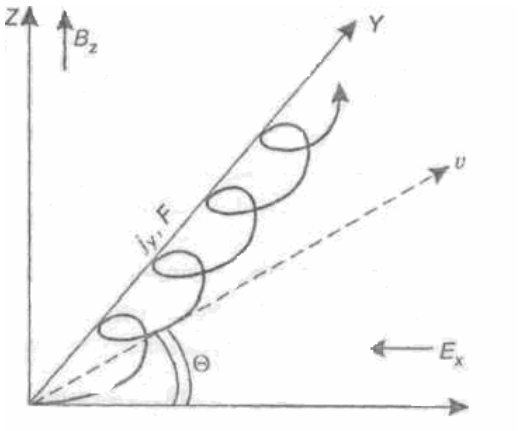

Figure 1.9. Part of motion of charge particle in the present of crossed magnetic and electric fields.

If electric field has x-direction $E = E_x$ and magnetic field has z-direction $B = B_z$ and there is no scattering of particles, then charge particles drift to y-direction. This direction is perpendicular to electric and magnetic fields. The path of motion is cycloid in the XY-plane (fig. 1.9). Y-direction velocity of particle is ratio E_x/B_z.

If there is scattering of the particles, the collision changes the trajectory of motion before the particle finishes cycloidal motion. The start of motion along new cycloid is shifted along the direction of electric field, y-direction. Thereby the longitudinal component of drift velocity v_x arises.

The tangency of angle Θ between drift direction and electric field is

$$tg\Theta = \mu B_z = \omega_c \langle \tau \rangle \quad . \tag{1.42}$$

If μB equals unity ($\mu B = 1$) then angle Θ equals 45° (Θ = 45°). This angle conventionally divides magnetic fields into strong and weak fields. If μB is less than unity ($\mu B << 1$) the field is weak, if μB is more than unity ($\mu B >> 1$) the field is strong.

In the case of strong field when angle Θ is near 90^0 ($\Theta \rightarrow 90^0$) the cyclotron frequency ω_c is the biggest and the cyclotron radius r_c is the smallest. There is practically no particle scattering.

In the case of weak magnetic field the path of motion considerably depends on scattering mechanism.

In the case of forming oxide film by electrochemical method there are particles with negative and positive charge. Magnetic field change motion trajectory of both types. The magnitude of the Lorentz force is:

$F_L = q\upsilon B \sin\varphi$,

where q is charge of the particle, v is particle velocity, B is magnetic field induction, and φ is the angle between v and B.

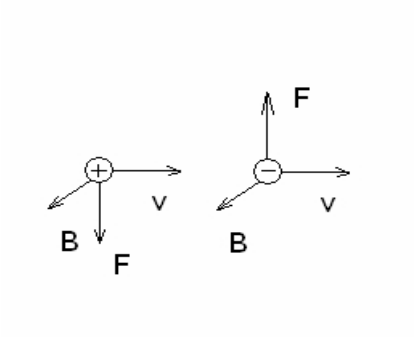

Figure 1.10. Direction of the Lorentz force for positive and negative charges.

The direction of Lorentz force is determined by the Right Hand Rule [22]. This rule is shown in figure 1.10.

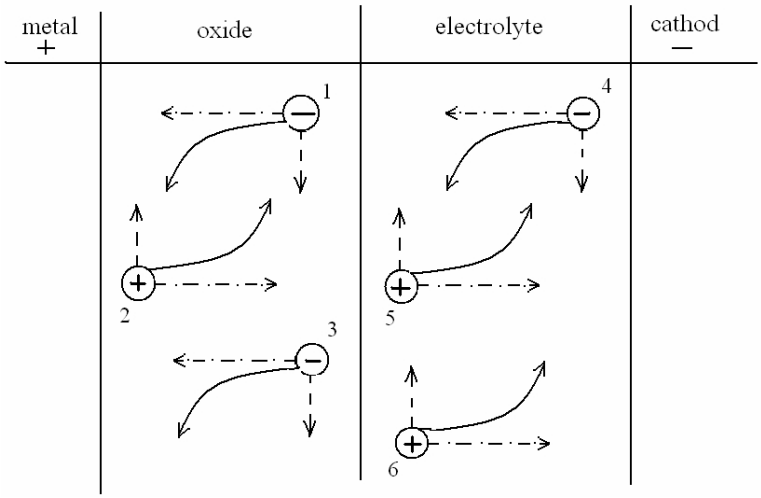

Figure 1.11. Motion of quasi-ions during forming of niobium oxide in the present of magnetic field. Where solid arrows are the Lorentz forces, dashed arrows with dot are electric forces, dashed arrows are expected trajectory, 1 is negative charge particle is $Me^{-}_{\frac{1}{2}(z+1)}$, 2 is positive charge particle is $Me^{+}_{\frac{1}{2}(z-1)}$, 3 is electron, 4 is hydrogen ion, 5 is oxygen ion and 6 is proton.

Figure 1.11 shows the scheme of motion of ions during growing of the oxide in the present of crossed electric and magnetic fields. There is involution of ions trajectories besides deviation from linearity.

Therefore magnetic fields can significant change trajectories of particle fluxes. It can be the reason for changing of process of oxide formation. In the presence of crossed electric and magnetic fields path of motion of charge particles is involution. The fluxes of positive and negative charge particles collide with it other on the phase boundaries. After this chemical reactions are occurred. If the conditions of this collisions or reactions are changed then results of reactions also can be changed. That why magnetic field can influence on the process and the result of the oxide formation.

1.2.4. Role of spin interaction in chemical and electrochemical reactions

1.2.4.1. Chemical kinetic

For understanding of the processes of chemical reactions taking place on phase boundaries we consider chemical kinetic. Chemical kinetics is the study of rates of chemical processes. Chemical kinetics includes investigations of how different experimental conditions can influence on the speed of a chemical reaction and yield information about the reaction mechanism and transition states, as well as the construction of mathematical models that can describe the characteristics of a chemical reaction. We will stop our consideration on the questions connected with influence of magnetic field on reaction process.

Consider qualitatively the nature of activation energy in chemical reaction. Any chemical reaction is connected with moving of atomic nucleus and transformation of electronic environment. According to Born-Oppenheimer approximation [23] set of electrons in molecule can be considered as a fast subsystem by reason of small mass of electrons comparison with mass of nucleus. The electron distribution is determined by the relative position of nucleus. Only one potential energy of system corresponds to

any of these relative positions of nucleus. Dependence of potential energy on a nuclear configuration can be expressed graphically as a surface of potential energy (in abbreviated form SPE). A point on the surface of potential energy corresponds to any nuclear configuration.

A molecule is characterized not only by one surface of potential energy but by a system of such surfaces. One surface is the basic and the others have higher energy and are excited. These surfaces of potential energy correspond to various electronic states of system - to the ground and excited states. The form of surfaces is various and consequently they can be crossed. Transition of the molecule from one of potential energy surface to another is connected with change of electronic and (or) spin state of the molecule.

In chemical reaction, two (or more) molecules taking part in this reaction are in strong interaction. This reactionary complex as well as the separate molecule has the system of potential energy surfaces. Change of position of nucleus during break or formations of chemical bond is a movement of a representation point on a surface of potential energy.

Exchange interaction leads to occurrence of the potential energy surface of the system of the atoms. There are two questions connected among themselves: 1) Does the chemical reaction always occur as movement of a representation point on such surface? 2) How big is the size of energy barrier of reaction? The exhaustive answer to these questions can be found, if surfaces of potential energy for each of possible electronic states of system are known.

If these surfaces have enough different energy (the energy gap between them is great during the time of reaction), influence of the higher electronic states on process of reaction can be neglected. In this case the height of a saddle point on the surface is activation energy of reaction [24].

1.2.4.2. Reactions of electron transport

Electron transport from one molecule or ion to another molecule or ion is one of the most widespread elementary reactions. Such stage necessarily is present at schemes of oxidation-reduction processes, electrochemical reactions, biochemical reactions of photosynthesis, breath, etc. The majority of such reactions occur in liquid solutions. Two fragments participate in the reaction of electron transport, namely an electron donor D (a reduction reagent) and an electron acceptor A (an oxidation reagent).

For experimental study of the elementary reaction of the electron transport the most simple model objects are chosen. In the case of such model objects, the observable reaction does not become complicated by transformation of the molecular structure. There are no breaks and formations of chemical bonds. The ions of transitive metals and their complex compounds can be used as model objects. There are two various types of reactions of electron transport.

If the donor and acceptor fragments are integrated into one molecule and are close to each other then it is the internal spherical reactions of electron transport. In this case the wave functions of the orbitals, from which electron leaves and to which it comes, are strongly crossed. Examples of the internal spherical reactions are reactions of oxidation or reduction of the central ion in complex compound by ligand, i.e. reaction of the electron transport from an ion to ligand or vice versa [25].

The external spherical reaction is a reaction of the electron transport between pair of particles, each of which can exist separately. During the external spherical reaction each of particles remains chemically individual and has own solvate or ligand environment.

Experimental investigation of those two types of reactions has led to following conclusions:

1. Even the exoergic reactions of the electron transport are activation, i.e. even if free energy of reaction is less than zero $\Delta G_{if} < 0$, activation energy is more than zero $E_a > 0$.

2. Rule of Polyani-Semenova [24] for activation energy is carried out

$\Delta E_a = \alpha \Delta G_{if} + \text{const.}$

In the case of an electron transport reaction: $\alpha = 1/2$.

3. Activation energy depends on permittivity (polarity) of the solvent. Activation energy increases with increasing of high-frequency permittivity ε_∞ and activation energy decreases with increasing of low-frequency permittivity ε_0.

It was found out that activation energy increases with decreasing of ion radius. Intuitively dependence should be opposite. Thus the main goal of the theory of the electron transport is to explain the nature of the energy barrier of the reaction. For this purpose Marcus model has been created [23].

1.2.4.3. Marcus model

Marcus model explains the experimental facts described above by means of following postulates [23]:

1. The nearest coordination sphere of reacting particles is not changed during process of electron transport. Therefore the internal nuclear coordinates of reacting particles are not considered at all, their change is negligibly small.

2. Balance between initial products in a solution and a donor-acceptor pair is established. This assumption means that diffusion stage of reacting pair formation in a cell of solvent is excluded from consideration. Division of the reaction products, i.e.

their output from a cell of solvent occurs fast. Thus only the kinetic regime of the reaction is considered.

3. The source of activation energy is the orientation polarization of environment (environment is molecules of solvent). The linear response of environment is supposed, i.e. a degree of the orientation polarization of environment in each point is proportional to intensity of electric field in this point (~εE).

According to these postulates the dipole molecules, situated around charge or dipole particles, are oriented. Each of molecules can be characterized by the angular dependence of energy. The angle describes orientation of molecule. In the case of linear polarization the angular dependence of energy is parabolic. It means that molecule of environment are in harmonic potential. The initial donor-acceptor pair is in equilibrium polarize environment. It is shown schematically in Figure 1.12.

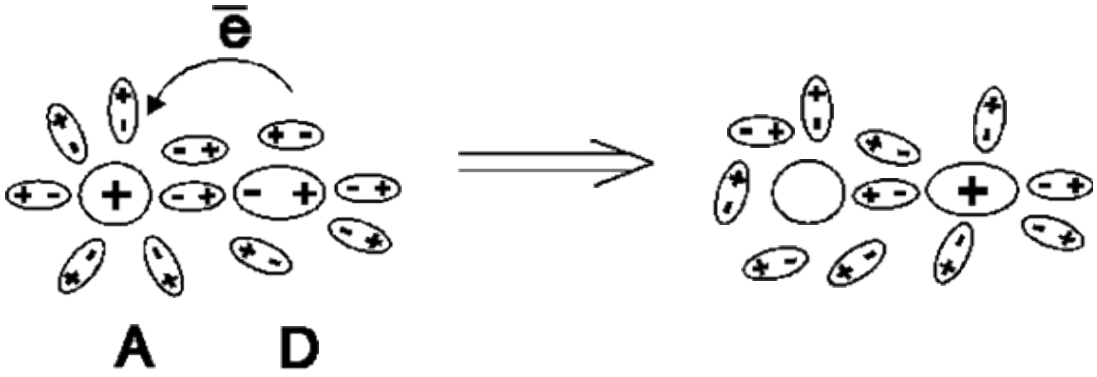

Figure.1.12. Reaction of electron transport.

Another equilibrium orientation polarize environment corresponds to products of reaction, i.e. to the same pair, but with transferred electron. The main idea of the model is the following. Set of molecules of environment near to the reacting pair particles is in continuous casual movement. To move the electron it is necessary to have polarization of the environment, corresponding to initial condition, broken in a random way and has moved to direction of the polarization, corresponding to products of reaction.

1.2.4.4. Spin and magnetic effects in chemistry

Previously it was supposed that reaction is spin-resolved. In reality, however, this condition is not always true. Consider reactions during which spin coordinates influence on the process of reaction. The spin state of molecular systems can be exactly described by the quantum mechanics.

1.2.4.4.1. Spin of microscopic particle

Spin *S* is intrinsic angular momentum. Spin of microscopic particle is described by spin quantum number *s*. The magnitude of angular momentum, *S*, can take only values according to the relation

$$|S| = \hbar[s(s+1)]^{1/2}.$$

The spin of elementary particles, such as protons, neutrons, atomic nuclei, and atoms have spin quantum number s =1/2. Nucleus and other microscopic particles, which consist of several particles, are characterized by integer or half-integer spin quantum number 0, 1/2, 1, 3/2 etc. Charged micropaticles (electron, proton and etc.) have the magnetic moment

$$\mu = -g\,\mu_\beta[s(s+1)]^{1/2},$$

where *g* is the gyromagnetic ratio and $\mu_\beta = \frac{e\hbar}{2m}$ is Bohr magneton. Thus, electrons, nucleus, atoms and molecules having nonzero spin are microscopic magnets.

Projection of spin S_z to any chosen axis z in space is quantized. This means, that exist *2s+1* possible values of S_z and $S_Z = \hbar m_s$ where m_s takes on the values from - s to s. Projection of the magnetic moment μ_z to any chosen axis *z* in space is also quantized and $\mu z = -g\,\mu_\beta m_s$.

Quantum states with different values of projections of spin and magnetic moment on the axis *z* are degenerate (i.e. their energy is equal). The presence of a magnetic field

breaks the degeneracy due to interaction between magnetic field of micropaticles and external field (The Zeeman effect).

Consider behavior of particle with spin quantum number s = 1/2 in external magnetic field H.

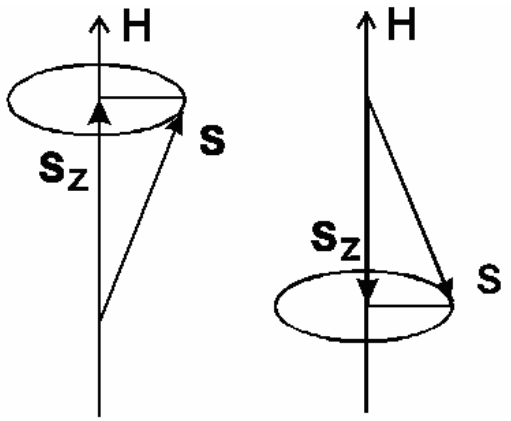

Figure 1.13 Particle with spin s = ½ in the external magnetic field.

Figure 1.13 shows that in the present of external magnetic field the particle can have two zeeman states. In each of these states external magnetic field interacting with the intrinsic magnetic moment of the particle induces force acting on the spin. As a result of this spin precesses around the direction of the external magnetic field. In one state a projection of the spin is directed to the direction of the external field, in the other state to the opposite direction. Energy different of these states is $\Delta E = g\,\mu_\beta H$.

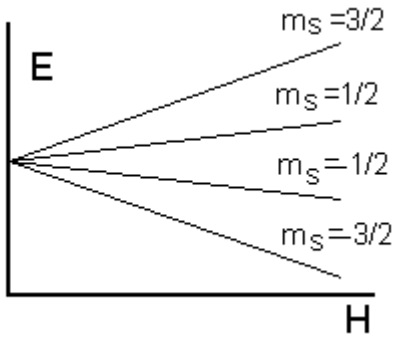

Figure 1.14. Splitting of energy levels of a particle with s=3/2 in external magnetic field.

If the spin is more than 1/2, then there are more than two possible states. For example in the case of a particle with spin s=3/2 the dependence of energy on strength of magnetic field is shown in Figure 1.14.

Thus the splitting of energy levels of a particle in the external magnetic field allows to determine the spin quantum number of the system. In the next consideration absolute values of spin and magnetic moment of microparticle is not interesting for us. Therefore the term "spin" will be used as the term "spin quantum number".

If the energy levels of the particles do not split in the present of magnetic field, then the particles have zero spin. It is named the singlet state and the particles are in the singlet state. If spin is equal to ½, it is doublet state. If spin of system is unity the state is named triplet and etc.

1.2.4.4.2. Dissociation and recombination reactions

Consider dissociation reaction of a molecule. During dissociation of a diatomic molecule it is possible to expect formation of two noncharged atoms (solid line) or two ions, cation and anion (dashed line), fig. 1.15.

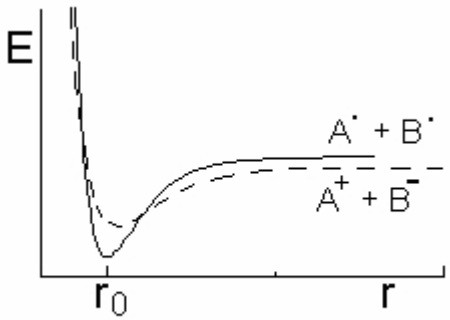

Figure1.15 Potential energy of dissociation reaction.

If the potential energy of two separated ions is less than the potential energy of two separated atoms then there is the heterolytic reaction. In the opposite case there is the homolytical bond breakage.

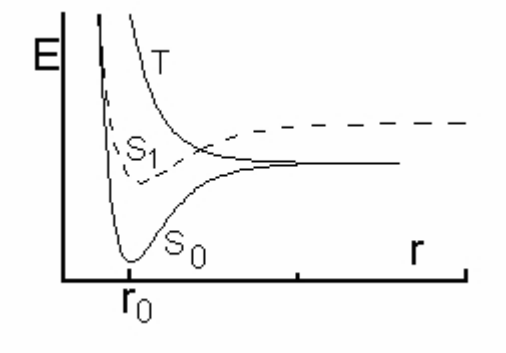

Figure 1.16 Diagram of dissociation process of diatom molecule.

The heterolytic dissociation is not interesting for spin dynamic because there is a transport of two electrons and total spin of this system is equal zero. In the case of homolytical dissociation there is a separation of electron pair which made chemical bond and formation of two atoms or radicals. This process is shown in Figure 1.16. The term S_0 corresponds to the pair of electrons which are situated on the one molecular orbit. These electrons have antiparallel spin orientation and total spin is equal zero, this is a singlet state. The term T is dissociation term. Here electrons have parallel spin orientation and total spin is equal unit, this is a triplet state. According to the Pauli Exclusion Principle these electrons are situated on the different molecular orbits. Therefore the triplet state is an excited state.

There exist infinitely many empty molecular orbits in the molecule, and each molecule has a set of singlet and triplet exited states. Some exited states can be completely dissociated or have small activation energy. Following two mechanism of dissociation reactions can be realized:

1. Thermal dissociation from ground state.
Energy of the bond breakage is concentrated on the corresponding vibrational mode. Formed radical pair has the same singlet spin state as the broken molecule, i.e. electrons have antiparallel spin orientation.

2. Dissociation from electron-excited state.
Usually electron-excited states have high energy. Therefore thermal excitation of molecule to the electron-excited state takes place only in high temperatures. Also the

electron-excited state can be created by the nonthermal source of energy, for example, by light. The surface of potential energy of an excited state is completely different by topology from the surface of the ground state. This difference is the reason of unexpected chemical reactions. The activation energy of dissociation reaction in the excited singlet state can be sufficiently small. During this reaction radical pair in the singlet spin state is formed. In the course of transition from the singlet to the triplet state molecule can undergo the internal spin conversion. The probability of this transient depends on the energy difference of these states, overlap of wave functions and spin-orbit interaction. In some molecules this probability can be great; in the other molecules this process can be completely forbidden. Also the triplet excited states can have small activation energy. In the case of dissociation reaction from triplet state, the pair of radicals with parallel spin is formed, and there is also radical pair in the triplet state.

Thus in the course of dissociation reaction, depending on mechanism, the pair of radicals or atoms in the singlet or triplet states is formed.

Consider now reverse reaction of recombination of two radicals. If colliding radicals have antiparallel spins (the radical pair in the singlet state), then formation of the chemical bond is possible. As a rule this reaction is non-activated, i.e. activation energy is approximate to zero. The formed molecule is in the ground electron state. The reaction proceeds quickly and efficiently. If colliding radicals have parallel spins (the radical pair in the triplet state), then only formation of molecule in the excited triplet state is possible. In overwhelming majority of the cases this reaction is impossible, because triplet states have high energy and reaction probability is small.

Consider recombination reaction of radicals which were born separately in some distance from each other. These radicals enter into reaction after random collision. In this case the spin state of the radical pair is also random. The radical pair formed in the course of random collision is named the diffusion radical pair. A part of them is in the singlet state, a part is in the triplet state. Let recombination of the radical pair occurs in the present of external magnetic field.

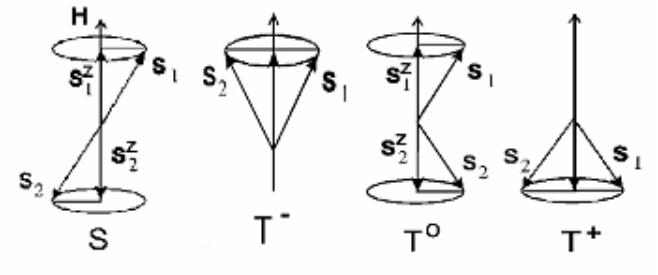

(a) (b) (c) (d)

Figure 1.17 Projections of the magnetic moment of radical pairs in the present of magnetic field.

Figures 1.17 describe possible mutual orientation of the projections of the magnetic moment of radicals, which random collides.

Figure 1.17(a) shows radicals with opposite projections of magnetic moments and the precession of radicals occurs in the antiphase. In this case both the total spin of the two radicals and the total projection of magnetic moments is equal to zero. It means that radical pair is in the singlet state and recombination is possible.

Figures 1.17 (b, c, d) show radical pairs with total spin equal to unit. Figure 1.17 (c) shows radicals with the opposite directed projections of magnetic moments. The total projection of magnetic moments is zero, but the precession of radicals is in-phase. Thereby total spin is equal to unit. In Figure 1.17 (b) projections of magnetic moment of both radicals are directed along the external magnetic field, in figure 1.17 (d) projections of magnetic moment have opposite direction. Therefore there are four possible spin states of the pair after random collision of two radical: one singlet state *S* ($s = 0$, $m_s = 0$) and tree triplet states *T*+, *T*o, *T*- ($s = 1$, $m_s = -1, 0, 1$). Consequently only a quarter of the collisions can be finished by the reaction of recombination and three-quarters of the collisions are finished by other reactions for example by reactions with solvent or radical trap, reaction of isomerization or dissociation of radical and etc.

Reactions are restricted by spin not only in the case of radical pair, but also in the case of molecules with spin more than ½.

Spin states of the particles substantially determine the reaction process and the composition of reaction products. This consideration is not full because spin state of reacting particles can change. This possibility is considered in the next chapter.

1.2.4.4.3. Molecular and spin dynamics of radical pair

The change of the spin state of molecules and atoms are characterize by relaxation times T_1 (time of the longitudinal relaxation or spin-lattice relaxation) and T_2 (time of the transverse relaxation or spin-spin relaxation) [26].

We illustrate these characteristics as follows. Let there be a set of particles with spin ½ in the sample. Two possible states of each particle are shown in figure 1.13. In the presence of an external magnetic field the energy of these states is different. The spin occupies these two states according to the Maxwell-Boltzmann distribution. Thus the difference between equilibrium Maxwell-Boltzmann populations of two states characterizes the equilibrium magnetization of the sample caused by an external magnetic field. If a part of spin states is changed by means of external influence then the magnetization of the sample is also changed. For example, if spins with the projection of the magnetic moment directed along the external field changes the projection of the magnetic moment to the opposite direction, then the equilibrium is broken. The broken distribution starts the process of relaxation to the equilibrium state. Such relaxation is called longitudinal, because it makes equilibrium along external magnetic field. This process is occurred by means of the spin flip. Excess energy is transmitted to the molecules of environment surrounding spin.

Now let all set of spins (such as in fig. 1.13) precesses in-phase. It means that the equilibrium is broken and the sample has the macroscopical oscillating transverse magnetization. During the relaxation to the balance the spins of the set should obtain various phases of precession so that the total transverse magnetization becomes equal to zero. This is the process of transverse (spin-spin) relaxation. Times of magnetic relaxation T_1 and T_2 are in the range of 10^{-5} - 10^{-8} sec.

So-called cell effect increases the times of magnetic relaxation. The colliding pair of molecules of reagents is situated in the cell of molecules of solvent. This cell can keep the pair together for a significant time. Thus, the radical pair has time for spin evolution in liquid solvent, i.e. for transition from one spin state to another.

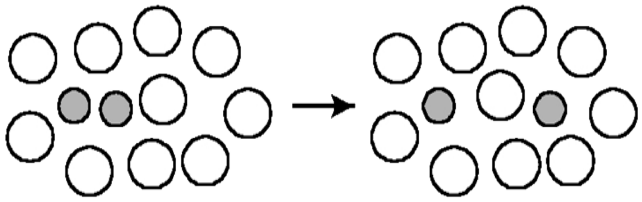

Figure 1.18 Cell effect.

1.2.4.4.4. Rate of spin evolution of radical pair

Consider a triplet radical pair. It can be in one of the three spin states: T^-, T^o or T^+. For transition from T^- or T^+ states to singlet state it is needed to change the direction of the magnetic moment projection of one of radicals to the opposite direction. This process is analogous to process of spin-lattice relaxation. For transient from T^0 state to singlet state it is needed to change the precession of spin from in-phase to antiphase. This process is analogous to process of spin-spin relaxation.

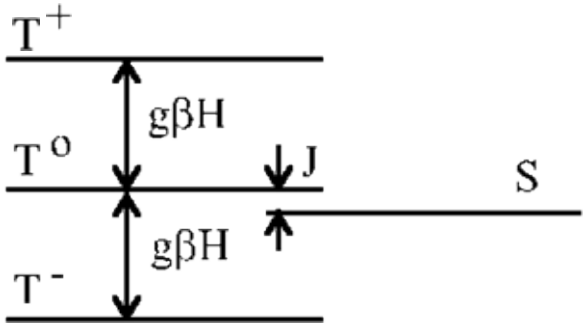

Figure 1.19. Energy levels in the presence of strong magnetic field.

To determine the rate of triplet-singlet evolution it is necessary to consider probability of all transitions: $T^- \rightarrow S$, $T^o \rightarrow S$ and $T^+ \rightarrow S$. The greatest contribution is given by the transient with smallest difference of energy. In the presence of external magnetic field

the energy of T^- and T^+ states is proportional to the field strength, but energy of S and T^0 does not depend on magnetic field. Energy levels in the presence of strong magnetic field are shown in Figure 1.19.

Thus the greatest contribution to the process of triplet-singlet evolution is given by transient from the T^0 state. Difference of energy between T^0 and S states is quantity of energy of the exchange interaction J.

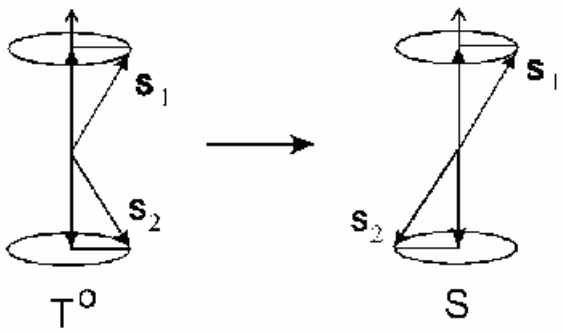

Figure 1.20. Transient $T^0 \rightarrow S$.

To realized the transient $T^0 \rightarrow S$ the difference of phases between precessing spins have to reach value π. Such difference of phases can be accumulated only if two spins precess with different frequencies. The precession frequency of each spin corresponds to frequency of respective EPR transient:

$$\begin{aligned} \omega_1 &= \hbar^{-1} g_1 \mu_\beta H \\ \omega_2 &= \hbar^{-1} g_2 \mu_\beta H \end{aligned} \qquad (1.43)$$

where ω_1 and ω_2 are frequencies of spins, g_1 and g_2 are g-factors of radicals.

Then time of triplet-singlet evolution is

$$\tau_{TS} = \frac{\pi}{\omega_1 - \omega_2} = \frac{\hbar\pi}{(g_1 - g_2)\mu_\beta H}. \qquad (1.44)$$

Thus the rate of triplet transient is proportional to the difference of g-factors of radicals. Such mechanism of spin evolution is called Δg-mechanism. The rate of spin evolution also depends on the strength of magnetic field. To take into account the

possibility of spin conversion of all tree states the dependence (1.44) become more complicated.

However, even without deep consideration of this dependence it is possible to note that the magnetic field is able to change the process of chemical reactions which are determined by the spin state of the reagents. This qualitative consideration explains how magnetic interaction with energy is much less than thermal energy and, especially, less than energy of chemical bonds nevertheless is able to influence on the chemical reactions.

In addition to Δg-mechanism there is another mechanism leading to change of the rate of the spin precession. This is the mechanism of the superfine interaction (SFI-mechanism). This mechanism is important if radicals have magnetic nucleuses. The magnetic nucleus create additional magnetic field on the unpaired electron. Energy of electron spin and the frequency of precession are changed by means of this additional field. For example let one of radical have a proton. The proton is a magnetic nucleus with spin 1/2. On the ordinary temperature half of radicals has the projection of magnetic moment of the nucleus directed along magnetic field, another half has opposite direction. The frequencies of precession of these radicals are

$$\begin{aligned} \omega_1 &= \hbar^{-1}(g_1\mu_\beta H + \frac{1}{2}a) \\ \omega_2 &= \hbar^{-1}(g_2\mu_\beta H - \frac{1}{2}a) \end{aligned}, \qquad (1.45)$$

where a is energy of superfine interaction.

The difference of frequencies which leads to spin conversion is:

$$\omega_1 - \omega_2 = \hbar^{-1}(g_1\mu_\beta H - g_2\mu_\beta H \pm \frac{1}{2}a) = \hbar^{-1}(\Delta g\mu_\beta H \pm \frac{1}{2}a). \qquad (1.46)$$

Thus the rate of spin conversion of such radicals is simultaneously determined by the Δg- and SFI- mechanisms. The rate of spin conversion depends on the direction of nuclear spin in magnetic field (signs '+' and '-' in formula (1.46)).

Formula (1.46) describes two very important chemical effects which are the magneto-isotopic effect and the effect of spin polarization of nucleuses.

1.2.4.4.5. Second generation of magnetic effects.

Previously the reasons of magnetic effect (influence of magnetic field on the chemical reaction) were described. In this process the spin evolution occurs spontaneously by means of nature terms of the system. But it is possible to create the controllable influence on the spin evolution by means of microwave electromagnetic radiation.

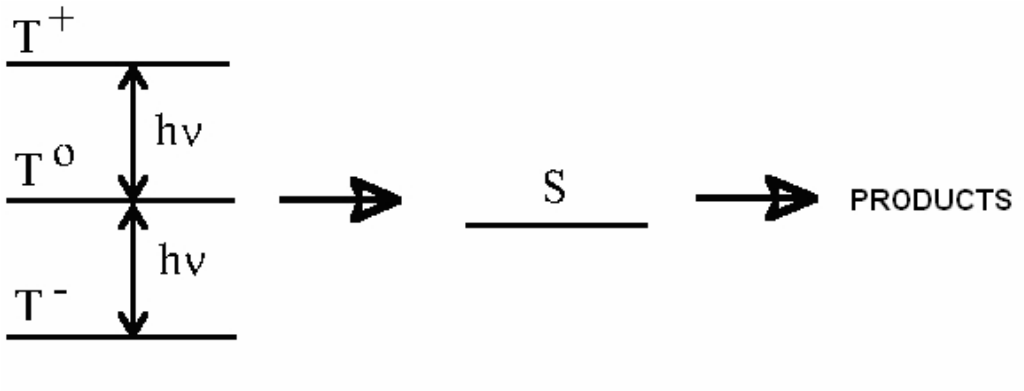

Figure 1.21. Transients $T^{+} \rightarrow T^{o}$ and $T^{-} \rightarrow T^{o}$.

Consider the triplet radical pair in magnetic field. Due to the smallest energy difference the fastest conversion is $T^{o} \rightarrow S$. But microwave radiation leads to transition: $T^{+} \rightarrow T^{o}$ and $T^{-} \rightarrow T^{o}$. Thereby if the radiation has enough intensity and the resonance condition holds then all triplet molecules have the same probability of the transition to the singlet state, fig. 1.21.

Thus the second generation of magnetic effect is the phenomena connected with influence of the microwave radiation on the chemical reaction.

2. EXPERIMENTAL TECHNIQUE

2.1. Synthesis of niobium oxide and calculation of kinetic characteristic

Niobium oxide was obtained by electrochemical method. This method has standard equipment scheme, Fig. 2.1. Where 8 is a container with electrolyte: 6 are cathodes and 7 is niobium anode. Stabilized current source B7-50 provides DC current. The current was measured by amperemeter Ц300 connected in series. The voltage was measured by voltmeter Ц300. The capacity was measured by capacity measuring instrument E7-15, after the electrolyte container was turned off from the current source.

The oxide was formed in phosphor acid solution $0.01NH_3PO_4$. Forming voltage was 122.5 V (U_f), and the current j = 1 mA/cm^2. Time dependence of voltage and current were fixed during films growth.

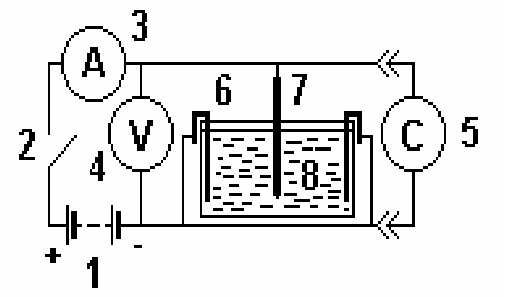

Figure 2.1. Equipment scheme. 1 is current source B7-50; 2 is key; 3 is amperemeter Ц300; 4 is voltmeter Ц300; 5 is capacity measuring instrument E7-15; 6 are electrodes; 7 is niobium anode; 8 is container with electrolyte.

Influence of DC and AC magnetic field on kinetic characteristics of oxidation processes and also on oxide properties was investigated. For this purpose magnetic and electric fields were applied in the sample at the same time during a process of oxide growing. AC magnetic field was applied by means of inductance coil and AC source.

To form niobium oxide different magnetic fields were used:

1. DC magnetic fields: B = 0.11 T, B = 0.23 T, B = 0.42 T and B = 0.6 T.
2. AC magnetic fields: B = 0.1 T, B = 0.19 T, B = 0.29 T, B = 0.38 T and B = 0.49 T.

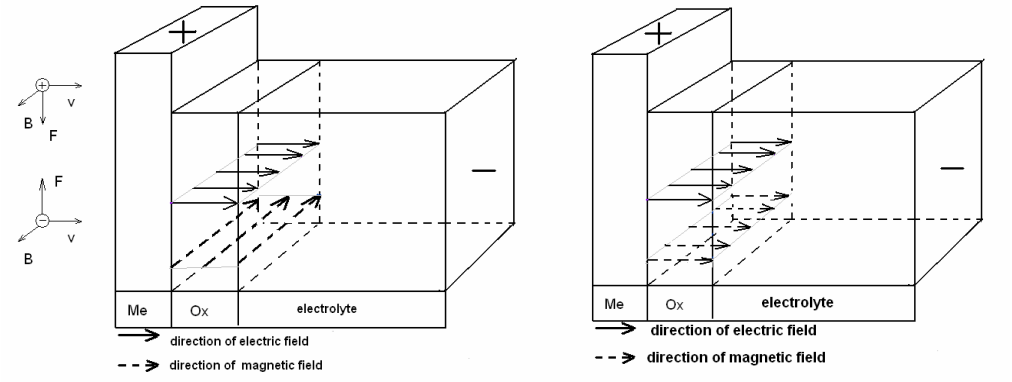

(a) (b)

Figure 2.2. Relative orientation of electric and magnetic fields in the sample: a) parallel fields, b) perpendicular; solid arrows show direction of electric field, dashed arrows show direction of magnetic field, “Me” is niobium and “Ox” is niobium oxide.

In addition, magnetic and electric fields had different configuration: parallel and perpendicular (fig. 2.2). It was realized by different sample orientation in the box with electrolyte (fig. 2.3).

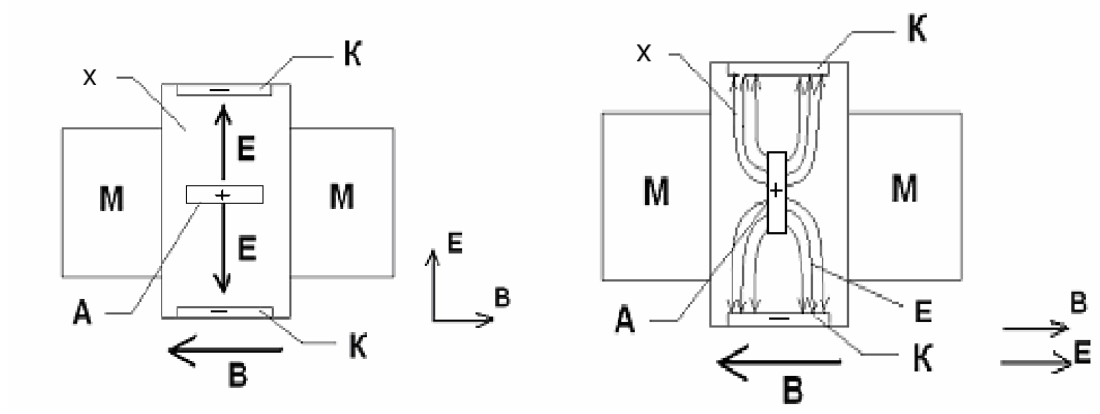

a b

Figure 2.3. Scheme of sample orientation in the box with electrolyte, which provide different configuration fields: a) parallel fields, b) perpendicular fields. X is box with electrolyte; K are cathodes (stainless steel); A is anode (niobium); M are dc or ac magnets; B and E are magnetic and electric fields directions.

When the oxide is formed by DC voltage, the voltage increase by dU results to thickness increase by dx [3]. According to Faraday's law [22], the oxide growth velocity is

$$\frac{dx}{dt} = \lambda \frac{M}{nz\rho F} j, \tag{2.1}$$

where M is the oxide molecular weight, ρ is oxide density, nz is the reaction valency, F is Faraday's constant, λ is the efficiency of the reaction and j is the current density.

The velocity of the voltage change across the oxide is

$$\frac{dU}{dt} = \frac{dU}{dx}\frac{dx}{dt} = E\frac{dx}{dt}. \tag{2.2}$$

Using (2.1) and (2.2), a connection between the velocity of the voltage change and the current can be established:

$$\frac{dU}{dt} = \lambda \frac{M}{nz\rho F} Ej \ . \tag{2.3}$$

The voltage U and the time t are obtained from the experiment, the other constants are known, and therefore the electric field strength E can be calculated.

Actually, during oxidation of such metals as niobium and tantalum the dependence $U(t)$ stays linear up to break down voltage. With further voltage increase the efficiency of the reaction λ becomes smaller than 100% due to the side reaction of oxygen discharge.

Constancy of dU/dt shows that chemical compound of the formed oxide does not change during synthesis process. If $U(t)$ is nonlinear, it means that either molar volume M/ρ or field E_{diff} changes or side reactions exist and efficiency of reaction λ decreases. Dependence $U(t)$ is a very informative characteristic [5].

Metal-oxide-electrolyte system can be considered as a plane capacitor. Then

$$d\frac{1}{C_{sp}} = \frac{1}{\varepsilon_0 \varepsilon E} \ , \tag{2.4}$$

where C_{sp} is a capacity of oxide layer of unit surface and ε is oxide dielectric permittivity. Therefore, if the thickness of the oxide is known E can be calculated as $E = \frac{dU}{dx}$ and giving permittivity ε can be calculated from equations (2.3) and (2.4).

2.2. Investigation of the samples by optical methods

Optical measurements give opportunity to determinate the thickness of obtained oxide films and the forming coefficient. The forming coefficient is the ratio of oxide thickness to forming voltage. Measurements were made by two methods, ellipsometric method and spectrophotometric analysis.

2.2.1. Ellipsometric method of film thickness determination

This is a measurement of interface between two different materials. The basic characteristics are ellipsometric polarization parameters of reflected light.

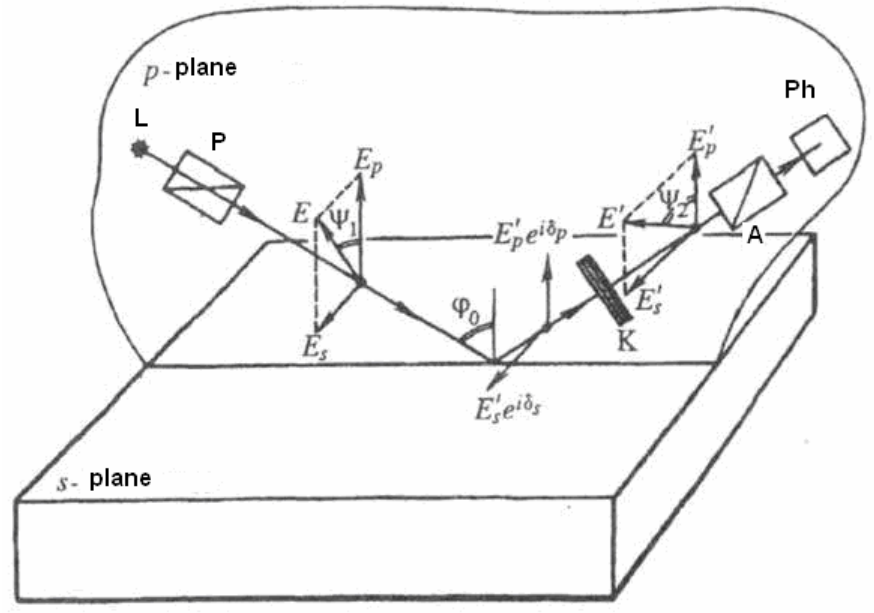

Figure 2.4 Operation ellipsometer scheme. L is light source, P is polarizer, A is analyzer, Ph is photodetector.

Monochromatic plane-polarized light becomes elliptically polarized after interaction with the material and reflection from it. It happens because electromagnetic

oscillations in different planes change the electromagnetic field amplitude E and initial phase of oscillation δ by different ways (fig. 2.4). There are a incidence plane (*p*-oscillations) and a perpendicular plane (*s*-oscillations). Complex amplitudes for *p*- and *s*-oscillations of incident wave ($\vec{E}_p = E_p e^{i\delta}, \vec{E}_s = E_s e^{i\delta}$) and reflected wave ($\vec{E}'_p = E'_p e^{i\delta}$, $\vec{E}'_s = E'_s e^{i\delta}$) are characterized by parameters *E* and δ. Amplitude ratios $\vec{R}_p = \vec{E}_p / \vec{E}_p$ and $\vec{R}_s = \vec{E}_s / \vec{E}_s$ are called complex reflection coefficients and can be calculated using reflection boundary model [28].

The main equation of ellipsometry is:

$$\frac{\vec{R}_p}{\vec{R}_s} = \frac{E'_p E_s}{E'_s E_p} e^{i(\delta_p - \delta_s)} = \frac{tg\psi_2}{tg\psi_1} e^{i\Delta} = tg\psi e^{i\Delta}$$

where ψ and Δ are ellipsometric angles, which can be measured by an ellipsometer.

Experimental results were calculated with help of program Mathcad 2001 Professional. Input information was:

1. ψ, Δ are ellipsometric angles.
2. Tabular data n_3, k_3 are real and imaginary refractive indexes of substrate, in our case substrate is niobium, $n_3 = 2.82$, $k_3 = 2.86$.

The refraction index and thickness of the oxide were calculated by the program.

2.2.2 Spectrophotometric analysis of film oxide

2.2.2.1 Operation principle of Spectrophotometer

The measurements were done on two spectrophotometers: SF-46, which is manual controlled model and SF-56, which is an automatic.

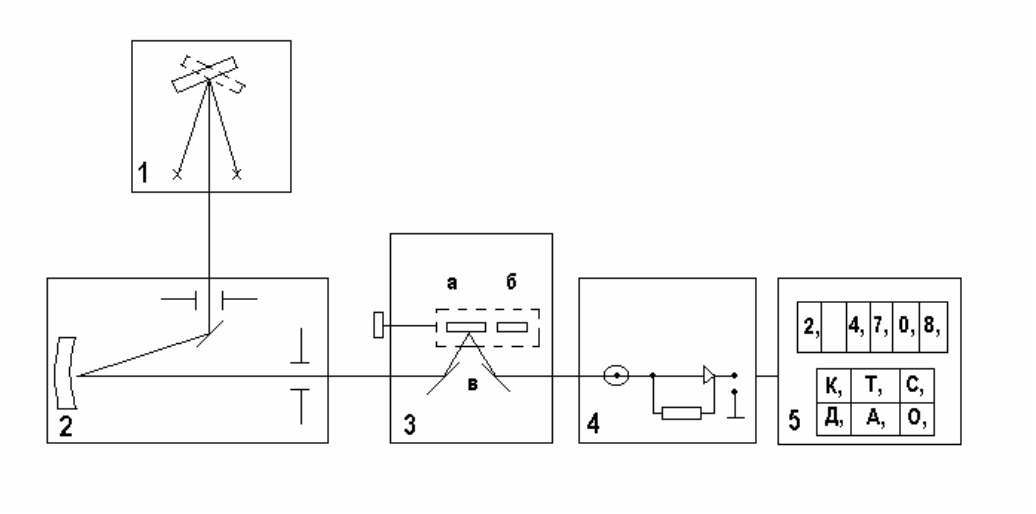

Figure2.5. Structure scheme of spectrophotometer SF-46. 1 is a light source, 2 is a monochromator, 3 is cuvette's bow with the reference sample and the observable sample, 4 is amplifier, 5 is microprocessor system.

The basic working principle of the spectrophotometer is a measurement and comparison of two light intensities. The first is the light from the observable sample and the second is the light from the control sample. Scheme of the spectrophotometer is shown in figure 2.5.

The light beam goes from illuminator to the monochromator through entrance slit and then it is decomposed by diffraction grating into spectrum. The reference sample and the observable sample are put one after another into monochromatic light beam. Observable film was opaque. Therefore the structure scheme of spectrophotometer SF-46 was changed. A block with two mirrors was added. The light goes from the sample to the photo element cathode in the receiver-amplifier block. Resistor R is included in anodic circuit of photo element. Electrical current goes through resistor and gives voltage drop on the resistor. This voltage drop is proportional to the light, which falls into photo cathode.

DC amplifier with amplification coefficient near 1 provides signal transmission into output microprocessor system (MPS). MPS measures voltages $U_т$, U_0 and U, which are proportional to dark current of photo element, flux through control sample, and flux through observance sample, respectively.

After the measurement, MPS calculates reflection coefficient R of observance sample by the formula

$R = [(U\text{-}U_T)/(U_0\text{-}U_T)]*100.$

The result is shown on the digital panel.

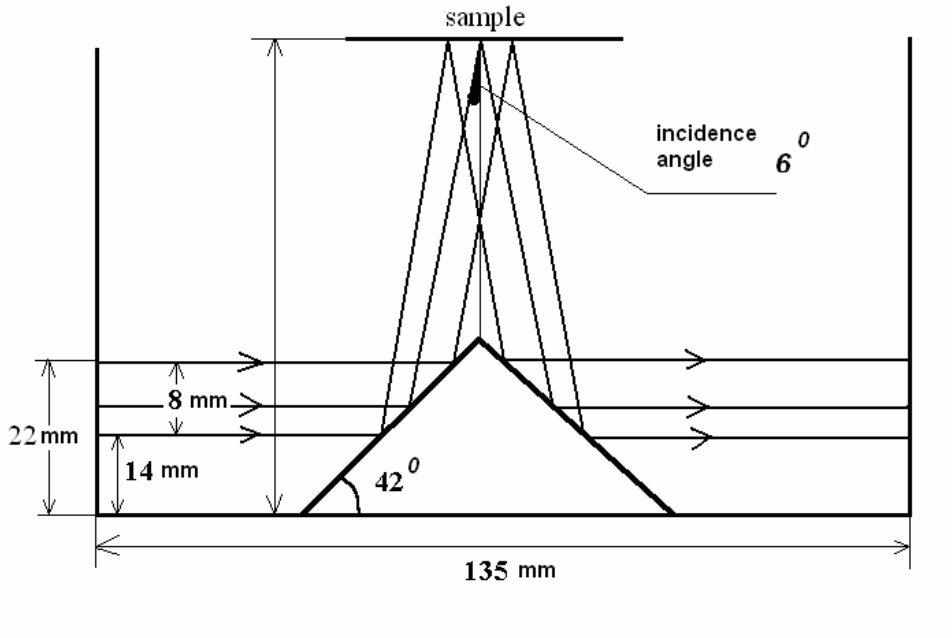

Figure 2.6. Additional block to spectrophotometer SF-46.

Additional block was used for obtaining a reflection coefficient $R(\lambda)$, Fig. 2.6.

Spectrophotometer SF-56 is automated and measuring data is sent to the computer.

2.2.2.2. Calculation of films thickness from reflection coefficient spectrum R(λ) using the first method

Optical interference in thin films and reflection coefficient $R(\lambda)$ are the basis of this method. The oxide film thickness is calculated from the maximum and minimum on the reflection coefficient spectrum $R(\lambda)$.

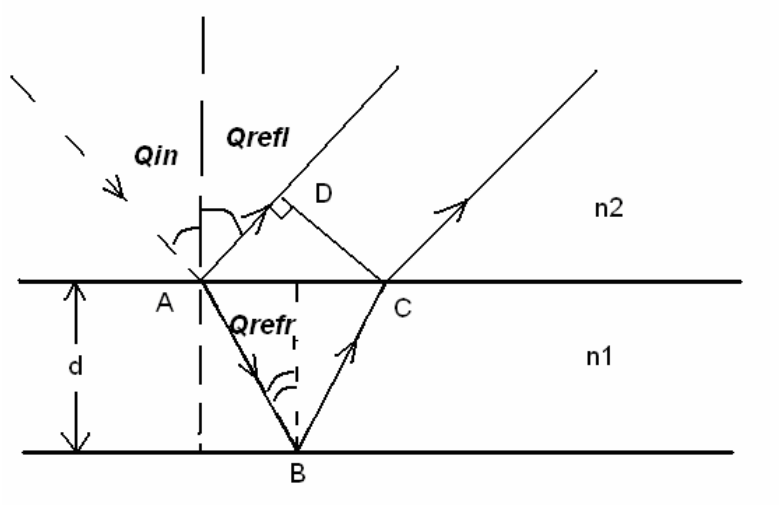

Figure 2.7. The ray path in thin film. Here d is the thickness of oxide film, n_1 and n_2 are refractive indexes of oxide and environment respectively, Q_{in} is incoming angle of incident and Q_{refl} is an angle of reflection and Q_{refr} is an angle of refraction.

The plane-parallel plate with thickness d is shown in Fig. 2.7. Monochromatic plane wave falls on the plate in angle Q_{in}. Refractive indexes of the environment n_2 and the film n_1 are known and $n_1 > n_2$.

Incoming wave is partly reflected and partly refracted on the upper surface of the film. Refracted wave is reflected from the lower surface. It is also reflected on the upper film surface. These two waves are coherent. The interference result depends on the optical path difference Δ. In turn, the optical path difference depends on the film thickness d. Therefore, the film thickness can be calculated from positions of interference maximum and minimum. Using the equations and formulas

$$\Delta = (|AB| + |BC|)*n_1 - |AD|*n_2 \quad (2.5)$$

$$\frac{\sin Q_{in}}{\sin Q_{refr}} = \frac{n_1}{n_2} \rightarrow \sin Q_{refr} = \frac{n_1}{n_2} \sin Q_{in}. \quad (2.6)$$

In our case $Q_{in} = 6^0$. Q_{refr} is calculated from (2.6).

Usually n is constant and product nd can be obtained from positions of the interferential maximums and minimums. λ_m and λ_{m-1} are wavelengths of neighbouring extremums.

$$2nd = m\lambda_m = (m - 1)\,\lambda_{m-1} \quad (2.7)$$

$$\frac{m}{m-1} = \frac{\lambda_{m-1}}{\lambda_m} \rightarrow m\lambda_m = m\lambda_{m-1} - \lambda_{m-1} \tag{2.8}$$

$$m = -\frac{\lambda_{m-1}}{\lambda_m - \lambda_{m-1}} \tag{2.9}$$

$$2nd = \frac{\lambda_{m-1}}{\lambda_{m-1} - \lambda_m \lambda_m} \tag{2.10}$$

$$2nd = \frac{\lambda_{m+1}}{\lambda_{m+1} - \lambda_m \lambda_m} \ . \tag{2.11}$$

Taking into account the angle of refraction the maximum condition is

$m\lambda = 2ndcos\ Q_{in}$. (2.12)

The equation for reflection minimum is

$$\frac{2\pi}{\lambda} dn_{ox} \cos Q_{refr} + \frac{\Delta}{2} = \frac{2m+1}{2}\pi \ . \tag{2.13}$$

The equation for reflection maximum is:

$$\frac{2\pi}{\lambda} dn_{ox} \cos Q_{refr} + \frac{\Delta}{2} = m\pi \ , \tag{2.14}$$

where m is interference order, d is film thickness, n_{ox} is oxide film reflective index.

Because reflective index of film is more than refractive index of environment ($n_1 > n_2$), maximums and minimums conditions of interferential reflection can be written in next forms:

Maximum condition: $d\cos Q_{\text{refl}} = ((2\text{m-}1)(\lambda_{\max}/2\ n_{\text{ox}})$

Minimum condition: $d\cos Q_{\text{refl}} = (\text{m}\lambda_{\min}/2\ n_{\text{ox}})$

The interference order m is obtained from these two previous formulas. The final equation for thickness is:

$d = (\lambda_{\min}*\lambda_{\max})/(4(\lambda_{\min} - \lambda_{\max})\ n_{\text{ox}} \cos Q_{\text{refl}},$ (2.15)

where n_{ox} is oxide film reflective index, λ_{min} is interferential minimum wavelength, λ_{max} is interferential maximum wavelength, Q_{refl} is refraction angel of oxide and d is the oxide film thickness.

Obtained thickness gives opportunity to estimate a forming coefficient of oxide film by formula:

$\alpha = d_{ox}/U_f$,

where U_f is forming voltage and d_{ox} is thickness of the oxide film.

2.2.2.3. Calculation of film thickness from spectrum of reflection coefficient R(λ) by the second method

This method is based on estimation of dispersion of reflection and absorption indexes from optical transmission spectrum [29, 30, 31]. The iterative method of thickness determination is represented in these works. We used this method for our case of reflection.

If the loss is small ($k^2 << n^2$), next formula describes the reflection index spectrum dependence [32]

$$R(\lambda) = \frac{Qch2\alpha_1 d + Rsh2\alpha_1 d + q\cos 2\beta_1 d + r\sin 2\beta_1 d}{Sch2\alpha_2 d + Tsh2\alpha_2 d + s\cos 2\beta_1 d + t\sin 2\beta_1 d} \quad (2.16)$$

Where $\alpha_1 = 4\pi k_1/\lambda$, $\alpha_2 = 4\pi k_2/\lambda$ $\beta_1 = 4\pi n_1 d/\lambda$ and Q, R, q, r, S, T, s and t are coefficients, which are dependent on optical constant.

$$Q = (n_0^2 + n_1^2)(n_1^2 + n_2^2) - 4n_0 n_1^2 n_2 \quad (2.17)$$

$$R = 2n_1 (n_0 + n_2)(n_1^2 + n_0 n_2) \quad (2.18)$$

$$q = (n_0^2 - n_1^2)(n_1^2 - n_2^2) \quad (2.19)$$

$$r = -2k_1(n_0 - n_2)(n_0 n_2 - n_1^2) \quad (2.20)$$

$$S = (n_0^2 + n_1^2)(n_1^2 + n_2^2) + 4n_0 n_1^2 n_2 \quad (2.21)$$

$$T = 2n_1 (n_0 + n_2)(n_1^2 + n_0 n_2) \quad (2.22)$$

$$s = (n_0^2 - n_1^2)(n_1^2 - n_2^2) \quad (2.23)$$

$$t = 2k_1(n_0 + n_2)(n_0 n_2 - n_1^2) \quad (2.24)$$

Here n_0 is air reflection index, n_1 is oxide reflection index, n_2 is metal reflection index.

Mathematical model of spectrum (2.16) with coefficients (2.18 - 2.24) can be obtained from conditions $\cos 2\beta_1 d = \pm 1$ or $\sin 2\beta_1 d = 0$, giving

$$R_M = \frac{Qch2\alpha_1 d + Rsh2\alpha_1 d + q}{Sch2\alpha_2 d + Tsh2\alpha_2 d + s} \tag{2.25}$$

$$R_m = \frac{Qch2\alpha_1 d + Rsh2\alpha_1 d - q}{Sch2\alpha_2 d + Tsh2\alpha_2 d - s} \ , \tag{2.26}$$

where M and m subscripts correspond to spectrum maximum and minimum respectively. If there are no losses $k_1 = 0$, $\alpha_1 = 0$ and $sh2\alpha_1 d = 0$, $ch2\alpha_1 d = 1$, then

$$R_M = \frac{Q + q}{S + s} \tag{2.27}$$

$$R_m = \frac{Q - q}{S - s} \ . \tag{2.27}$$

Value of R_M and R_m are determined from spectrum,

$$\frac{R_m}{R_M} = \frac{2n_1^4 - 4n_1^2 n_0 n_2 + (n_0 n_2)^2}{2n_1^2 (n_2 - n_0)^2} \ . \tag{2.28}$$

This is a fourth-degree equation. Solution of this equation gives zero-order approximation of refraction index.

After that, zero-order approximation of film thickness is calculated. Equations for maximum and minimum are obtained from condition $\cos 2\beta_1 d = \pm 1$:

$$\frac{4\pi n_1}{\lambda_j^M} d_M = 2s\pi \tag{2.29}$$

$$\frac{4\pi n_1}{\lambda_j^M} d_m = (2s+1)\pi \text{ , s = 1,2,3…} \tag{2.30}$$

where d_M and d_m are film thicknesses, which are calculated from spectrum maximum and minimum respectively; s is interference order for minimum λ_j, numeration is started from long-wave spectrum part; and λ_j^M is wave length of maximum, which is situated on the right of minimum λ_j. The interference order is unknown, therefore two sequences of data are formed from formulas (2.29) and (2.30):

$$d_M = \frac{s\lambda_j^M}{2n_1} \text{ and } d_m = \frac{\lambda_j}{4n_1} + \frac{s\lambda_j}{2n_1} \tag{2.31}$$

We chose this value of s from two sequences of data, for which the amount $\left|d_M - d_m\right|$ is minimum.

In additional, formulas (2.29), (2.30) and (2.31) describe the case of transition. We have reflection. Reflection coefficient is connected with transmission coefficient by formula $R + T = 1$. Therefore maximum and minimum exchange places.

2.3. Oxide conductivity on DC signal

2.3.1 Oxide metallization

Metal-oxide-metal system was needed for next measurement. A standard vacuum plant with wolfram thermal evaporator was used. Aluminium disc electrode was placed over the evaporator and current through evaporator was regulated. Pressure inside vacuum chamber was less than 10^4 Torr.

In thermal evaporation is the bond break between atoms at evaporated surface atoms. Aluminium bound breakage energy is about $5*10^{-19}$ J, or 3 eV, and melting temperature is 660^0 C.

The material starts to evaporate when the temperature is more than 0 K. It happens because instantaneous kinetic energy of surface atoms can be randomly changed and become more than averfase thermal energy (average kinetic energy). The probability of this effect exponentially increases with temperature. Evaporation temperature is the temperature, when vapour pressure over surface is $p_s = 1.33$ Pa or 10^{-2} Torr.

The forced regime is always used to decrease harmful effect of residual gas inside operation volume.

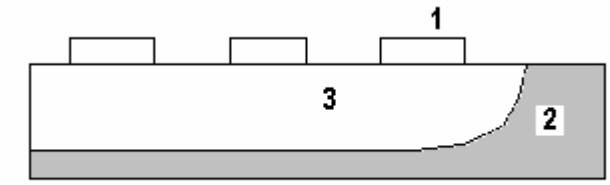

Figure 2.8. Sandwich-structure type film in section. 1 are aluminium metal contacts, 2 is niobium substrate and 3 is niobium oxide.

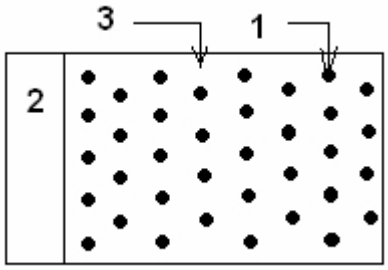

Figure 2.9. Sample plan view. 1 are aluminium metal contacts, 2 is niobium substrate and 3 is niobium oxide.

The sample with mask was put on the table at a distance of 10 cm from the evaporator. Obtained sandwich structure is shown in figures 2.8 and 2.9. Aluminium contacts have a size about 1-1.5 mm.

Determination of evaporated contact square. Microscope and length standard were used for determination of evaporated contact square. First microscope division value was estimated and then aluminium contact diameters were measured. Average diameter and contact square were calculated.

2.3.2. Conductivity measurement in strong field

Volt-ampere characteristics of samples were measured. This gives information about the type of sample conductivity. Standard equipment was used. Block scheme is shown in fig. 2.10. This equipment uses DC. DC voltage was given from a power source into Nb-Nb_2O_5-Al structure through a load box 3. One contact was connected into niobium substrate, the other into aluminium contact. The voltage was measured using universal electrometer B7-38 panel. У5-11 is an electrometric DC current amplifier. It amplifies current in the range 10^{-3}-10^{-12}A. Electrometric voltmeter B7-34A measure sample

voltage drop. Current through oxide field can be calculated as a ratio of the voltage drop to the 10^n, where n is fixed order on the amplifier У5-11.

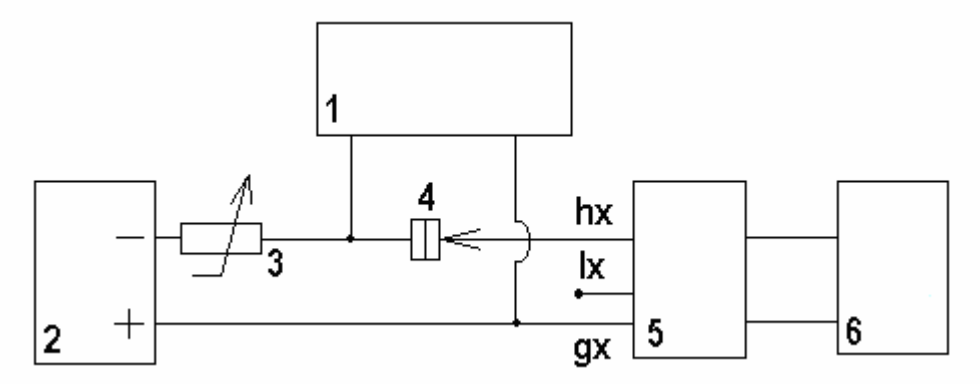

Figure 2.10. Block-scheme of conductivity measurement equipment. 1 is universal electrometer B7-38, 2 is power supply, 3 is resistance box, 4 is sample, 5 is amplifier У5-11 and 6 is electrometric voltmeter B7-34A.

Thereby, it was possible to measure niobium oxide DC volt-ampere characteristics in the range from zero to forming voltage.

2.3.3 Film oxide investigation by volt-ampere characteristic analyzes

The volt-ampere characteristic analysis is a method which determines charge transport mechanism inside oxide films. It is needed to draw volt-ampere characteristics in different coordinate for determination of electroconductivity mechanism. Different coordinates correspond to different electroconductivity mechanisms. If volt-ampere characteristic is linear in some coordinate and the experimental tangent of slope angle ($\beta = \mathrm{tg}\ \alpha$) is equal to the theoretical amount of β_{th}, then corresponding electroconductivity mechanism exist in the sample. α is slope angle of experimental volt-ampere characteristic, β is experimental value of tangent of slope angle and β_{th} is theoretically calculated value of tangent of slope angle.

Logarithmical coordinates $\ln j = \mathrm{f}(\ln U)$ correspond to space charge limited current. If tangents of slope angle is more than 2 ($\beta \geq 2$), then the space charge limited current exist in the sample. $\beta = 2$ corresponds to classical situation, when dielectric has no

traps and the Henry-Mott law [5] is held, this mechanism is called quadratic space charge limited current. β = 3-10 corresponds to transition region and in this case all traps are occupied by electrons. If β = 1, then ohm conductivity exists and Ohm law is held, this is case of weak electric field. The other two mechanisms are described by Schottky and Poll-Frenkel equations. Coordinates $\ln j = f(U^{1/2})$ correspond to Schottky mechanism and coordinates $\ln (j/U) = f(U^{1/2})$ to Poll-Frenkel mechanism. β_{Sch} is the Schottky coefficient and $\beta_{P\text{-}F}$ is the Poll-Frenkel coefficient. These two coefficients can be calculated by using the formula

$\beta_{P\text{-}F} = 2\beta_{Sch} = 2(q^3/4\pi\varepsilon\varepsilon_0 d)^{1/2}(1/kT)$,

where q is charge of electron.

2.4. Analysis of spectrum of dielectric permittivity

Experimental investigation of dielectric polarization includes measurement of real ε' and imaginary ε'' parts of complex dielectric permittivity.

LCR-meter gives an opportunity to measure tangency of loss angle tg φ and sample capacity C_p versus frequency f.

Real ε' and imaginary ε'' parts of complex dielectric permittivity can be calculated by formulas

$$\varepsilon' = \frac{C_p(\omega)}{C_0} \tag{2.32}$$

$$\varepsilon'' = \varepsilon' tg\varphi\,, \tag{2.33}$$

where C_0 is geometric sample capacity without dielectric:

$$C_0 = \frac{\varepsilon_0 S}{d}\,.$$

Here $\varepsilon_0 = 8.85*10^{-12}$ F/m, S is contact square, d is sample thickness.

Therefore, after S, d, tg φ, C_p obtaining it is possible to paint a dependences $\varepsilon'(\omega)$, $tg\varphi(\omega)$, $C_p(\omega)$. Those dependences include information about polarization character.

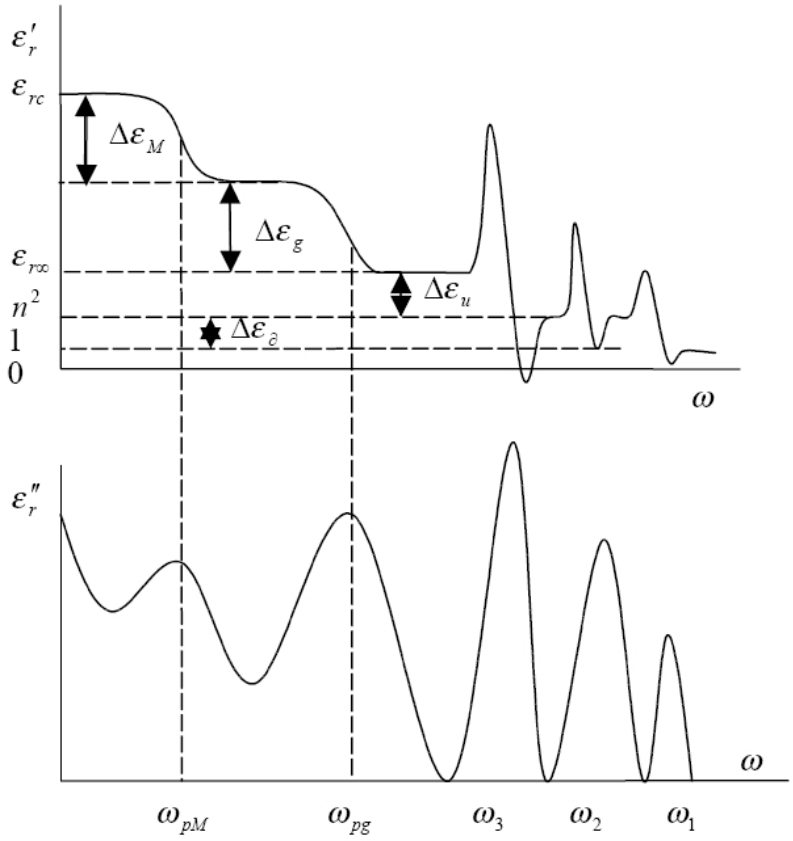

Figure 2.11. Frequency dependencies of real $\varepsilon^{/}$ and imaginary $\varepsilon^{//}$ permittivity [33], symbols are described in the text.

Consider general frequency dependence of the complex dielectric permittivity in wide range, from 0 to 10^{17} Hz. Figure (2.11) shows the frequency dependencies of real and imaginary permittivity.

In the gamma-line and X-ray frequency range (more than 10^{17} Hz), real permittivity is equal unit ($\varepsilon^{/} = 1$) and imaginary permittivity is zero ($\varepsilon^{//} = 0$). For frequency in the ultraviolet region, there is electron polarization in the solid and liquid dielectric, and it gives contribution to the real part of complex permittivity. In the range of dispersion of electron polarization (10^{14} - 10^{16} Hz), when frequency of external field is equal to natural-vibration frequency of the electron shell ω_1, then there are narrow maxima of the imaginary part of permittivity. The imaginary part of permittivity characterizes the dielectric losses. Thereby these maximum are the optical absorption spectrums. In the infrared range (10^{12} - 10^{14} Hz) more heavy particles, ions, become to shift after change of electric field, it means that ionic polarization arises and real part of permittivity

increases on amount $\Delta\varepsilon_u$. At the resonance frequencies of ions (ω_2 and ω_3) there are also maximum of resonance absorption. In the radio-frequency range (10^{13}-10^{11} Hz) for polar dielectric there is dipole polarization and $\varepsilon^{/}$ increases by the amount $\Delta\varepsilon_g$. In the range of relaxation dispersion, dipole has not time to reorient for a half-cycle of change of electric field, and relaxation losses are observed. In heterogenic dielectric at low frequency there is interlayer polarization changing $\varepsilon^{/}$ on $\Delta\varepsilon_M$, and ω_{pM} is resonance frequency of interlayer polarization. The largest real permittivity is on the lowest frequency, it is the static permittivity. The smallest permittivity is on the largest frequency, it is optical dielectric permittivity or refractive index.

In our investigation it was possible to measure spectrum of permittivity only in the range from 20 to 10^6 Hz and only this range of spectrum was analyzed. But it give information about static permittivity and losses of the formed oxide films.

3. EXPEREMENTAL RESULTS AND DISCUSSIONS

3.1 Growth kinetics of niobium oxide

The oxide film Nb_2O_5 was obtained on niobium surface foil. The sizes of samples are 1.3 × 2.5cm, 1 × 2cm. Niobium foil was preprocessed by alcohol C_2H_5OH. Electrolyte was phosphoric acid H_3PO_4 solution with concentration 0.01N.

Two oxide forming regimes were used. First was galvanostatic regime. During this regime current density was constant and voltage was increasing to the formation voltage U_f. After that voltagestatic regime starts, when voltage is constant and current density was decreasing.

Niobium oxide Nb_2O_5 has the following characteristics [34]: density $\rho = 4950$ kg/cm^3, valence of reaction $nz = 10$, molar mass $M = 266$ g/mole and forming coefficient $\lambda = 1$.

Three series of sample have been made. In this work we refer to samples obtained in series 1, 2 and 3. In names of the samples the first number refers to the series and the second number refers to the magnetic field strength, as described in the lists below.

1. First series samples: Constant magnetic field

For all samples were used the equal terms of forming: $U_f = 200$V, electrolyte was solution of H_3PO_4 with concentration 0.01N, density of current was $j = 1$ mA/cm and samples area $S = 0.0004$ m^2.

Following constant magnetic fields were applied perpendicular to electric field during synthesis of oxide: $B = 0$ T, Sample № 1-10. $B = 0.11$ T, Sample № 1-8. $B = 0.23$ T, Sample № 1-11, 1-12, $B = 0.42$ T, Sample. № 1-3.

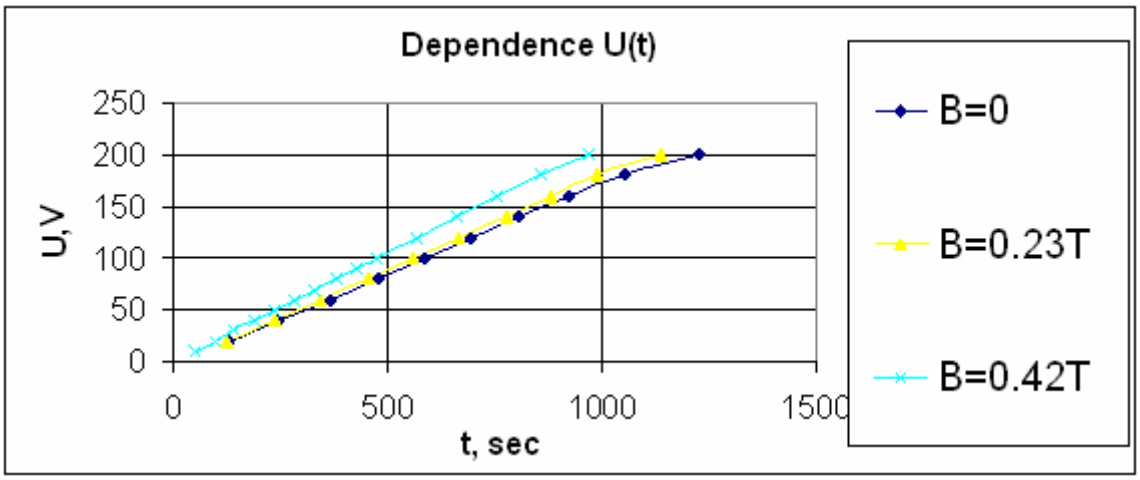

Figure 3.1 Voltage-time dependences U(t) for the samples formed in different applied magnetic fields: B = 0 T, B = 0.23 T, B = 0.42 T.

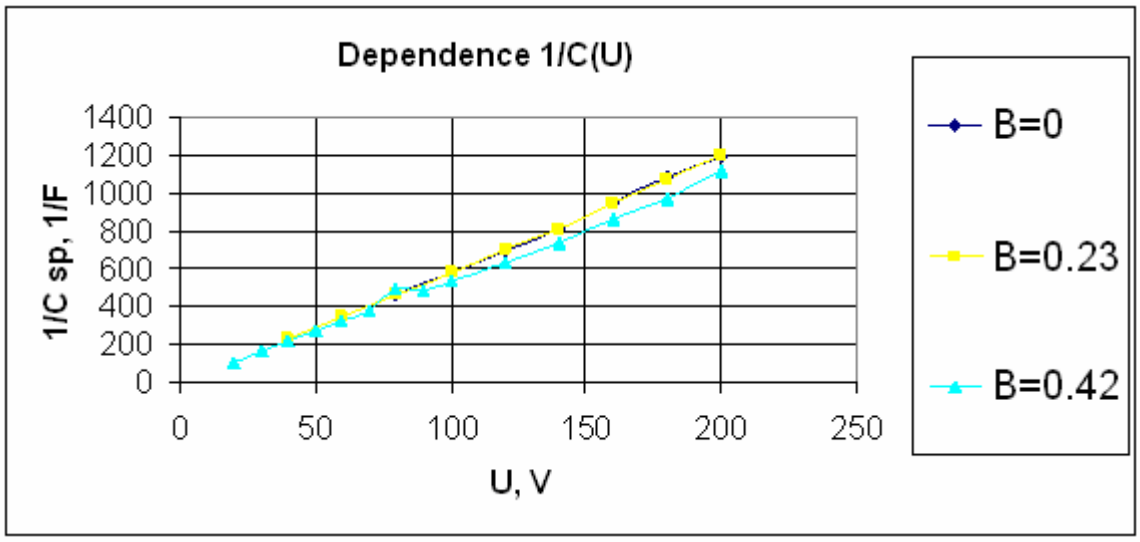

Figure 3.2 Experimental voltage dependence of the inverse capacity 1/C for the samples formed in different applied magnetic fields of B = 0 T, B = 0.23 T, B = 0.42 T.

Figure 3.1 shows experimental voltage-time dependencies $U(t)$ for the samples formed in different applied magnetic fields. Experimental voltage dependence of the inverse capacity 1/C is shown in Figure 3.2.

Table 3.1 Calculation results of the differential electric field strength E_{diff} and velocity of oxide growth *dU/dt* for the samples formed in different applied magnetic fields

	B = 0	B = 0.11	B = 0.23	B = 0.23	B = 0.42
sample №	1-10	1-8	1-11	1-12	1-3
dU/dt	0.17	0.178	0.182	0.184	0.209
d(1/C)/dU	6.1	5.94	6.05	6.05	5.39
E_{diff},V/m	3.05E+08	3.20E+08	3.27E+08	3.30E+08	3.76E+08

The differential electric field strength and the rate of oxide growth were calculated from the slope angle of the dependence *U(t)* by the method described in chapter 2.1. Results of calculation are shown in table 3.1.

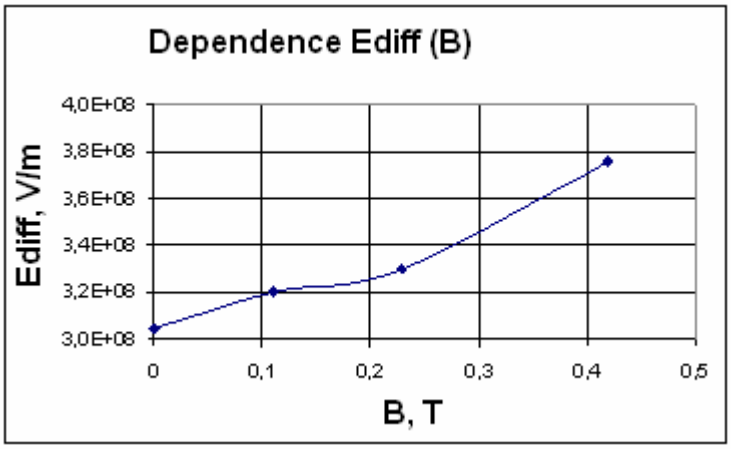

Figure 3.3. Dependence of differential electric field strength E_{diff} on magnetic field strength B applied during synthesis of the oxide.

Figure 3.3 shows dependence of differential electric field strength on magnetic field strength applied during synthesis of the oxide.

2. Second series samples: Pulsed magnetic field

For all samples were used the equal terms of forming: U_f = 160 V, electrolyte was solution of H_3PO_4 with concentration 0.01N, density of current was j = 1 mA/cm and samples area S = 0.0004 m^2.

Following constant magnetic fields were applied perpendicular to electric field during synthesis of oxide: B = 0 T, Sample № 2-5. B = 0.1 T, Sample № 2-7. B = 0.19 T, Sample. № 2-8. B = 0.29 T, Sample. № 2-9. B = 0.38 T, Sample. № 2-11.

Frequency of pulsed magnetic field was f = 50 Hz.

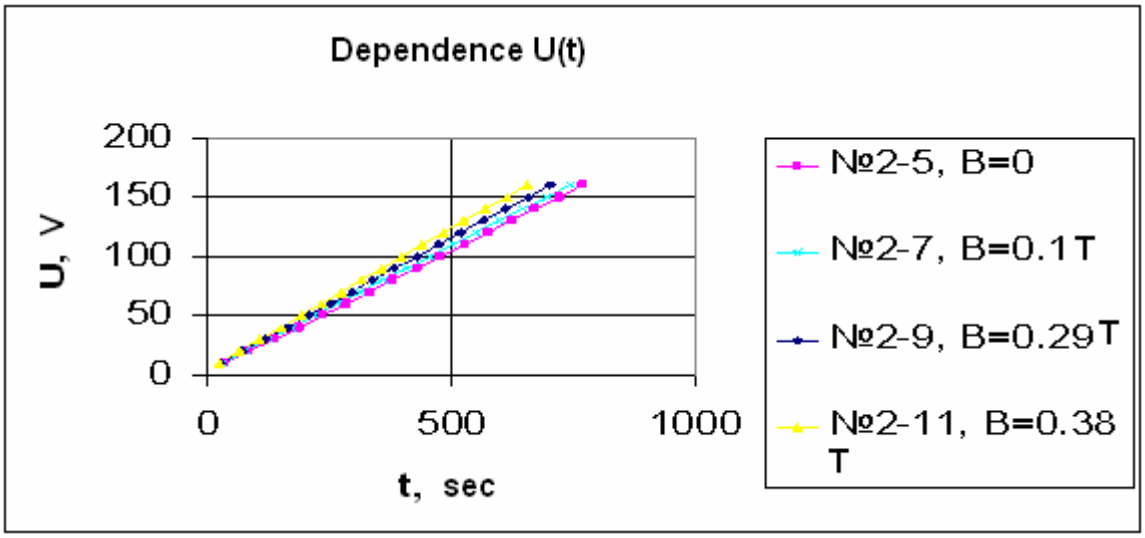

Figure 3.4 Voltage-time dependences $U(t)$ for the samples formed in different applied magnetic fields: B = 0 T, B = 0.1 T, B = 0.29 T, B = 0.38 T.

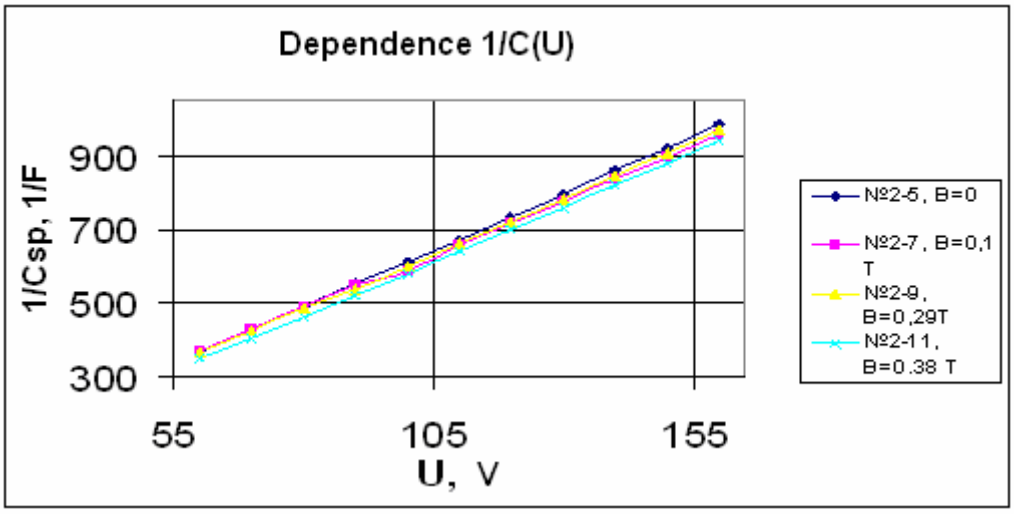

Figure 3.5 Experimental voltage dependence of inverse capacity 1/C for the samples formed in applied magnetic fields: B = 0 T, B = 0.1 T, B = 0.29 T, B = 0.38 T.

Figures 3.4 shows experimental voltage-time dependences $U(t)$ for the samples formed in different applied magnetic fields. Experimental voltage dependence inverse capacity $1/C$ is shown in Figure 3.5.

Table 3.2 Calculation results of the differential electric field strength E_{diff} and velocity of oxide growth dU/dt for the samples formed in different applied magnetic fields

	B = 0 T	B = 0.1T	B = 0.19T	B = 0.29T	B = 0.38T
sample.№	2-5	2-7	2-8	2-9	2-11
dU/dt	0.205	0.211	0.226	0.223	0.229
$d(1/c)/dU$	5.845	5.946	6.184	6.152	6.399
E_{diff},V/m	3.69E+08	3.78E+08	4.06E+08	4.01E+08	4.11E+08

Differential electric field strength and velocity of oxide growth were calculated from slope angle of the dependence $U(t)$ by the method described in part 2.1. Results of calculation are shown in table 3.2.

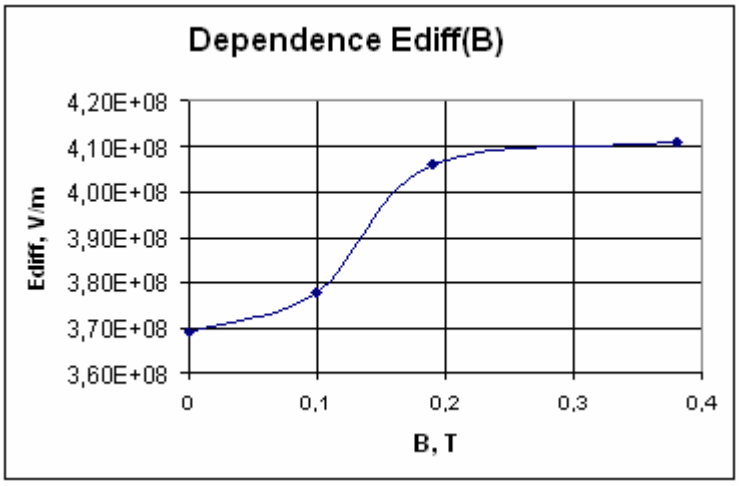

Figure 3.6. Dependence of differential electric field strength E_{diff} on magnetic field strength B applied during synthesis of the oxide.

Figure 3.6 shows dependence of differential electric field strength on magnetic field strength applied during synthesis of the oxide.

In these two series constant and pulsed magnetic fields, applied during oxide syntheses, accelerate the synthesis. Differential electric field strength is also increased.

Dependences $U(t)$ shown in Figs. 3.1 and 3.4 are linear during all oxide growth process. The magnetic field applied in these two series was perpendicular to electric field. In this case there is Lorentz force. Lorentz forces change trajectories of charge particles movement as was described in part 1.2.3. In the next series of experiments were realized parallel magnetic and electric field. This configuration of fields eliminates the possibility of the present of Lorentz force.

3. Third series samples: Constant and pulsed magnetic fields perpendicular and parallel to electric field

For all samples were used the equal terms of forming: U_f = 122,5 V, electrolyte was solution of H_3PO_4 with concentration 0.01N, density of current was j = 2 mA/cm and samples area S = 0.0006 m^2.

Following constant magnetic fields were applied perpendicular to electric field during synthesis of oxide:

1. Pulsed magnetic fields perpendicular to electric field were applied during synthesis of oxide: B = 0 T for Sample. № 3-7. B = 0.29 T for Sample. № 3-5. B = 0.49 T for Sample. № 6.

2. Pulsed magnetic fields parallel to electric field were applied during synthesis of oxide: B = 0 T for Sample. № 3-1. B = 0.29 T for Sample № 3-2 and Sample. № 3-4. B = 0.49 T for Sample № 3-3.

3. Constant magnetic field of B = 0.6 T was applied parallel to electric field during synthesis of oxide, Sample № 3-8.

Frequency of pulsed magnetic field was f = 50 Hz.

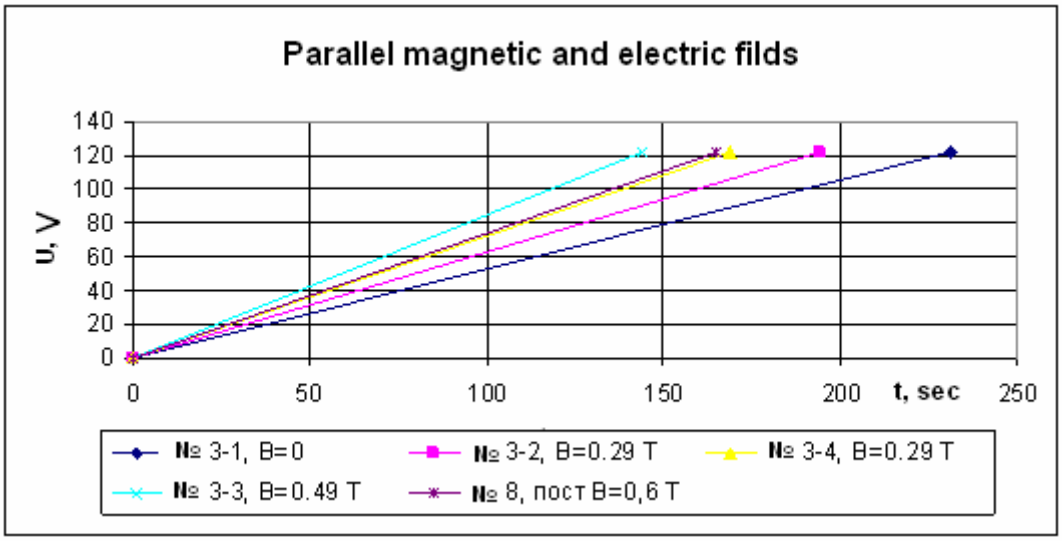

Fig. 3.7. Kinetic characteristics of synthesis processes in the presence of constant and pulsed magnetic fields parallel to electric field.

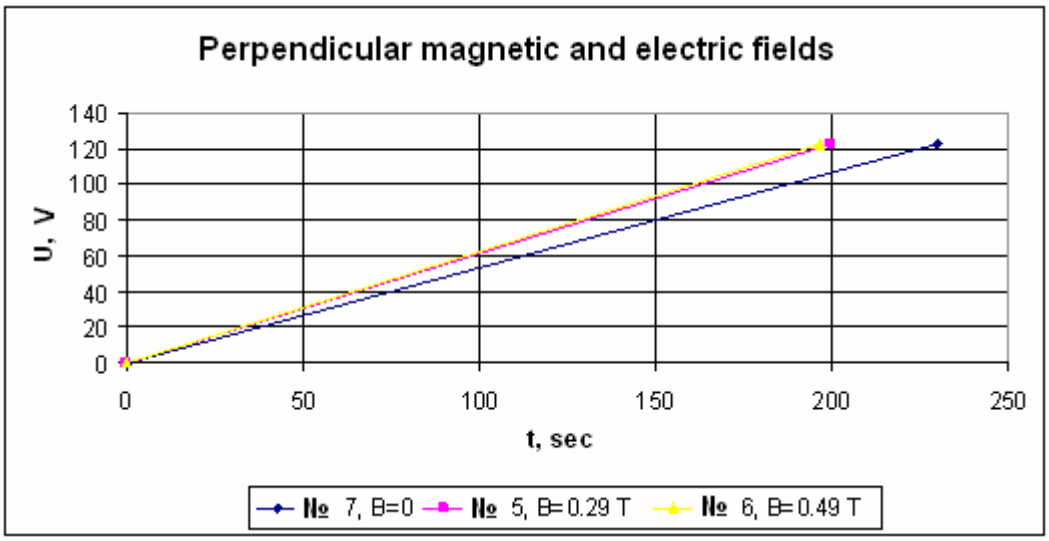

Figure 3.8. Kinetic characteristics of synthesis processes in the presence of pulsed magnetic fields perpendicular to electric field.

Kinetic characteristics of synthesis processes in the present of constant and pulsed magnetic fields parallel to electric field are shown in Figure 3.7. Kinetic characteristics of synthesis processes in the present of pulsed magnetic fields perpendicular to electric field are shown in Figure 3.8.

Table 3.3. Calculated results of the differential electric field strength E_{diff} and velocity of oxide growth *dU/dt* for the samples formed in different magnetic fields parallel to electric field. Here *T* is time of oxide growth

	Parallel fields				
	Pulsed magnetic fields				**Constant magnetic field**
B, T	**0**	**0.29**	**0.29**	**0.49**	**0.6**
Sample №	3-1	3-2	3-4	3-3	3-8
T, sec	231	194	169	144	165
dU/dt, V/sec	0,530	0.631	0.725	0.851	0.742
E_{diff},V/m	4.76E+08	5.67E+08	6.51E+08	8.98E+08	6.67E+08

Table 3.4. Calculated results of the differential electric field strength E_{diff} and velocity of oxide growth *dU/dt* for the samples formed in different magnetic fields perpendicularl to electric field. Here *T* is time of oxide growth

	Perpendicular fields		
B, T	**0**	**0,29**	**0,49**
Sample №	3-7	3-5	3-6
T, sec	230	200	197
dU/dt, V/sec	0.53261	0.6125	0.62183
E_{diff},V/m	4.8E+08	5.5E+08	5.6E+08

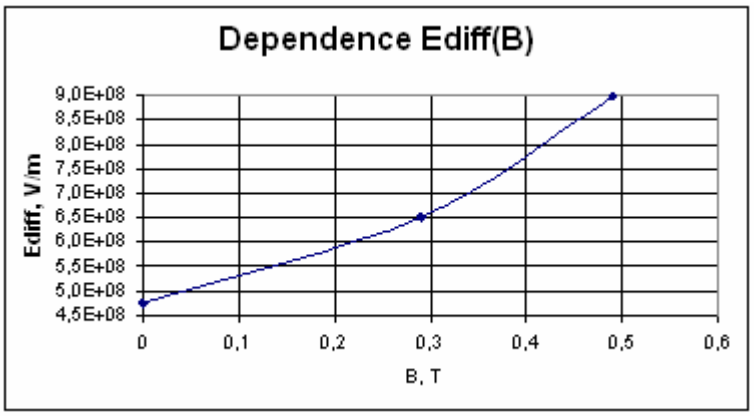

Figure 3.9. Dependence of differential electric field strength E_{diff} on pulsed magnetic field strength *B* applied during synthesis of the oxide in the case of parallel magnetic and electric fields.

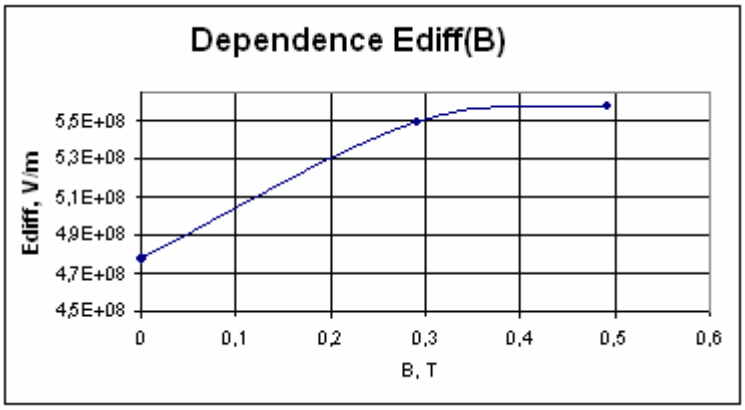

Figure 3.10. Dependence of differential electric field strength E_{diff} on pulsed magnetic field strength B applied during synthesis of the oxide in the case of perpendicular magnetic and electric fields.

Figures 3.9 and 3.10 show dependencies of differential electric field strength on magnetic field strength applied during synthesis of the oxide in the cases of parallel and perpendicular fields, respectively.

Results of these series of experiments also established magnetic fields applied during oxide syntheses increase velocity of oxide growth and differential electric field strength.

These experiments show that Lorentz force is not the only reason for magnetic field influence on the process of the oxide synthesis. Magnetic field influence on transport mass and charge, and also on the chemical reactions taking place on the phase boundaries and on the spin state of particles entered into those reactions. Therefore magnetic field can effect to the structure of formed oxide.

Next we investigate optical and electrical properties of the oxide samples.

3.2. Film thickness determination and optical properties of oxide

Wave length dependence of the reflection index $R(\lambda)$ of the samples synthesized in the second and third series (chapter 3.1) were obtained by the spectrophotometer СФ-46 with the additional block and by the spectrophotometer СФ-56.

Optical investigation of the samples obtained in series 3

Figure 3.11 shows experimental dependences of the reflection index on the wave length $R(\lambda)$. Positions of spectral maximums and minimums are given in Table 3.5. These positions can be used to determine the film thickness. Figure 3.11 and Table 3.5 show that positions of maximums and minimums are different for films synthesized in different magnetic field and in different field configuration. Therefore film thicknesses are also different.

Table. 3.5. Positions of spectral maximums and minimums of interference spectrums of samples synthesized in different crossed electric and magnetic fields (series 3).

	Perpendicular fields				Parallel fields	
B, T	0	0.29	0.49	0.6	0.29	0.49
Samp.№	**3-1**	**3-4**	**3-3**	**3-8**	**3-5**	**3-6**
max	212	213	211	211	213	215
min	226	228	229	224	228	225
max	249	247	250	250	250	248
max	357	332	354	355	354	333
min	377	395	368	366	369	353
max	410	425	400	402	401	403
min	455	477	441	436	445	447
max	519	541	496	489	504	509
min	615	674	584	566	599	603
max	792	930	715	688	771	777
min	1021		959	946	984	985

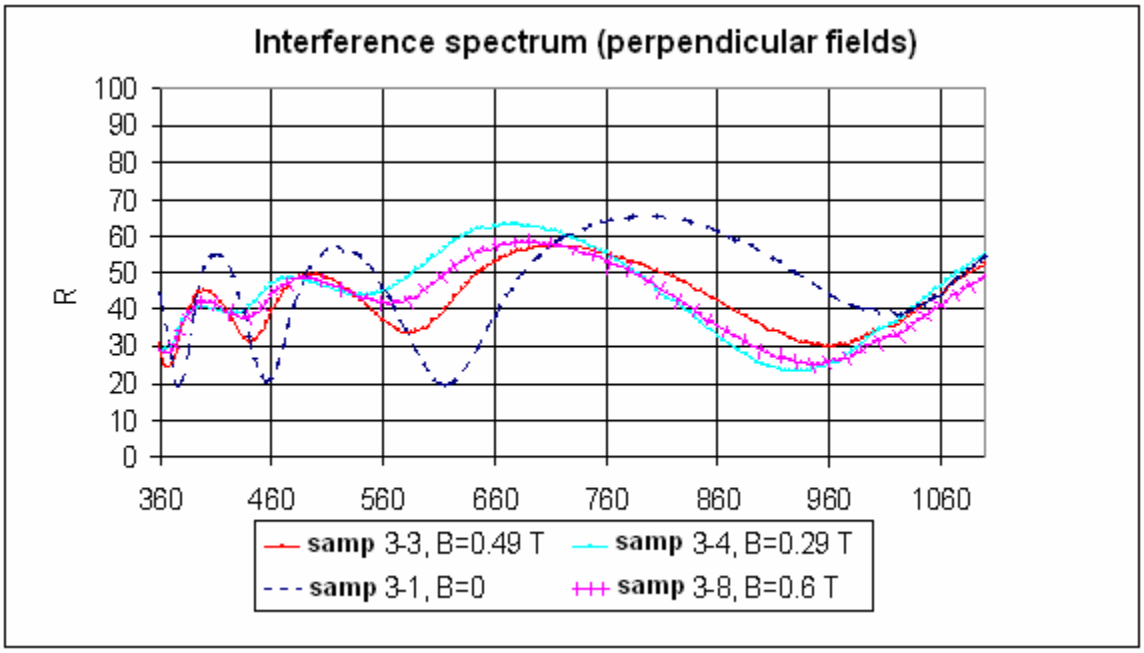

(a)

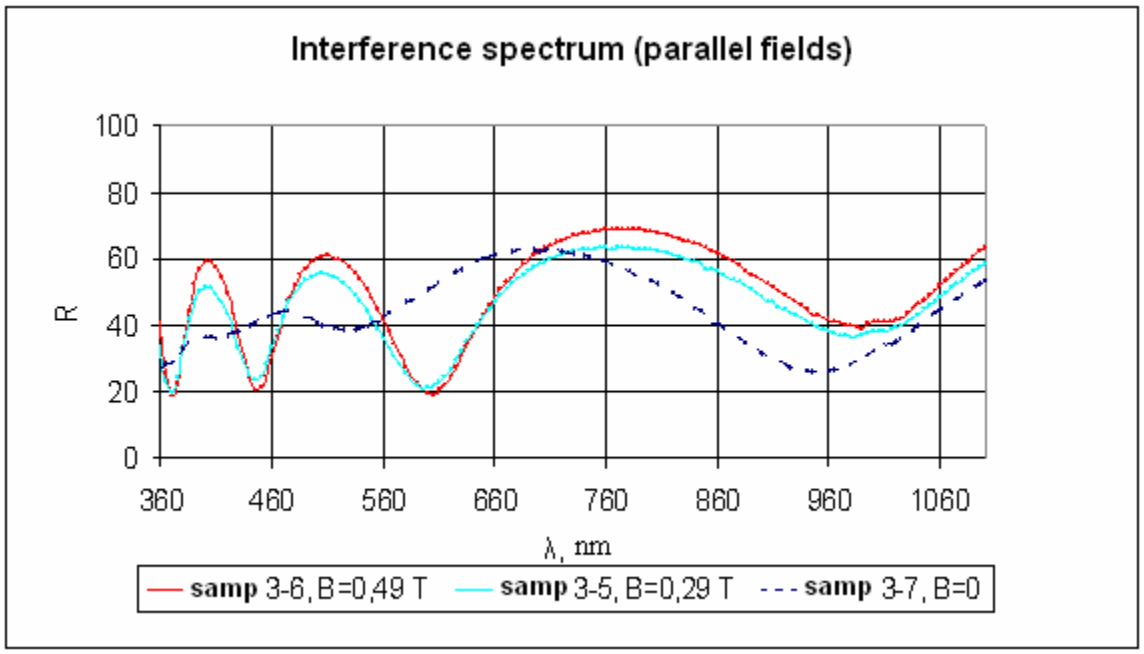

(b)

Fig. 3.11. Interference spectrums of samples synthesized in different crossed electric and magnetic fields (series 3): a) perpendicular fields; b) parallel fields.

Moreover spectrums are also different for samples synthesized in the present of equal strength of magnetic field but in different configuration of electric and magnetic fields.

This is seen in Figure 3.12. Interference spectrum for samples obtained using parallel magnetic and electric fields are more diffused than in the case of perpendicular fields. Maximums and minimums are more diffuse. It shows the change of optical properties. It is possible to draw a conclusion that magnetic field, applied during sample preparation, influences on optical properties of the samples.

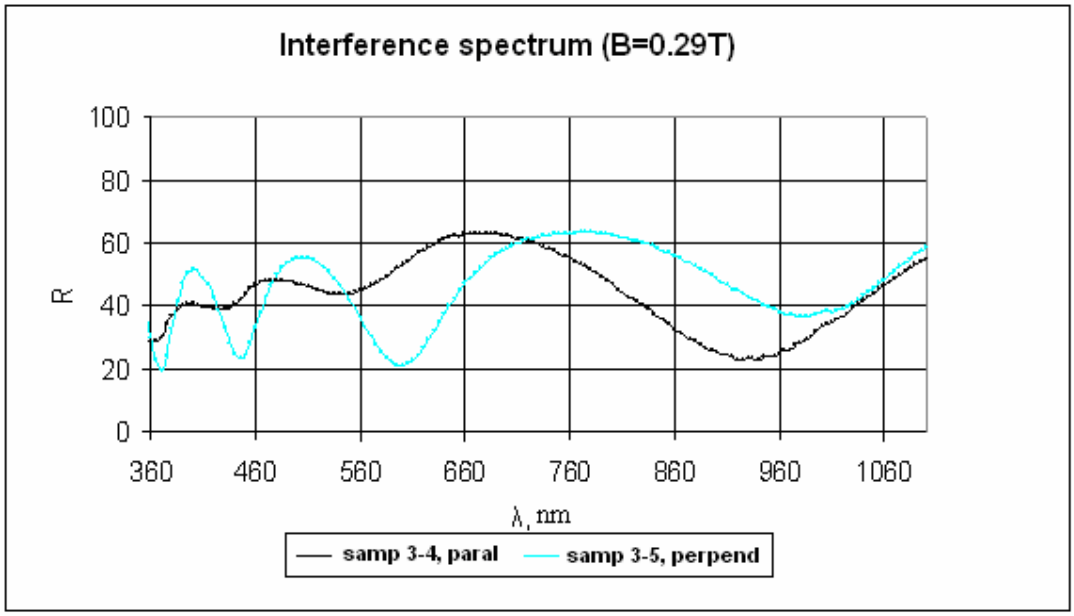

(a)

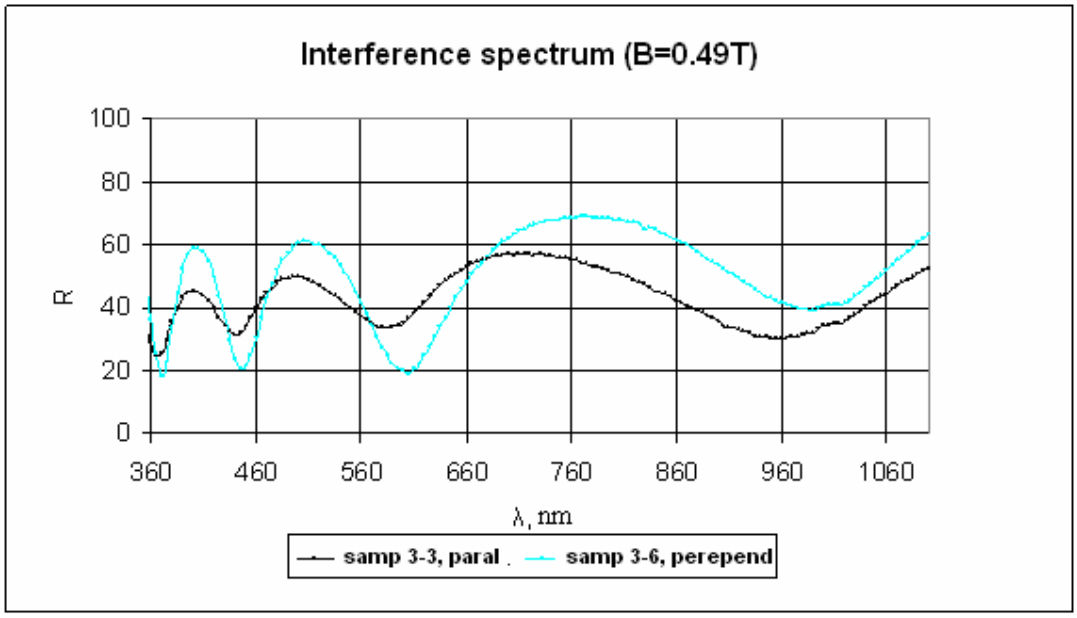

(b)

Figure 3.12. Comparison of interference spectrums of the samples synthesized in the present of equal strength of magnetic field but with different configuration of electric and magnetic fields (series 3). a) B = 0.29 T; b) B = 0.49 T.

Calculation method of film thickness described in chapter 2.2.2.3 has been developed in our laboratory. This method is new to the case of reflection. Therefore we have considered and have applied all possible variants of calculations. This method also allows to calculate the refraction index of the oxide.

Variant 1.
Positions of maxima and minima of interference spectrum did not exchange the places and theoretical value of the refraction index of the oxide was substituted into formulas (n = 1.95).

Variant 2.
Positions of maxima and minima of interference spectrum did not exchange the places and calculated value of the refraction index of the oxide was substituted into formulas.

Variant 3.
Positions of maxima and minima of interference spectrum exchanged the places and theoretical value of the refraction index of the oxide was substituted into formulas (n = 1.95).

Variant 4.
Positions of maxima and minima of interference spectrum exchanged the places and calculated value of the refraction index of the oxide was substituted into formulas.

Results for all four variants are given in Table 3.6.

Table 3.6. Results of film thickness determination for sample 3-1 by spectrum of reflection coefficient $R(\lambda)$ with the second method, symbols are described in the text.

	Variant 1						
№	s_{max}	s_{min}	λ_{max}, nm	λ_{min}, nm	d_{max}, nm	d_{min}, nm	d_{max}-d_{min}, nm
1	3	3	410	377	315.38	338.33	-22.95
2	2	2	519	455	266.15	291.67	-25.51
3	1	1	792	615	203.08	236.54	-33.46

	Variant 2						
№	s_{max}	s_{min}	λ_{max}, nm	λ_{min}, nm	d_{max}, nm	d_{min}, nm	d_{max}-d_{min}, nm
1	3	3	410	377	199.86	214.41	-14.54
2	2	2	519	455	168.29	184.42	-16.13
3	1	1	792	615	130.63	152.16	-21.52
№	R_m	R_M	R_m/R_M	X_1	X_2	n	
1	19	53	0.36	9.47	0.74	3.08	
2	20	55	0.36	9.51	0.74	3.08	
3	19.8	61	032	9.19	0.77	3.03	
	Variant 3						
№	s_{max}	s_{min}	λ_{max}, nm	λ_{min}, nm	d_{max}, nm	d_{min}, nm	d_{max}-d_{min}, nm
1	3	3	377	410	290.00	367.95	-77.95
2	2	2	455	519	233.33	332.69	-99.36
3	1	1	615	792	157.69	304.62	-146.92
	Variant 4						
№	s_{max}	s_{min}	λ_{max}, nm	λ_{min}, nm	d_{max}, nm	d_{min}, nm	d_{max}-d_{min}, nm
1	3	3	377	410	183.78	233.17	-49.40
2	2	2	455	519	147.54	210.36	-62.83
3	1	1	615	792	101.44	195.95	-94.51
№	R_m	R_M	R_m/R_M	X_1	X_2	n	
1	19	53	0.36	9.47	0.74	3.08	
2	20	55	0.36	9.51	0.74	3.08	
2	19.8	61	0.32	9.19	0.77	3.03	

Here the “max” and “min” subscripts correspond to maximum and minimum of spectrum respectively, s_{min}, s_{max} are order for interference minimums and maximums, λ_{min}, λ_{max} are wave length of minimums and maximums, d_{min}, d_{max} are thicknesses calculated by formulas 2.31, (d_{min}-d_{max}) is difference between d_{min} and d_{max}, R_m, R_M are values of envelope curve of minimums and maximums for respective wave length, X_1, X_2 are roots of equation 2.28, n is calculated refracted index of oxide. The most true value of thickness is the value of d_{min} which corresponded to minimum difference between d_{min} and d_{max}.

Total results of calculation and analysis are given in Table 3.7.

Table. 3.7. Total results of film thickness determination of samples from third series by spectrum of reflection coefficient $R(\lambda)$ with the second method described in chapter 2.2.2.3.

	Parallel fields				Perpendicular fields	
B, T	0	0.29	0.49	0.6	0.29	0.49
Samp.№	**3-1**	**3-4**	**3-3**	**3-8**	**3-5**	**3-6**
№	Variant 1, d_{min}, nm					
1	338	330	330	328	331	334
2	292	283	283	279	285	287
3	237	225	225	218	230	232
№	Variant 2, d_{min}, nm					
1	214	183	192	212	204	216
2	184	151	159	179	175	184
3	152	121	130	141	146	150
№	Variant 3, d_{min}, nm					
1	368	359	359	361	360	362
2	333	318	318	313	323	326
3	305	275	275	265	297	299
№	Variant 4, d_{min}, nm					
1	233	199	208	233	222	234
2	210	170	179	201	198	209
3	196	148	159	172	188	194

Grey color in the table indicate the most true values of thickness. These values correspond to smallest difference between d_{min} and d_{max}. It is impossible to speak, that the method is completely correct because it has been applied for the first time. To prove reliability of this method it is necessary to make a series of experiments on other materials and to compare result with theoretical data. But it can be noted, that calculations give quite reasonable results close to theoretical.

Table. 3.8. Calculated reflective indexes.

Sample №	*B*, T	Configuration of fields	*n*
3-1	0	parallel	3.06
3-2	0.29	parallel	3.18
3-4	0.29	parallel	3.6
3-3	0.49	parallel	3.4
3-8	0.6	parallel	3.02
3-5	0.29	perpendicular	3.14
3-6	0.49	perpendicular	3.02

Results of calculation of refractive index are presented in table 3.8. These results will be used for next calculations, because determined reflective indexes were the same for every samples in all variants of calculation.

Method described in chapter 2.2.2.2 is more reliable than previous. Thicknesses of films are calculated by this method for all neighbouring maximums and minimums. To calculate average value of thickness, taken into account only those values which are computed by maxima and minima belong to wavelength range from 350 nm to 600 nm are. This is because reflective index is calculated for this wavelength range using method 2.2.2.3, and for another wave lengths reflective index has dispersion. Average thickness d_{aver} is calculated from values of d_4, d_5, d_6, d_7. Results are presented in Table 3.9.

Table. 3.9. Calculated results of films thicknesses using spectroscopy method (series 3).

	Parallel fields				Perpend. fields	
B, T	0	0.29	0.49	0.6	0.29	0.49
Samp. №	3-1	3-4	3-3	3-8	3-5	3-6
d_1, nm	280	254	197	301	258	400
d_2, nm	200	233	201	178	206	201
d_3, nm	550	164	684	978	693	602
d_4, nm	383	440	338	338	368	387
d_5, nm	338	307	317	427	323	339
d_6, nm	301	317	293	333	302	303
d_7, nm	271	215	242	298	253	271
d_8, nm	225	193	235	264	214	223
d_9, nm	0	0	206	0	284	305
d_{aver}, nm	324	319	297	349	311	325

Forming coefficients were calculated as a ratio of average oxide thickness to forming voltage: $\alpha = d_{ox}/U_f$. Results are presented in Table 3.10

Table. 3.10. Calculated forming coefficients.

	B, T	d_{aver}	α,Å/V
samp. №3-1, parallel fields	0	324	25.9
samp. №3-4, parallel fields	0.29	319	25.5
samp. №3-3, parallel fields	0.49	297	23.8
samp. №3-8, parallel fields	0.6	349	27.9
samp. №3-5, perpendicular fields	0.29	311	24.9
samp. №3-6, perpendicular fields	0.49	325	26.0

Optical inverstigation of samples obtained in series 2.

Spectrums of the reflection index on the wave length $R(\lambda)$ of samples synthesized in the second series were obtained by spectrophotometer СФ-46 with the additional

block. Calculations are analogous to previously described method. Positions of maximums and minimums are presented in Table 3.11 and calculated thicknesses are presented in Table 3.12.

Table. 3.11. Positions of maximums and minimums of interference spectrum (series 2).

B, T	0	0.1	0.29	0.38
samp. №	**2-5**	**2-7**	**2-9**	**2-11**
max	365	365	370	370
min	390	385	390	390
max	420	420	420	420
min	450	450	460	450
max	500	500	510	500
min	560	560	570	560
max	650	660	650	650
min	770	770	780	780

Table. 3.12. Calculated results of films thicknesses by means of spectroscopic method. (series 2).

B, T	0	0.1	0.29	0.38
samp. №	**2-5**	**2-7**	**2-9**	**2-11**
d_1, nm	464	572	588	588
d_2, nm	445	376	445	445
d_3, nm	513	513	393	513
d_4, nm	367	367	382	367
d_5, nm	380	380	394	380
d_6, nm	330	301	377	330
d_7, nm	340	376	318	318
d_{aver}, nm	397	395	403	387
α,Å/B	24,8	24,7	25,2	24,2

Average thickness d_{aver} is calculated from values of d_3, d_4, d_5.

One more sample №2-13 was synthesized. The only difference from the second series was forming voltage of 200 V and magnetic field B = 0. For this sample result of optical analysis gave d_{aver} = 477 nm and α = 23,9 Å/V.
Thicknesses and forming coefficients of films were also determined by means of ellipsometric method.

Experimental equipment allows to determine thickness of sample in the range from several Å to 3000 Å. Theoretic thickness of sample is calculated as a product of theoretical forming coefficient and forming voltage. Theoretical forming coefficient of niobium oxide is α = 23 Å/V. All previous samples have thickness near maximum permissible value 300 nm. Therefore films with smaller thickness were synthesized. All those samples were formed without present of magnetic field. The main goal of this experiment is to estimate forming coefficient.

The terms of forming samples were: electrolyte was solution of H_3PO_4 with concentration 0,01N; density of current was j = 1 mA/cm; square of samples was S = 0.0002 m^2, U_f was different for different samples.

Next samples were synthesized: Sample № E-1, U_f = 60 V. Sample № E-3, U_f = 40 V. Sample № E-2, U_f = 30 V. Sample № E-4, U_f = 20 V.

Values of ellipsometric angles ψ and Δ were obtained for all samples from experiment and oxide thickness was calculated as described in chapter 2.2.1. Measurements were taken in different direction of the film: along and across the film.

Theoretical predicted thickness is the thickness calculated by formula
$d = \alpha_{th} * U_f$,
where α_{th} is theoretical forming coefficient, for niobium oxide α_{th} = 23 Å/V.

Table. 3.13. Calculated results of films thicknesses and forming coefficients by means of ellipsometric method.

Sample E-1 U_f = 60 V, theoretical predicted thickness about 120 nm.						
	ψ	Δ		*n*	*d, nm*	α,Å/V
	30.025	106.116	z.ap.:	3.1	150-210	
	30.908	107.405				
average	**30.4665**	**106.7605**		**2.587**	**174.04**	**29.0**
Sample E-3 U_f = 40 V, theoretical predicted thickness about 80 nm.						
	ψ	Δ		*n*	*d, nm*	α,Å/V
	26.783	223.433	z.ap.:	3.1	100-180	
	30.517	223.916				
	26.1	225.183				
average	**27.8**	**224.1773**		**2.95**	**114.06**	**28.5**
Sample E-2 U_f = 30 V, theoretical predicted thickness about 60 nm.						
	ψ	Δ		*n*	*d, nm*	α,Å/V
	35.433	-83.334	z.ap.:	3,1	50-180	
	35.675	-81.534				
	33.325	-83.317				
	35.5	-83.267				
average	**34.98325**	**-82.863**		**2.865**	**93.28**	**33.1**
Sample E-4 U_f = 20 B, theoretical predicted thickness about 40 nm.						
	Ψ	Δ		*n*	*d, nm*	α,Å/V
			z.ap.:	3.1	50-100	
	67.125	-11.484		**2.943**	**71.64**	**35.82**

Results of experiments and computations are presented in Table 3.13, where “z.ap.” is zero-order approximation of thickness and reflective index of oxide film, which are

input data for the program; extra bold indicates calculated values. The calculated thickness values are more than theoretical thickness.

All results of optical experiments are combined in Table 3.14. There are given thicknesses and forming coefficients, calculated by different method, for samples synthesized in the presence of different magnetic fields, and different configuration of electric and magnetic fields.

Table 3.14. Calculated results of films thicknesses and forming coefficients by means of ellipsometric method and first method of spectroscopy.

Sample №	Configuration of fields	B, T	U_f V	d, nm		α, Å/V
				СФ-56	Ellipsometr.	
2-13		0	200	477		23.9
2-5		0	160	397		24.8
2-7	perpendicular	0.1	160	395		24.7
2-9	perpendicular	0.38	160	403		25.2
2-11	perpendicular	0.49	160	387		24.2
3-1		0	122.5	324		25.9
3-4	parallel	0.29	122.5	319		25.5
3-3	prallel	0.49	122.5	297		23.8
3-8	parallel	0.6	122.5	349		27.9
3-5	perpendicular	0.29	122.5	311		24.9
3-6	perpendicular	0.49	122.5	325		26.0
E-1		0	120	270		22.5
E-2		0	60	147	174	24.5
E-4		0	40		114	28.5
E-3		0	30		93	31.0
E-5		0	20		71	35.5

Using data of Table 3.14 it is possible to draw dependence of film thickness on forming voltage.

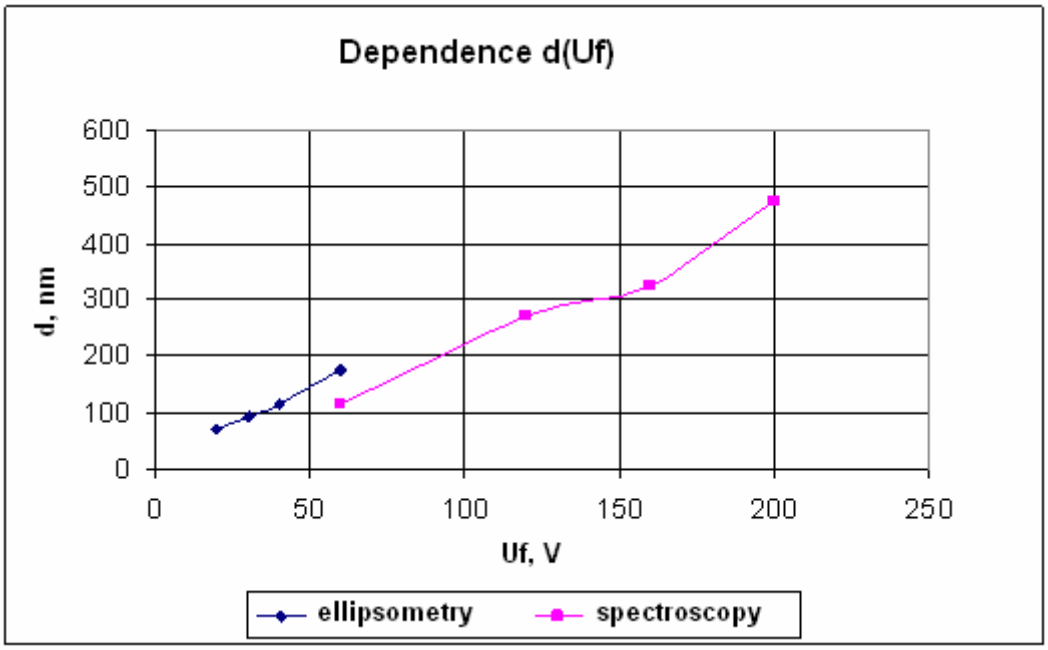

Figure 3.13. Dependence of film thickness on forming voltage.

Linearity of dependence $d(U_f)$ confirm validity of all described methods of thickness determination within the bounds of the theory of oxide film growth. According to this theory increase of forming voltage by fixed value causes increase of oxide thickness by fixed value. Thickness d and forming voltage U are proportional to each others and proportionality, or the slope angle, is the forming coefficient. Data of Table 3.14 show that calculated value of forming voltage sufficiently coincides with theoretical value. For method of ellipsometry result of the thickness determination is overestimated, maybe because not correct calculation model.

3.3. Determination of dc conductivity of niobium oxide

Aluminium contacts were evaporated on the surface of the third series samples by method described in chapter 2.3.1.2. Area of contacts were measured. Results are shown in Table 3.15.

Table. 3.15. Area of evaporated aluminium contacts.

Samp. №	*B*, T	point	*S*, m^2
3-1	0	(2,3)	1.43E-06
3-2	0.29	(5,4)	1.43E-06
		(4,2)	1.43E-06
3-3	0.49	(2,3)	1.65E-06
		(3,1)	7.80E-07
		(3,4)	1.13E-06
3-5	0.29	(3,3)	1.13E-06
3-6	0.49	(3,3)	1.54E-06
		(2,3)	1.54E-06
3-7	0	(2,2)	1.32E-06
3-8	0.60	(3,3)	1.13E-06
		(3,4)	1.13E-06
		(2,2)	1.13E-06
		(2,4)	1.13E-06

Volt-ampere characteristics of niobium oxide films U(I) were obtained by means of method described in chapter 2.2.3. Subject to thicknesses of films and squares of contacts the strengths of electric field E [V/m] and density of current j [A/m^2] were determined. The strength of electric field is ratio of voltage U to thickness of film d, the density of current is ratio of current I to square of contact. The obtained data of volt-ampere characteristics were drawn with different coordinates, Fig. 3.14 and 3.15. Those coordinates are:

1. Logarithmical coordinates $\ln j$ ($\ln U$).
2. Schottky coordinates $\ln j$ ($E^{1/2}$).
3. Pul-Frenkel coordinates $\ln j/E$ ($E^{1/2}$).

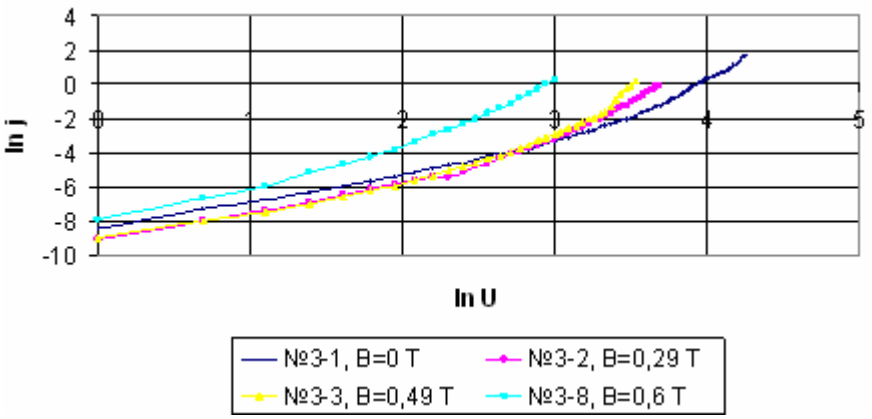

(a) Logarithmical coordinates.

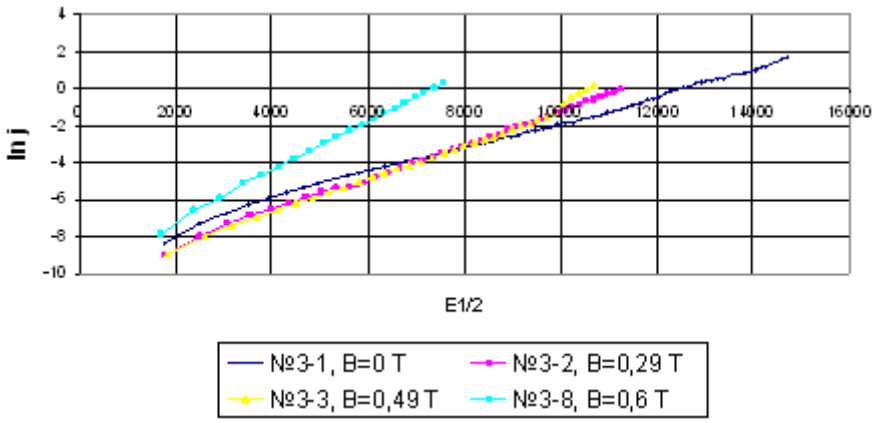

(b) Schottky coordinates.

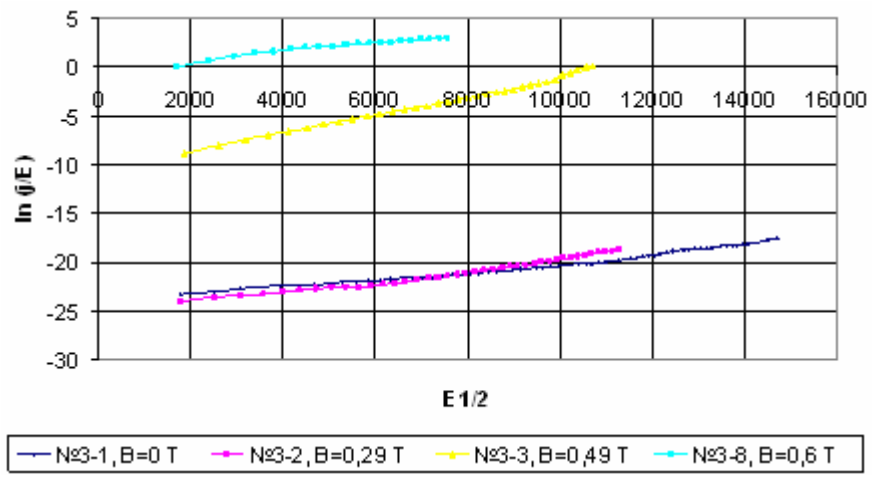

(c) Pul-Frenkel coordinates.

Figure 3.14. Volt-ampere characteristics of samples synthesized in the present of parallel magnetic and electric fields.

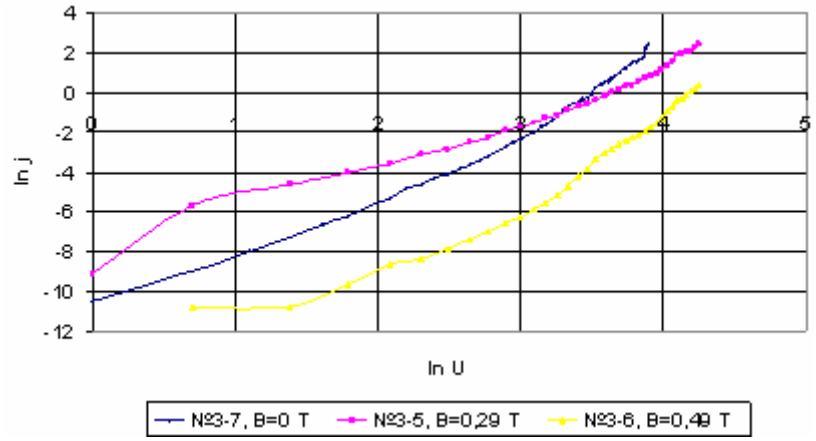

(a) Logarithmical coordinates.

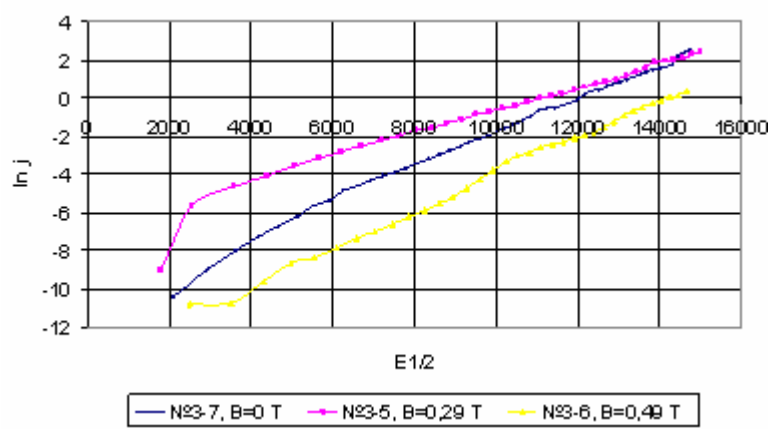

(b) Schottky coordinates.

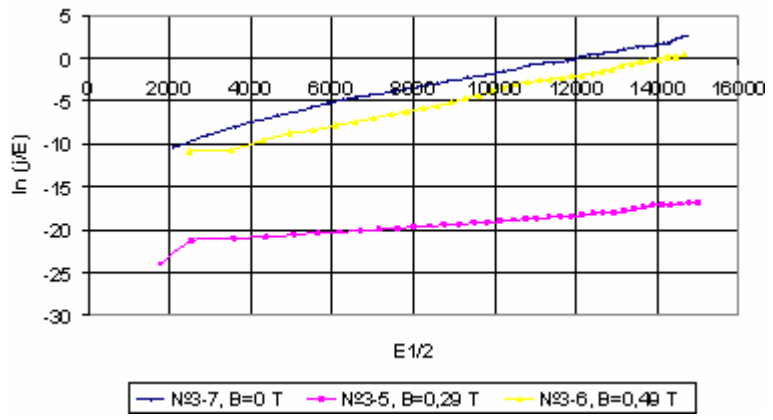

(c) Pul-Frenkel coordinates.

Figure 3.15. Volt-ampere characteristics of samples synthesized in the present of perpendicular magnetic and electric fields.

To establish mechanism of conductivity it is needed to consider two factors: 1. Is the volt-ampere characteristic linear in some coordinates? 2. What is the experimental value of Schottky or Pul-Frenkel constants? If there is linear range in volt-ampere dependence and if calculated values of Schottky or Pul-Frenkel constants are equal to theoretical ones, then there is Schottky or Pul-Frenkel mechanism of conductivity, respectively.

Theoretical Schottky and Pul-Frenkel constants are calculated by formulas

$$\beta_{Sch} = \left(\frac{e}{4\pi\varepsilon\varepsilon_0 (kT)^2} \right)^{1/2} \quad \text{and} \quad \beta_{P-F} = 2\beta_{Sch} \quad \text{, respectively.}$$

Where e is electron charge, ε is permittivity of oxide, $\varepsilon = n^2$. The calculation gives $\beta_{Sch} = 5*10^{-4}$, $\beta_{P-F} = 1*10^{-3}$.

Volt-ampere characteristics have linear range both in Schottky coordinates and in Pul-Frenkel coordinates, Fig. 3.14 (b,c) and 3.15 (b,c). To determine the mechanism of oxide conductivity, experimental Schottky and Pul-Frenkel constants were estimated. These constants are equal to slope angles in the respective coordinates. Results are shown in Table 3.16.

Table 3.16. Calculated results of Schottky and Pul-Frenkel constants in different range of voltage U.

		range of U	β_{Sch}	range of U	β_{P-F}	mechanism	
						Sch	P-Fr
Parallel magnetic and electric fields							
№ 1	B = 0 T	average	6.99E-04	average	4.43E-04	+	
		(17-70)	7.29E-04	(17-70)	5.38E-04		
№ 2	B = 0.29 T	average	8.96E-04	average	5.71E-04	+	+
		(10-40)	9.32E-04	(10-40)	6.86E-04		
№ 3	B = 0.49 T	average	9.57E-04	average	6.18E-04	+	+
		(9-27)	8.94E-04	(9-27)	6.21E-04		

		(27-34)	1.74E-03	(27-34)	1.55E-03		+
№ 8	B = 0.6 T	average	1.34E-03	average	8.79E-04		+
		(4-20)	1.29E-03	(4-20)	9.07E-04		+
Perpendicular magnetic and electric fields							
№ 7	B = 0 T	average	6,20E-04	average	6,69E-04	+	
		(10-50)	6,71E-04	(10-50)	6,25E-04		
№ 5	B = 0.29 T	average	6,68E-04	average	4,04E-04	+	
		(5-50)	6,04E-04	(5-50)	3,32E-04		
№ 6	B = 0.49 T	average	9,73E-04	average	7,26E-04		+
		(10-50)	9,69E-04	(10-50)	7,59E-04		

Data in Table 3.16 show that applied magnetic field change mechanism of conductivity of synthesized oxide. Schottky mechanism exists in oxide film formed without applied magnetic field. Schotky coefficient increases with increasing of applied magnetic field. Pul-Frenkel mechanism exists in the samples formed in the present of high magnetic field. Consequently magnetic field both perpendicular and parallel to electric field influences on the electric properties of synthesized oxide.

Temperature dependences of conductivity were measured and activation energies were calculated from slope of ln j (1/T) by formula

$$\Delta E = \frac{k}{e}\frac{\Delta \ln j}{\Delta\left(\frac{1}{T}\right)}, [eV]$$

Where k is Boltzmann constant and e is charge of electron. Calculated results are presented in Table 3.17.

Figures 3.16 (a, b) and 3.17 (a, b) show temperature dependences of conductivity of samples formed without magnetic field and in the presence of maximum magnetic, field respectively.

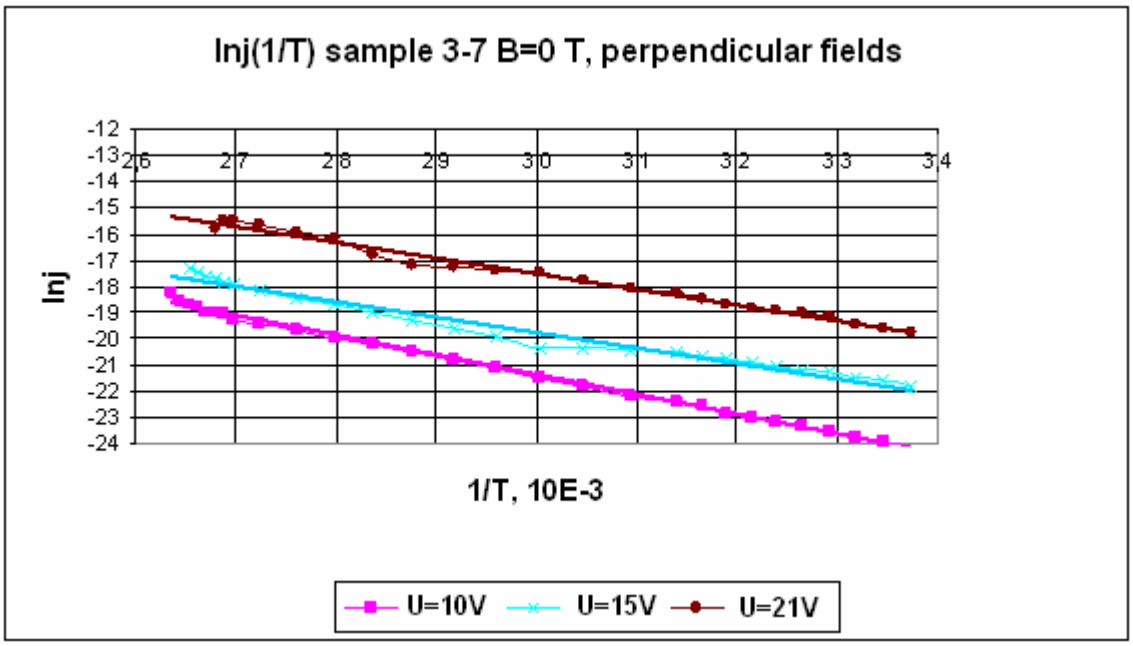

(a)

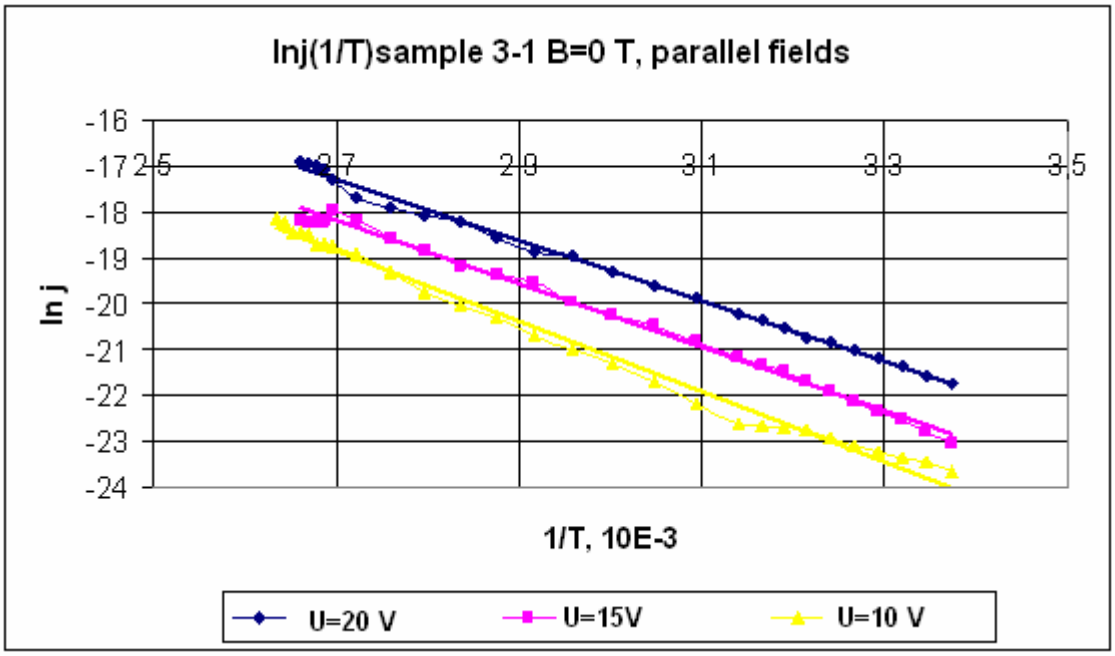

(b)

Figure 3.16 Temperature dependencies of conductivity for different sample voltage U, with B = 0 T.

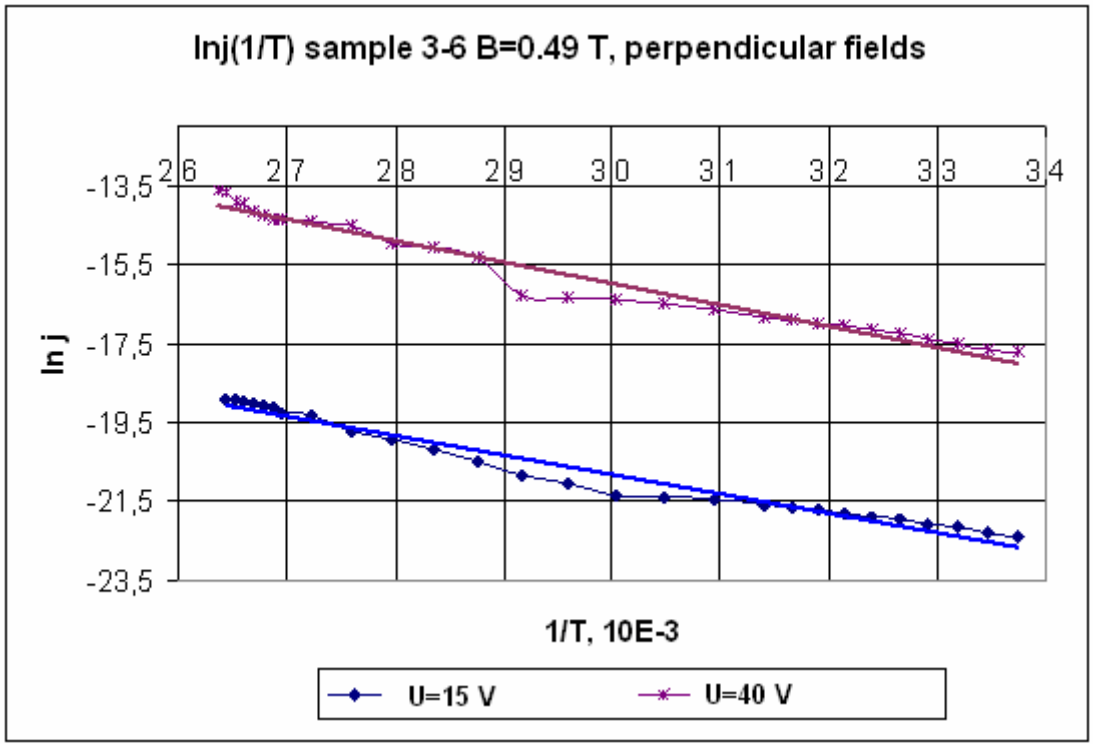

(a)

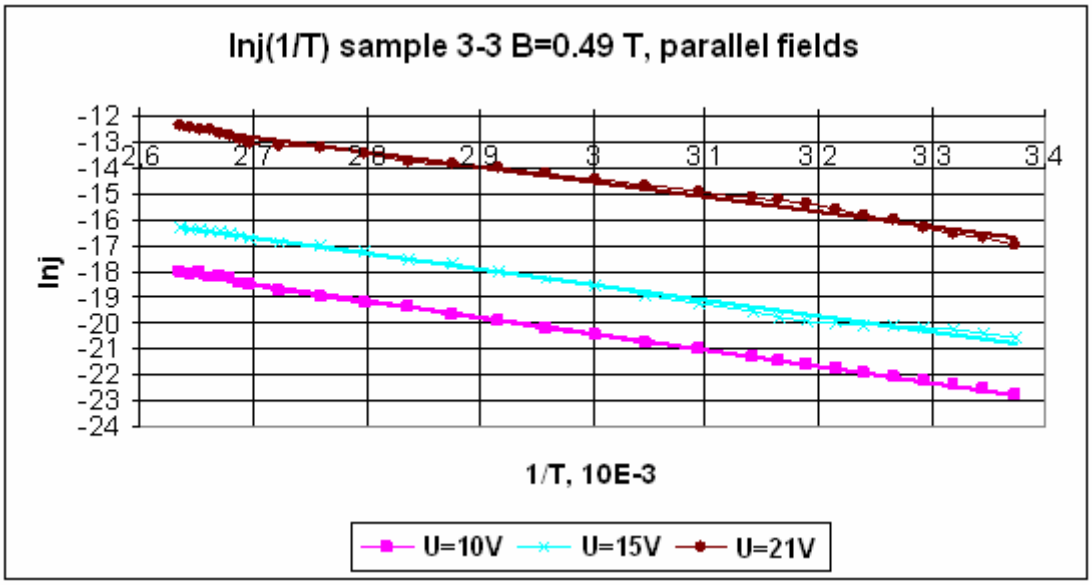

(b)

Fig. 3.17 Temperature dependencies of conductivity for different sample voltage U, with B = 0.49 T.

Table 3.17. Calculated activation energies of charge carriers for different samples.

	Activation energy, eV						
	B = 0		B = 0.29 T		B = 0.49 T		B = 0.6 T
№	3-7	3-1	3-5	3-2	3-6	3-3	3-8
U, B	perpend.	paral.	perpend.	paral.	perpend.	paral.	paral.
10	1.6	1.68	1.58	1.06		1.38	0.85
15	1.71	1.58		1.13	1.43	1.46	0.9
20	1.63	1.45	1.6	0.96		1.11	0.79
30			1.48		1.29		
40					1.11		

Data of Table 3.17 show that there is tendency of activation energy decriase with increasing of magnetic field applied during oxide syntheses. It means that magnetic field influences on the energy structure of the samples.

3.4. Analysis of permittivity spectrum and determination of niobium oxide static permittivity

The main idea of this investigation is to determine the static permittivity of niobium oxide formed in the presence of different magnetic field and also an analysis of permittivity spectrum. Experimental equipment LRC-meter gives opportunity to measure spectrum dependence in the range from 20 Hz to 1 MHz. As it was shown in chapter 2.4 this range of frequency describes only initial spectrum of permittivity. To analyze full spectrum of permittivity much higher frequency is needed. Anyhow this spectrum range is enough to determine static permittivity and to analyze and compare the losses in this frequency range.

For research study five samples were synthesized, using forming voltage U_f = 122.5 V, electrolyte was solution of H_3PO_4 with concentration 0,01N, density of current was j = 2 mA/cm, square of samples was S = 0.0004 m^2

During the synthesis the following magnetic fields were applied:

1. Sample 1 with B = 0 T, parallel configuration.
2. Sample 2 with B = 0.49 T, pulsed magnetic field, perpendicular configuration.
3. Sample 3 with B = 0 T, perpendicular configuration.
4. Sample 4 with B = 0.6 T, constant magnetic field, parallel configuration.
5. Sample 5 with B = 0.49 T, pulsed magnetic field, parallel configuration.

Alumunium contacts were evaporated using method described in chapter 2.3.1. The areas of contacts were determined.

LRC-meter measures C_p, tg φ of the samples for different frequency, where C_p is the capacity of sample and tg φ is a tangency of loss angle. Using area and thickness of contacts it is possible to calculate the geometrical sample capacitance, C_0. The film thickness was calculated by formula:

$d = \alpha U_f$

where α is forming coefficient. This is determined for all magnetic field and different configuration in chapter 3.2 and U_f is forming voltage 122.5 V for all samples.

The real and imaginary parts of permittivity are calculated by formulas (2.32) and (2.33), respectively. For all samples three different contacts were measured, the error is less than 2-3 per cent. Therefore why in the following discussion the average values of $\varepsilon'(\omega)$, $\varepsilon''(\omega)$, tg φ(ω), C (ω) will be used.

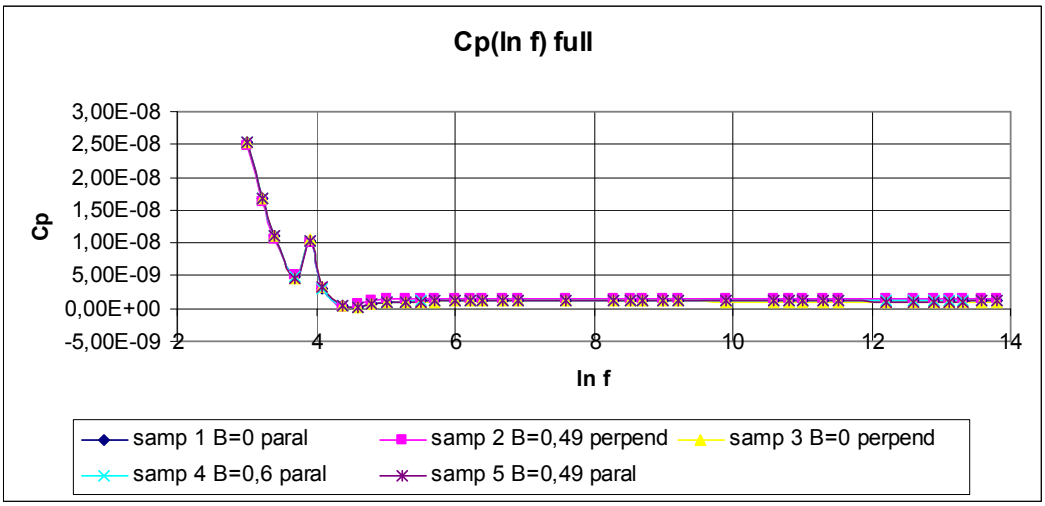

(a)

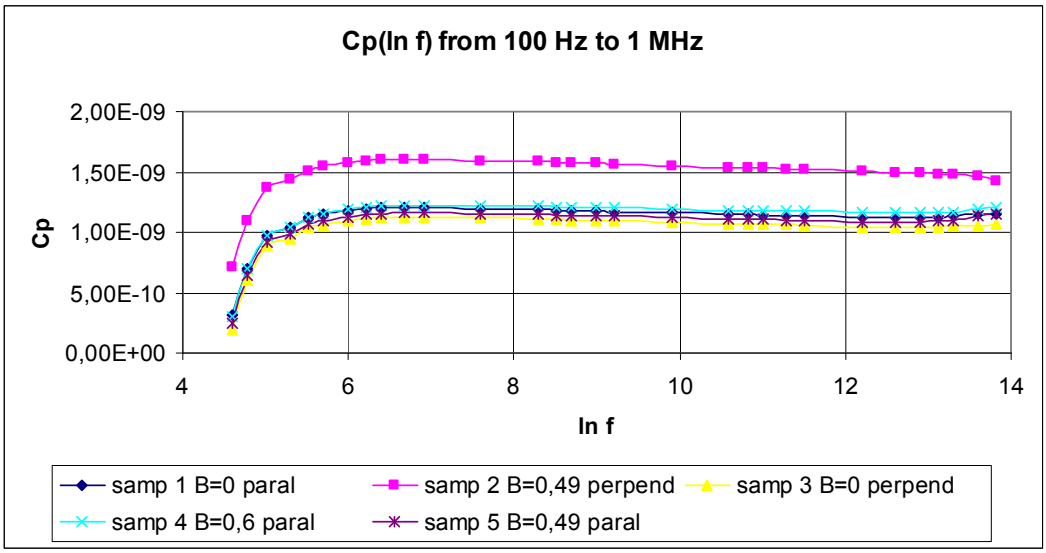

(b)

Figure 3.18. Frequency dependences of measured capacitance of samples. a) frequency range from 20 Hz to 1 MHz b) frequency range from 100 Hz to 1 MHz.

In figure 3.18 the frequency dependences of measured capacitance of samples are shown. The character of the dependences is similar for all samples. On low frequencies, less than 100 Hz, the values of capacitance is too big and does not correspond to value predicted by theory. Possible reasons are, for example, the measuring equipment has characteristic which can not give true value on low frequency. But on frequency more than 100 Hz the measured values of capacity is close to theoretical value. Therefore only this range of frequency is taken into account.

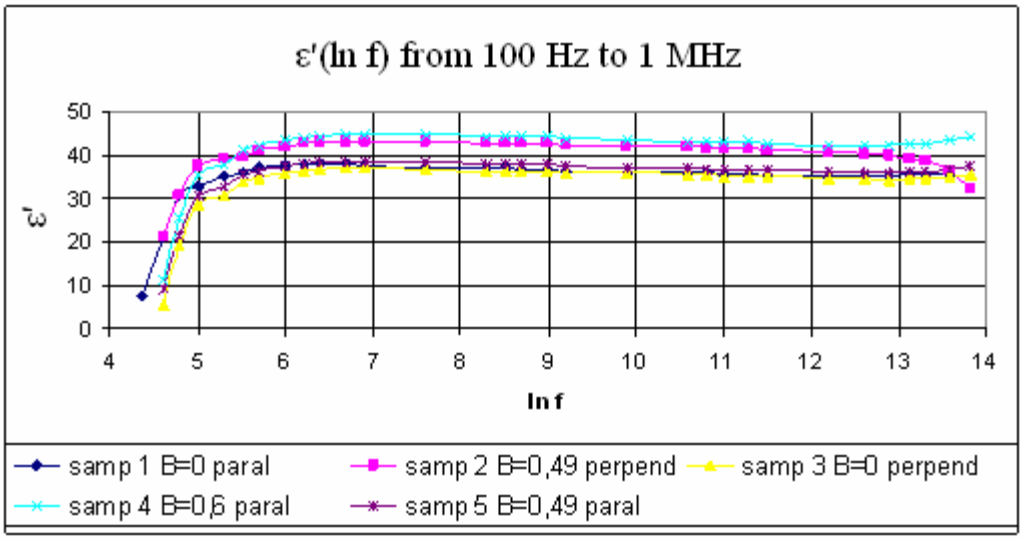

Figure 3.19. Frequency dependences of real part of permittivity, with frequency range from 100 Hz to 1 MHz.

In figure 3.19 dependence of real part of permittivity is shown. It can be noted that for samples formed in the present of magnetic field the permittivity is higher.

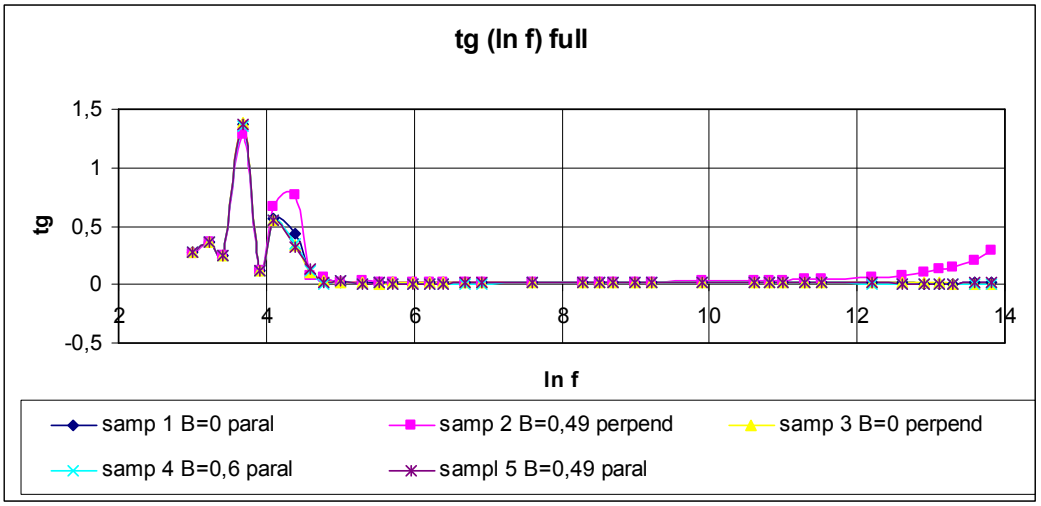

Figure 3.20. Frequency dependences of tangency of loss angle.

Similar to permittivity, frequency dependence of loss angle has insufficient data at the low frequencies. Therefore low frequencies are not taken into account.

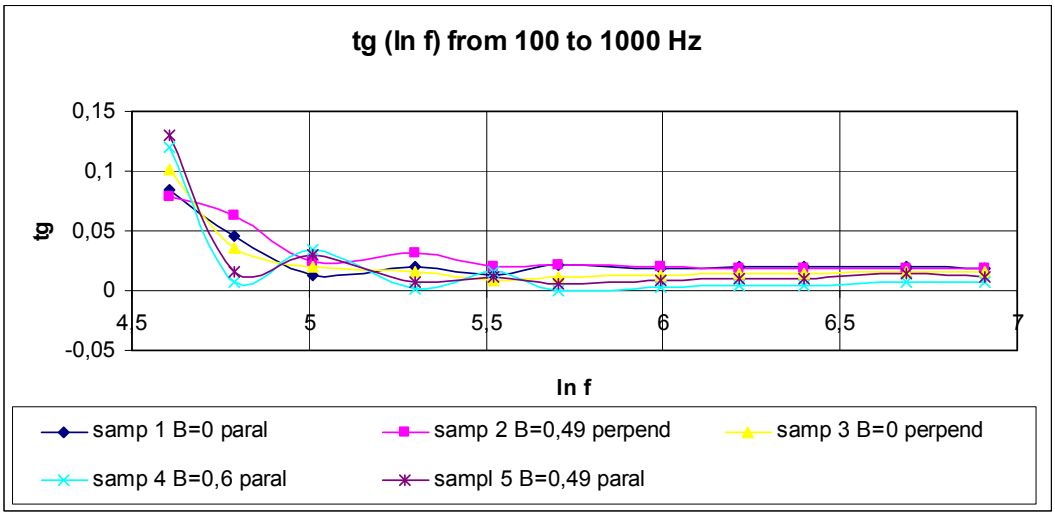

Figure 3.21. Frequency dependencies of tangent of loss angle with frequency range from 100 to 1000 Hz.

In figure 3.21 the frequency dependencies of tangent of loss angle with frequency range from 100 to 1000 Hz is shown. In this range there are oscillations of tangent value, and oscillations are more visible for samples formed in the present of magnetic field. But above frequency about 500 Hz the value of tangent becomes stable. At the high frequencies there is difference between tangents. The value of tangent of loss angle of the sample formed in the present of pulsed magnetic field parallel to electric field increases above 40 kHz frequency, Fig. 3.23.

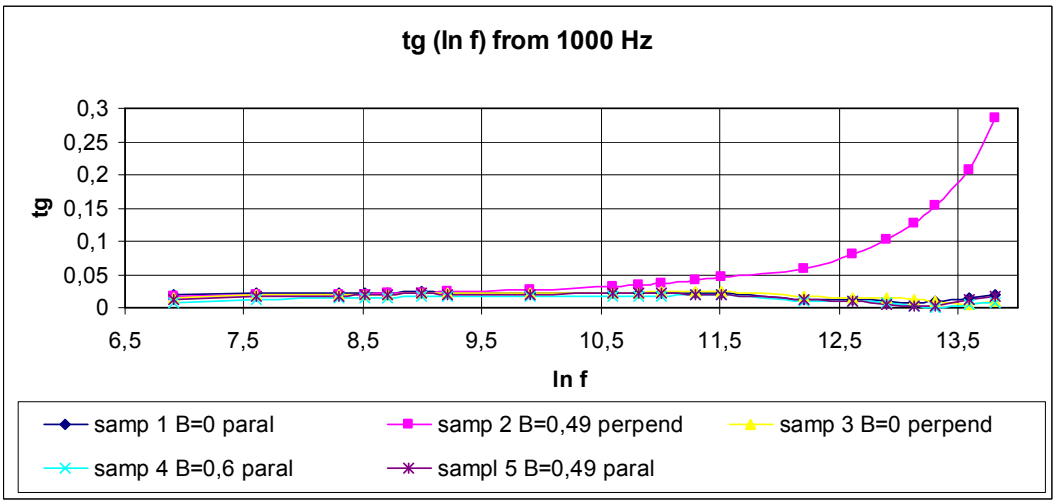

Figure 3.22. Frequency dependences of tangency of loss angle with frequency range from 1000 Hz to 1 MHz.

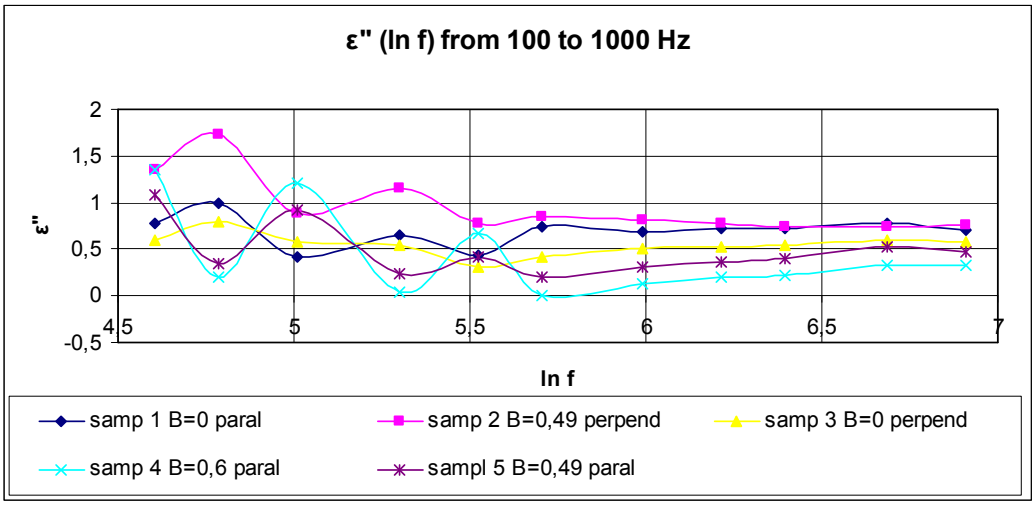

Figure 3.23. Frequency dependences of imaginary part of permittivity with frequency range from 100 to 1000 Hz.

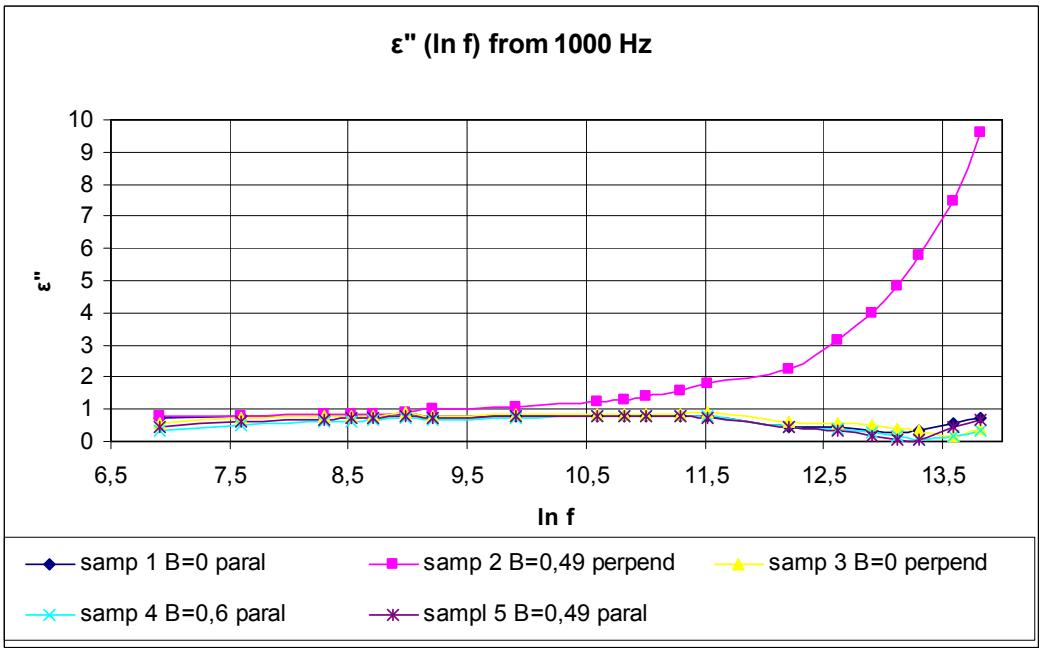

Figure 3.24. Frequency dependences of imaginary part of permittivity with frequency range from 1000 Hz to 1 MHz.

In Figures 3.23 and 3.24 frequency dependencies of imaginary part of permittivity in different frequency range are shown. The tangency of loss angle and imaginary part of permittivity characterizes dielectric losses in the sample. Figures 3.22 and 3.24 show that the dielectric losses of sample formed in the present of pulsed magnetic field perpendicular to electric field increase with high frequencies. The value of losses of

this sample is ten times more than for the other samples on the frequency 1 MHz. Therefore it can be noted that magnetic field is able to change the parameters of formed materials.

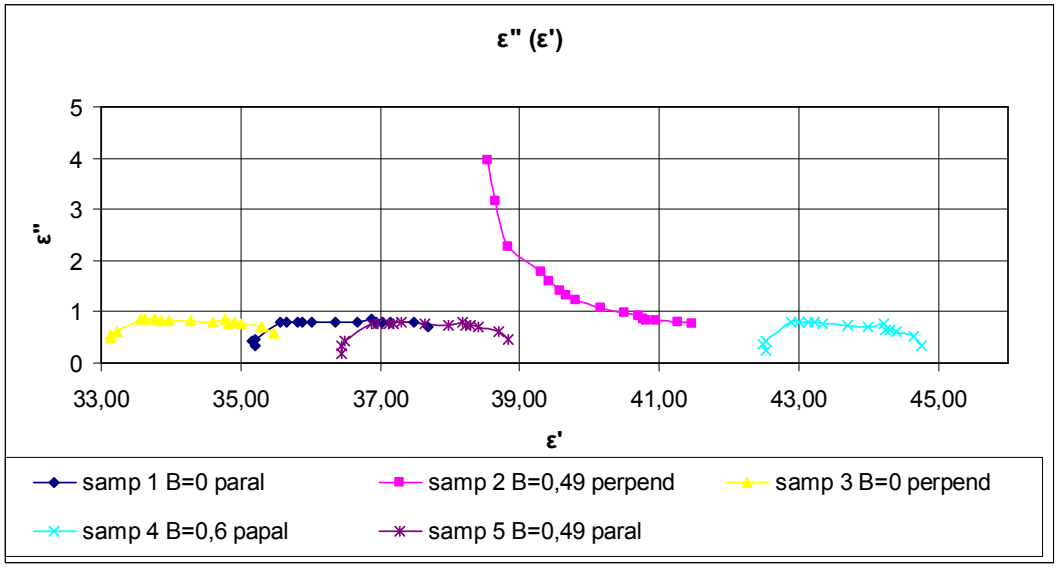

Figure 3.25. Diagrams Cole-Cole.

In figure 3.25 Cole-Cole diagrams are shown. This diagrams show dependence of imaginary part on real part. The left part of diagram characterizes the static permittivity of material. The approximation of left part of diagrams to zero gives the value of static permittivity. Theoretical value of permittivity of niobium oxide is 41. The data in these diagrams demonstrate that static permittivity for the samples formed in the presence of magnetic field have higher values than in the absence of the field. Moreover sample 2 have different character of dependence $\varepsilon^{//}$ ($\varepsilon^{/}$). It can be connected with change of losses characteristic.

CONCLUSIONS

As it was noted above, the process of oxide formation is: 1. Process of mass and charge transport through the phase boundaries of electrolyte-oxide and oxide-metal; 2. Transport of charge particles, electrons and ions of both signs, through the oxide; 3. Reactions of oxide formation on the phase boundaries. Magnetic field can influence on any of these processes.

As a first approximation it was considered that the reason for influence of magnetic field on the process of oxide formation and on the properties of formed material is Lorentz force acting on the charged particles in crossed magnetic and electric fields. This force can change the trajectory of the fluxes of particles, moving through phase boundaries and oxide volume and entering into the reaction of oxide formation, therefore magnetic field would change the conditions of the mass transport. Series of experiments of formation the niobium oxide films in parallel magnetic and electric fields have been done and in such conditions Lorentz force is absent. The effect of increase of growth rate of oxide was also observed. Therefore Lorentz forces is not the unique reason of influence of magnetic field on oxide synthesizing.

Increase of diffusion rate of electrolyte near oxide-electrolyte boundary by means of pulse magnetic field was considered as one more possible reason of increase of growth rate of the film. Crossed pulse magnetic and constant electric fields lead to presence of Lorentz force. This force changes the direction with frequency equal to frequency of magnetic field, in our case f = 50 Hz. Thus, Lorentz forces influences on the trajectory of charged particles in electrolyte near phase oxide-electrolyte boundary accelerate diffusion processes and provide faster mass transition through the phase boundary. To exclude an opportunity of influence of magnetic field on diffusion in the electrolyte, a constant magnetic field was applied. The effect was also observed. This has confirmed that there are other reasons of influence of magnetic field on process of the oxide formation.

All these processes can be reasons of influence of magnetic field on the oxide formation. However, the described analysis has shown that the magnetic field influences not only an processes of the mass transport through oxide and phase boundaries, but it is necessary to consider possible variants of influence of magnetic field on the reaction of oxide formation. Electric and optic properties of formed oxide are changed, it means that structure of formed materials can also change and magnetic field can influences on the reaction occurring on the phase boundaries during the synthesis.

In the presence of magnetic field electron energy is split into sublevels. The reaction of the electron transport is the basic reaction of oxidization, and it is logical to assume that magnetic field, thus, changes the process of reaction. In addition magnetic field influences on the spin states of the reagents. Spin of the particle is also the determinative during the reaction. Only the spin resolved reactions can be carried out. Investigation shows that pulsed and constant magnetic field, perpendicular and parallel to electric field, influences on the oxide formation and changes the process of synthesis and the properties of formed materials.

Experimental conclusions are:

1. In the presence of magnetic field the rate of oxide growth is increased.

2. The thickness of oxide film formed in the presence of magnetic field is less than the thickness of the film synthesized without a magnetic field. The thickness of the film decreases with increasing of magnetic field strength.

3. The mechanism of conductivity is changed. The films formed without magnetic field has Schotky's mechanism of conductivity. With increasing of applied magnetic field the mechanism of conductivity changes to Poll-Frenkel mechanism.

4. Activation energy of charge particles is decreased in the films formed in the presence of stronger magnetic field.

5. The permittivity of formed oxides increases with increasing of the applied magnetic field.

REFERENCES

1. http://www.xumuk.ru/spravochnik/251.html.
2. Del'Oka S.G., Pulfri D.L., Young L.-V. Physics of thin films. vol. 6, 1973.
3. Jung L. Anodic oxide films, 1967.
4. Shishakov N.A., Andreeve V.V., Andrushenko N.K. Structure and formation mechanism of oxide films on the metals. 1959.
5. Odinetz L.L., Hanina E. Physics of oxide films.1981.
6. Pavlov P.V., Hohlov A.F. Solid-state physics. 2000.
7. Aleshina L.A., Fofanov A.D. X-ray structural analysis of amorphous materials. 1987.
8. Bardina N.G., Anodic oxide films. 1964.
9. Mirzoev R.A., Davidov A.D, Dielectric films on the metals. 1990.
10. Shcherbachev D.R., Sorokin I.N., Nazarov N.G. Modeling of growth kinetics of barrier anodic oxide. 1991.
11. Shcherbachev D.R., Sorokin I.N., Growth kinetics of barrier anodic oxide. 1989.
12. T. Hurlen, E Gulbrandsen Growth of anodic films on valve metals // Electrochimica Acta, Vol. 39, No.14 pp. 2169-2172, 1994.
13. Zubric A.I. Process of condensation of tellurium thin films in the present of magnetic and electric field. 1998.
14. Hans Conrad. Influence of an electric or magnetic field on the liquid – solid transformation in materials and on microstructure of the solid // Materials Science and Engineering. 2000, 205-212.
15. Osipjan U.A., Morgunov R.B. Baskakov A.A., Orlov A.M, Skvortzov A.A. magnetic resonance ordering of silicon monocrystal. 2004.
16. Morgunov R.B. Spin micromechanics. 2004.
17. Levin M.N., Postnikov V.V., Palagin M. Selective action of weak magnetic field on the ferroelectric crystals with hydrogen bond. 2003.
18. Bugachenko A.L. Sagdeev R.Z. Magnetic and spin effects of chemical reactions. 1978.

19. Postnikov V.V., Levin M.N., Semenova G.V., Suschkova T.P. Structure transformation of solid solution Sb-As by means of pulsed magnetic field. 2002.
20. Dargunov V.P., Neizvesnii I.G., Grudchin V.A. Theory of nanoelectronics. 2000.
21. Kravchenko A.F., Ocsuk V.N., Electron processes in reduced dimension solid-state systems. 2000.
22. Mogaev V.V., Chernoutza M. Electricity and magnetism. 1994.
23. Salixov K.M. 10 lections of spin chemistry. 2000.
24. Stepanov N.F. Potential surface of chemical reactions. 1996.
25. Eyring G., Lin S.M., Lin S.G. Theory of chemical kinetics. 1983.
26. Voronin A.I., Oscherov V.I. Dynamics of molecular reactions. 1990
27. Bychenko A.L., Second generation of magnetic effects in chemical reactions. 1993
28. http://www.xumuk.ru/
29. Babirin A.A., Mezenov A.M., Shapavalov V.I. Determination of dispersion of reflection and refraction indexes of dielectric film by optical spectrum. 2005.
30. K. Ayadi, N. Haddauoi. A new approach to determination of optical constants and thickness of thin dielectric transparent films. //Journal of materials: materials in electronics 11 (2000)163-167.
31. Ljashenko S.P., Miloslavskii V.K. Simple method of determination of thickness and optical constant of semiconductor and dielectric layers. 1964.
32. Born M., Volf E. Optics. 1973.
33. Shcherbachenko L.A. Research of complex dielectric permittivity of dielectric on the radio frequencies.
34. Rabinovich V.A., Havin Z. Chemical reference book. 1978.